ABSTRACT

Title of dissertation: IONIZING RADIATION-INDUCED COPOLYMERIZATION OF 2-ETHYLHEXYL ACRYLATE AND ACRYLIC ACID AND IONOMER FORMATION

Alia Weaver, Doctor of Philosophy, 2007

Dissertation directed by: Professor M. Al-Sheikhly
Department of Materials Science and Engineering

The ionizing radiation-induced polymerization of acrylate esters is a technique employed for the curing of such materials for a variety of adhesive, coating, ink, and lithographic applications. The work presented in this dissertation involves the synthesis of a copolymer composed of 2-ethylhexyl acrylate (2-EHA) and acrylic acid (AA) using pulsed electron beam and gamma irradiation. The structure and synthesis kinetics of this copolymer were investigated by ^{1}H nuclear magnetic resonance (NMR), electron pulse radiolysis with kinetic spectroscopic detection (PR-KSD), and Fourier transform infrared spectroscopy (FTIR). The effects of total dose, dose rate, and acrylic acid content on the polymerization reaction were studied. The conversion of 2-EHA monomer into polymer at a given total dose was found to be enhanced at lower dose rates and higher concentrations of acrylic acid.

The pulse radiolysis investigation of the polymerization of 2-EHA and AA was performed through studies of four different types of systems: (i) neat 2-EHA, (ii) 2-EHA/methanol (MeOH) solutions, (iii) mixtures of 2-EHA and AA, and (iv) 2-EHA/AA/MeOH solutions. The effect of acrylic acid on the build-up of transient species has been studied by pulse radiolysis. The build-up of carbon-centered neutral 2-EHA

free radicals in neat 2-EHA was found to obey a second order rate law with a rate coefficient of $((7 \pm 3) \times 10^8)\varepsilon_{EHA\bullet}$, whereas in 2-EHA/AA mixtures it was found to obey a pseudo-first order rate law with a rate coefficient of $(1.5 \pm 0.3) \times 10^{10}$ mol^{-1} dm^3 s^{-1}. This phenomenon is suggested to originate in the increased H^+ ion concentration in the presence of acrylic acid, which leads to a faster neutralization step of 2-EHA radical anions as they are transformed into neutral free radicals during the initiation step of the reaction. An enhancement of the rate of build-up was also observed in the methanol solutions, with the build-up in 2-EHA/MeOH following a second order rate law with a rate coefficient of $((1 \pm 0.1) \times 10^8)\varepsilon_{EHA\bullet}$, while the build-up in 2-EHA/AA/MeOH followed a pseudo-first order rate law with a rate coefficient of $(2.5 \pm 1) \times 10^9$ mol^{-1} dm^3 s^{-1}.

An investigation of the formation of ion-containing copolymers (known as ionomers) was performed using the radiation-synthesized poly(2-EHA-co-AA). A two-step synthesis method was used, which included (i) mixture of the copolymer with a metal salt (ferrous acetate ($(CH_3COO)_2Fe$) or ferric chloride ($FeCl_3$)) and (ii) dialysis. Verification of successful incorporation of iron into the copolymer was determined through FTIR analysis, and was identified by an asymmetric carboxylate stretch at 1600 cm^{-1}. A greater uptake of iron was displayed by ionomers formed using ferrous acetate. The ionomers were also characterized by transmission electron microscopy (TEM) and energy dispersive x-ray spectrometry (EDS). TEM analysis of poly(2-EHA-co-AA)/Fe^{2+} ionomers formed from formulated compositions involving a 2:1 mole ratio of ferrous acetate to acrylic acid exhibited ionic clusters of approximately 100 nm in diameter, which may include up to 350 ferrous cations.

IONIZING RADIATION-INDUCED COPOLYMERIZATION OF 2-ETHYLHEXYL ACRYLATE AND ACRYLIC ACID AND IONOMER FORMATION

by

Alia Weaver

Dissertation submitted to the Faculty of the Graduate School of the
University of Maryland, College Park in partial fulfillment
of the requirements for the degree of
Doctor of Philosophy
2007

Advisory Committee:

Professor Mohamad Al-Sheikhly, Chair
Professor Emeritus Joseph Silverman
Professor Lourdes Salamanca-Riba
Professor Sandra Greer
Professor Aaron Barkatt
Dr. Dianne Poster

ACKNOWLEDGEMENTS

There are a number of people whose support has made the completion of this project possible and I am sincerely grateful for their kind help. First and foremost is my advisor, Dr. Mohamad Al-Sheikhly, who I wish to thank for the opportunity to pursue this degree and for his encouragement through all of the stages in the process of completing this dissertation.

I would also like to thank Dr. Joseph Silverman for his guidance and challenging discussions of radiation chemistry and polymers. He served as an endless source of insight into many aspects of this project.

A very special thanks goes to Dr. Douglas Weiss, one of the foremost experts in electron beam curing of acrylates, for his generosity with his time in offering suggestions at every step along the way. I could call on him at any time for advice and he was always very responsive to my questions.

I am also very grateful to Mr. Vincent Adams for the enormous amount of help with the ionizing radiation facilities employed in this work. This includes the training as well as assistance with any number of pieces of customized equipment which he helped to design and construct.

I wish to thank all of the members of the committee, including Dr. Sandra Greer, Dr. Aaron Barkatt, and Dr. Dianne Poster, for taking the time out of their busy schedules to review this dissertation and offer suggestions for improvement.

The assistance with various other experimental aspects of this work is gratefully acknowledged. This includes Dr. Bindhu Varughese and Dr. Janice Reutt-Robey for their help with XPS measurements, Dr. Yu-Fai Lam for his help with NMR, Dr. Lourdes

Salamanca-Riba for her help with TEM and EDS characterization, and Mr. Timothy Zhang for his help with equipment in the microanalysis center.

There are students from various research groups in the university who have been kind enough to allow me to use equipment in their laboratories. These included Dr. Robert Walker and students in his group, including Okan Esenturk and Michael Pomfret. Dr. Peter Kofinas and students in his group, including Arthur von Cresce, Ayan Ghosh, and Joshua Silverstein.

I wish to thank all of the members of the radiation and polymer science group. There are several whom I would like to thank especially for the help they have given me with various aspects of the laboratory work involved, including Jung-Chul An, Mahnaz Chaychian, Joon-Hyuk Yang, and Ali Mohamed.

I would also like to thank the Department of Energy for the financial support which made this project possible.

TABLE OF CONTENTS

LIST OF FIGURES

LIST OF TABLES

1. Theoretical Background

The purpose of this chapter is to give an introduction to the basic theoretical background information that is relevant to the work presented in this dissertation. An overview of the major theoretical definitions and principles related to the interaction of ionizing radiation with matter will be provided in this chapter. The emphasis of this section of the chapter will be on the chemical effects of ionizing radiation induced in materials. An introduction to polymer chemistry will then be provided, with additional explanation of the kinetics of polymerization reactions initiated by ionizing radiation. Finally, a brief description of the major properties associated with magnetic materials will be described.

1.1 Interaction of Ionizing Radiation with Matter

Ionizing radiation consists of radiation with sufficient energy to ionize atoms or molecules in the material through which it passes, and usually involves energies in the 10 keV to 100 MeV range. This includes electromagnetic radiation with wavelengths below 10 nm (x-rays, γ-rays) and atomic or subatomic particles (electrons, protons, neutrons, positrons, alphas, mesons, heavy ions) [1]. Both types of radiation may originate from either radioactive nuclides or particle accelerators. In this thesis, only gamma radiation and high energy electrons are used.

1.1.1 Electron Radiation

Electrons tend to interact with matter and lose energy in three major ways: Coulomb interactions, bremsstrahlung emission, and Čerenkov radiation emission [1]. Coulomb interactions with electrons and nuclei in the medium through which the electrons travel are the predominant type of interaction for fast electrons at energy of 7 MeV. (The size of the nucleus in comparison with that of the entire atom is so small that the number of nuclear collisions is relatively small.) These interactions include what are known as elastic and inelastic scattering. Elastic scattering involves the deflection of the electrons by the Coulomb potential of the nuclei of atoms within the material through which they are traveling, without leading to any loss of energy by those electrons. Inelastic scattering includes interactions which result in a loss of kinetic energy by the electrons, and is the process whereby excitation and ionization of the material under irradiation is induced. This is the most significant type of interaction of fast electrons from the radiation chemistry perspective in the work reported in this dissertation. Excitation involves the promotion of a bound electron to a higher energy orbital - this electron eventually returns to its ground state and may emit a photon. Ionization involves the ejection of an electron from the atom which then becomes a positive ion. The ejected electron may ionize other atoms or undergo some other type of interaction which causes it to lose its energy and stop. The positive ion eventually recombines with an electron to become neutral.

The energy loss of an electron as a function of the distance traveled through a material is described by what is known as the stopping power [1], dT/dx, (in units of MeV m^{-1}):

$$\frac{dE}{dx} = 4\pi r_0^2 \frac{mc^2}{\beta^2} NZ \left\{ \ln\left(\frac{\beta\gamma\sqrt{\gamma - 1}}{I} mc^2 \right) + \frac{1}{2\gamma^2} \left(\frac{(\gamma - 1)^2}{8} + 1 - (\gamma^2 + 2\gamma - 1)\ln 2 \right) \right\} \quad (1)$$

where $r_0 = 2.818 \times 10^{-15}$ m is the classical electron radius, $mc^2 = 0.511$ MeV is the rest mass energy of the electron, $\beta = v/c$ is the ratio of the speed of the electron to the speed of light ($c = 3 \times 10^8$ m s^{-1}), $N = \rho(N_A/A)$ is the number of atoms per m^3 of material through which the electron is traveling (ρ is the density (g cm^{-3}), $N_A = 6.02 \times 10^{23}$ atoms mol^{-1} is Avogadro's number, A is the atomic mass, Z is the atomic number, and $\gamma = 1/(\sqrt{(1 - \beta^2)})$.

Bremsstrahlung is a type of secondary electromagnetic radiation produced when accelerated charged particles (primary radiation) are deflected by other charged particles, such as the electrons or protons in a material [1]. Fast electrons typically undergo deceleration in response to Coulomb interactions with a material, thereby losing some of their kinetic energy in the form of Bremsstrahlung radiation.

Čerenkov radiation is a type of visible electromagnetic radiation emitted when the electron travels through a medium at a velocity greater than the speed of light in that medium [1]. The passage of a charged particle through a medium generates disruption in the local electromagnetic fields contained within that medium. This results in the displacement and polarization of bound electrons in the medium by the electromagnetic field of the passing charged particle. After the charged particle has finished passing through the medium, the electrons in the materials restore equilibrium by emitting

photons. If the velocity of these electrons is greater than the speed of light in the medium, then they interfere constructively with one another, thereby producing Čerenkov radiation.

An electron traveling through a medium undergoes a series of interactions with the atoms in the material and loses its energy until it eventually stops. The distance traveled until stopping is known as the CSDA (continuous slowing down approximation) range:

$$R = \int_0^T \left(\frac{-dx}{dT} \right)^{-1} dT \qquad (2)$$

where dT/dx is the stopping power, T is the energy of the electron deposited in the medium, and x is the distance traveled by the electron [2]. The range depends on the initial energy of the electron and the material through which it is traveling. The depth of penetration of 7 MeV electrons in water is approximately 3.6 g cm^{-2}.

1.1.2 Gamma Radiation

The ^{60}Co radionuclide undergoes nuclear decay which leads to the release of an equal number of γ-photons of 1.33 and 1.17 MeV energies. γ-rays, like all photons, are uncharged and possess no mass or charge. Figure 1.1 shows the three types of phenomena that take place as they interact with matter: the photoelectric effect, the Compton effect, and pair production [3].

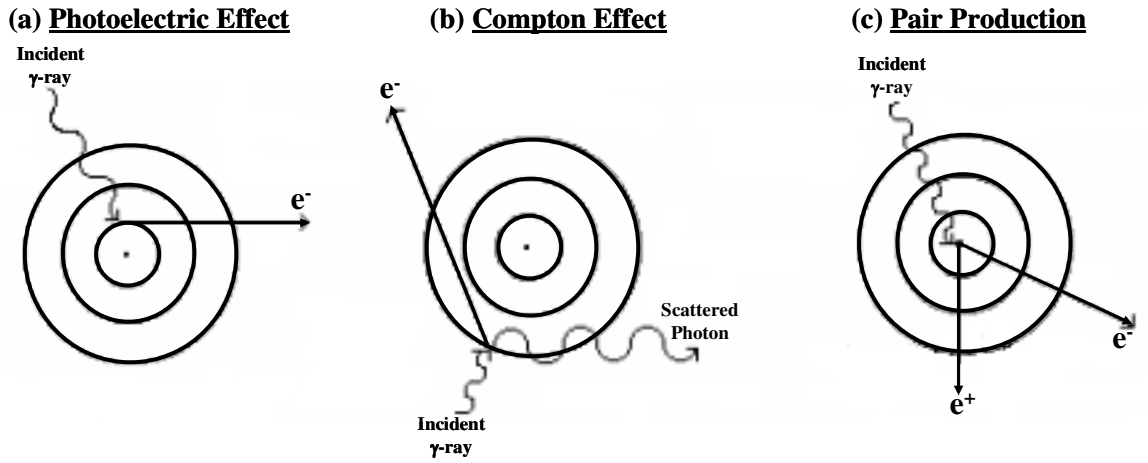

Figure 1.1. Interaction mechanisms of ^{60}Co γ-photons with matter: (a) photoelectric effect, (b) Compton effect, (c) pair production.

The photoelectric effect is an interaction that takes place between a photon and a bound electron in a material, and predominates when the photon energy is below 0.2 MeV. It involves transfer of all of the photon's energy to the electron such that the electron is ejected from the material (this type of electron is known as a photoelectron), while the photon disappears:

$$T = E_\gamma - B_e \tag{3}$$

where T is the kinetic energy of the photoelectron, E_γ is the energy of the incident photon, and B_e is the binding energy of the electron.

The Compton effect, the predominant interaction mechanism for photon energies of 0.2 - 10 MeV, takes place when a photon transfers a fraction of its energy to a freed electron, causing both of their energies and directions to change:

$$T = E_{\gamma} - E_{\gamma'} \tag{4}$$

where T is the kinetic energy of the scattered electron and $E_{\gamma'}$ is the kinetic energy of the scattered photon.

Pair production is an interaction between a photon and a nucleus in which an electron-positron pair is produced, while the photon disappears:

$$T_{e-} + T_{e+} = E_{\gamma} - (mc^2)_{e-} - (mc^2)_{e+} \tag{5}$$

where T_{e-} and T_{e+} are the kinetic energies of the electron and positron respectively, and $(mc^2)_{e-}$ and $(mc^2)_{e+}$ are the rest mass energies of the electron and positron, respectively. This type of interaction makes a negligible contribution to the energy loss interactions of ^{60}Co photons, since their average energy (1.25 MeV) is only slightly greater than the threshold energy required for pair production ($2mc^2$ = 1.02 MeV, where m is the rest mass of the electron and c is the speed of light).

1.1.3 Track Structure

The passage of ionizing radiation through a material generates ions and excited species that are concentrated along the path that the radiation travels. Figure 1.2 shows a schematic of the distribution of excited and ionized species in the track of a fast electron [4]. Energy is dissipated during this process in a series of discrete steps [3]. The isolated regions along the path where radiation energy is deposited are known as spurs, and

consist primarily of transient excited species. If these excited clusters are sufficiently close to one another, they may coalesce to form a columnar track.

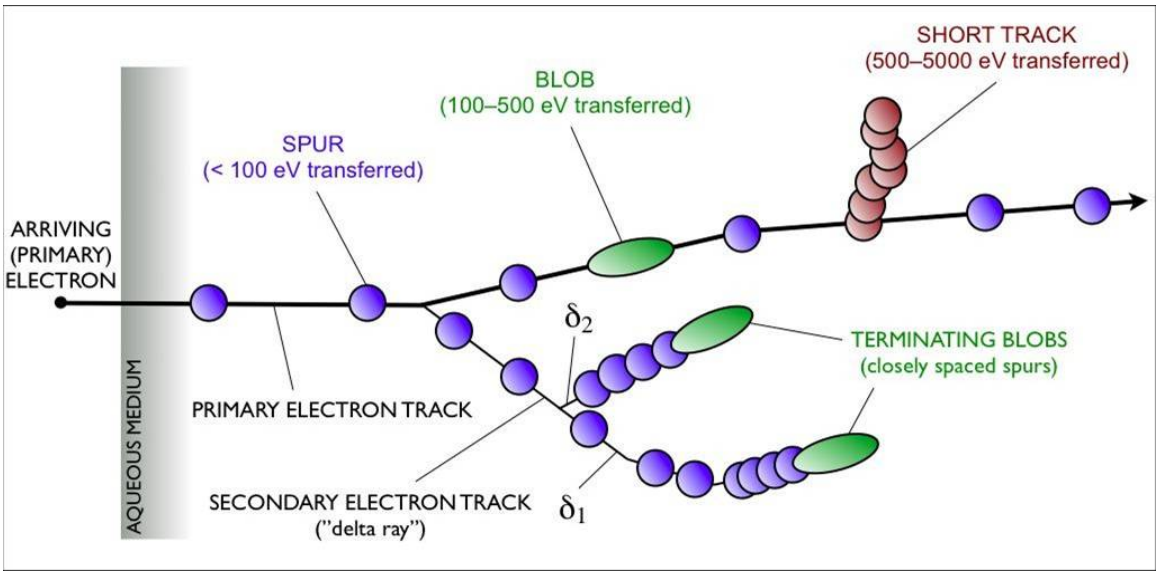

Figure 1.2. Distribution of excited and ionized species in the track of a fast electron [4].

The type of track structure which results depends on the energy of the ionizing radiation and type of absorbing material. For example, secondary electrons with energies of 100 eV will produce a relatively small region (~2 nm diameter) of ionization and/or excitation in water. However, secondary electrons with energies close to 10 keV contain sufficient energy to branch off from the primary track and form a new path; these are known as δ-electrons.

If the ion pairs produced in a material by ionizing radiation are separated by a distance smaller than the Onsager escape distance (distance at which the kinetic energy of the electron is comparable to its potential energy in the Coulomb field of its parent ion) [5], then they recombine within the spur. These are known as geminate ions, and they do

not participate in chemical reactions. However, if the ion pairs produced are separated by a distance greater than the Onsager escape distance, then they may diffuse out of the spur. These are known as free ions, and they may initiate a polymerization reaction or participate in other radiation chemical events (e.g., capture electrons, transform into free radicals, disproportionate, etc...).

1.1.4 Radiation Chemical Yield (G-value)

The amount of product generated per amount of ionizing radiation energy absorbed by a material is described by the radiation chemical yield (G-value), the SI unit of which is mol J^{-1}. It may also be described as the number of product molecules formed per 100 eV of radiation energy absorbed:

$$G = \frac{M}{N} \times \frac{100}{W} \tag{6}$$

where M is the number of molecules consumed, N is the number of ion pairs formed, and W is the mean energy required to produce an ion pair. One molecule per 100 eV is equal to 0.1036 μmol J^{-1} [6]. The G-values of the various transient species generated by ionizing radiation are significant for the work presented in this dissertation, since most of the work is focused on investigating the chemical effects of radiation on materials.

1.1.5 Absorbed Dose

The absorbed dose is the ionizing radiation energy deposited per unit mass of an absorbing material. The SI unit of absorbed dose is the gray (Gy), which is equal to one J kg^{-1}:

$$Absorbed\ Dose\ (Gy) = \frac{J}{kg} \tag{7}$$

The quantitative determination of the dose absorbed by a particular material is known as dosimetry. The relationship between the radiation chemical yield and the absorbed dose is given by:

$$G(product) = (9.648 \times 10^{6}) \times \frac{Radiation\ Chemical\ Yield}{Absorbed\ Dose} \tag{8}$$

where *G(product)* is the G-value of a particular product species in molecules per 100 eV, radiation chemical yield is in units of mol kg^{-1}, and absorbed dose is in units of Gy.

1.1.6 Time Scale of Radiation-Induced Phenomena

Figure 1.3 shows a time scale of ionizing radiation-induced phenomena in materials [7]. The first major events involve excitation and ionization, which take place during the first 10^{-15} - 10^{-6} seconds of irradiation. These species eventually transform into free radicals which, although highly reactive and short-lived, are the basis for most of the chemical reactions investigated in this dissertation.

Radiation-Induced Phenomena		**Time (s)**
Excitation	$M \rightsquigarrow M^*$	10^{-15}
- superexcited state, Rydberg state		
- singlet		
- triplet		
Ionization	$M \rightsquigarrow M^{\bullet+} + e^-$	
	$M^* \rightsquigarrow M^{\bullet+} + e^-$	
Charge separation, electron thermalization		10^{-14}
Cation fragmentation	$(A\bullet B)^{\bullet+} \rightarrow A^+ + B^\bullet$	10^{-13}
Excited energy transfer	$M^* + N \rightarrow M + N^*$	10^{-12}
Excited energy relaxation	$M^* \rightarrow M + h\nu$	
- intersystem crosslinking		
- internal conversion		
Geminate electron recombination	$M^{\bullet+} + e^- \rightarrow M^*$	10^{-11}
Electron scavenging		10^{-10}
- by ground-state molecule	$M + e^- \rightarrow M^-$	
- by radical ion	$M^{\bullet+} + e^- \rightarrow M^*$	
Positive ion scavenging		10^{-9}
Ion-molecule reactions		
Neutral radical reactions		
Products		

Figure 1.3. Time scale of ionizing radiation-induced phenomena [8].

1.2 Polymers

A polymer is a molecule containing a long sequence of repeating chemical units which are linked together by covalent bonds [9]. The subunits which are bonded together to form a polymer are low molecular weight compounds known as monomers. Polymeric materials may be classified in several different ways, including categories based on skeletal structure, repeat unit distribution, and synthesis reaction.

The skeletal structure of a polymer may be linear or non-linear. Linear polymers consist of a single chain (backbone) containing two ends. There are two major types of non-linear polymers: branched and network polymers. Branched polymers contain side chains (branches) that are attached to the backbone at positions known as junction points.

Network (crosslinked) polymers contain junction points which connect all the chains in a system together.

There are two major types of repeat unit structure found in polymers: homopolymers and copolymers [10]. Homopolymers contain a single type of repeat unit, whereas copolymers contain more than one type of repeat unit. The distribution of the repeat units in a copolymer leads to several different subcategories of these materials: statistical, alternating, block, and graft copolymers. Statistical copolymers are composed of a repeat unit sequence that obeys statistical laws (e.g., repeat unit sequence obeys Markovian statistics) [11]. Alternating copolymers are composed of two different types of repeat units which are positioned in alternating sequence along the chain. Block copolymers contain repeat units arranged in long sequences (blocks) of the same type. Graft copolymers are a type of branched copolymer containing branches which are different in chemical structure than the main chain.

Polymerization is a chemical reaction in which polymer is formed by linking monomers together in a chain of many repeating units. The various types of polymerization reactions may be classified into two major subcategories with regards to the underlying mechanisms on which they are based: step and chain reactions. Step polymerization consists of successive reactions between the functional groups of pairs of molecules [12]. Chain polymerization involves the sequential addition of repeat units to the end of a growing chain containing what is known as an active site, which may be a free radical, cation, or anion. This type of polymerization may be further subdivided into two categories, depending on the type of active site involved: free radical and ionic polymerization. The kinetics and mechanism of chain reactions, particularly those

involving free radicals, will be explained in the most detail in the following overview, since this is the type of polymerization studied in this dissertation.

1.2.1 Free Radical Chain Polymerization

Free radicals are species containing an unpaired electron. Free radical chain polymerization reactions involve growth of a polymer chain through the addition of monomer to a free radical reactive site at the end of the chain. It is the most widely employed type of chain polymerization used on the industrial scale [13]. There are five major types of reactions which take place during free radical polymerization: initiation, propagation, termination, chain transfer, and inhibition [11].

Initiation involves the formation of an active site, and usually takes place through the dissociation of an initiator molecule into a reactive species such as a free radical:

$$I \xrightarrow{k_{di}} 2R^{\bullet} \tag{9}$$

where I is the initiator, k_d is the rate coefficient for dissociation, and $R^{\bullet}$ is the initiator radical. A monomer then adds to this initiator radical to generate an initiator-monomer radical:

$$R^{\bullet} + M \xrightarrow{k_i} RM_1^{\bullet} \tag{10}$$

where M is a monomer, k_i is the rate coefficient for initiation, and $RM_1^{\bullet}$ is an initiator-monomer radical. The formation of the initiator radical is usually the slower step in the

initiation process, so the rate of initiation for a free radical polymerization reaction may be described as follows:

$$R_i = \frac{d[R^\bullet]}{dt} = 2k_d[I] \tag{11}$$

where R_i is the rate of initiation, $d[R^\bullet]/dt$ is the change in initiating radical concentration as a function of time, *[I]* is the concentration of initiator, and *2* refers to the stoichiometry shown in equation (9), in which two radicals $(R^\bullet)$ are generated per dissociation of initiator molecule.

Propagation is the repeated addition of new monomeric repeat units to the end of the growing chain:

$$M_i^\bullet + M \xrightarrow{k_p} M_{i+1}^\bullet \tag{12}$$

where $M_i^\bullet$ and $M_{i+1}^\bullet$ are growing chain radicals containing *i* and *(i+1)* repeat units respectively, and k_p is the rate coefficient of propagation. Each time a monomer is added to a chain end, the active site is transferred to this new unit, and the addition reaction is then repeated. The rate of propagation is described as follows:

$$\frac{-d[M]}{dt} = k_p[M][M^\bullet] \tag{13}$$

where *-d[M]/dt* is the rate of consumption of monomer as a function of time, and *[M]* and *[M•]* are the concentrations of monomer and chain radicals, respectively.

Termination of a polymerization reaction occurs when the active site undergoes a reaction which leads to the end of propagation and results in the formation of a 'dead' (unreactive) polymer molecule. There are two major ways in which termination of a free radical polymerization reaction may take place. One is known as combination termination, and it involves the coupling of two growing chains to form a single polymer molecule:

$$M_i^{\bullet} + M_j^{\bullet} \xrightarrow{k_{tc}} M_{i+j} \tag{14}$$

where $M_i^{\bullet}$ and $M_j^{\bullet}$ are growing chain radicals with *i* and *j* repeat units, respectively, k_{tc} is the rate coefficient for combination termination, and M_{i+j} is the final polymer molecule formed containing *(i + j)* repeat units. The other type of termination mechanism takes place through a disproportionation reaction, and results in the formation of two separate polymer molecules:

$$M_i^{\bullet} + M_j^{\bullet} \xrightarrow{k_{td}} M_i + M_j \tag{15}$$

where k_{td} is the rate coefficient for disproportionation termination. The overall rate of termination is described by:

$$R_t = \frac{-d[M^\bullet]}{dt} = 2k_{tc}[M^\bullet][M^\bullet] + 2k_{td}[M^\bullet][M^\bullet] = 2k_t[M^\bullet]^2 \qquad (16)$$

where R_t is the rate of termination, $-d[M^\bullet]/dt$ is the rate of consumption of chain radicals, $[M^\bullet]$ is the concentration of chain radicals, and the overall rate coefficient for termination is $k_t = k_{tc} + k_{td}$.

Chain transfer reactions are other reactions besides combination and disproportionation which result in the termination of chain growth:

$$M_i^\bullet + T - A \xrightarrow{k_{tr}} M_i - T + A^\bullet \qquad (17)$$

where T - A is a molecule in the system, k_{tr} is the rate coefficient for chain transfer, M_i - T is a 'dead' polymer molecule, and $A^\bullet$ is a radical that may then initiate the growth of a new chain by reacting with monomer:

$$A^\bullet + M \rightarrow AM_1^\bullet \qquad (18)$$

Any molecular species present may act as a source of chain transfer, including monomer, polymer, solvent, or initiator [14]. Chain transfer to solvent is the most common type of chain transfer, and leads to premature termination which results in a reduction of the degree of polymerization [15]. Most of the polymerization reactions studied in the work presented in this dissertation were conducted in the absence of solvent, and the effect of chain transfer was therefore not investigated.

Inhibition of a polymerization reaction occurs when a compound reacts with radicals to generate species which are not capable of further polymerization. A polymerizable system which contains inhibitors will undergo an induction period towards the beginning of the reaction during which time the inhibitor is consumed. After the induction period has been completed, the polymerization proceeds at the same rate that it would in the absence of inhibitor.

1.2.1.1 Steady-State Kinetics

During the early stages of a free radical polymerization reaction, the rate of radical formation is faster than the rate of radical consumption ($R_i >> R_t$). The concentration of radicals increases rapidly as the reaction proceeds, and eventually the system attains what is known as a steady-state condition, in which there is no net change in radical concentration. Under these conditions, the rate of radical formation and consumption are comparable ($R_i = R_t$):

$$R_i = 2k_t[M^\bullet]^2 \tag{19}$$

The steady-state concentration of radical species is described by:

$$[M^\bullet] = \left(\frac{R_i}{2k_t}\right)^{1/2} \tag{20}$$

This expression for radical concentration may be substituted into equation (13) to describe the rate of polymerization under steady-state conditions:

$$\frac{-d[M]}{dt} = k_p[M][M^\bullet] = k_p[M]\left(\frac{R_i}{2k_t}\right)^{1/2} = \left(\frac{k_p}{2^{1/2}k_t^{1/2}}\right)R_i^{1/2}[M] \qquad (21)$$

1.2.1.2 Non-Steady-State Kinetics

The ability to experimentally measure the rate of initiation (R_i), rate of propagation (R_p) and monomer concentration ($[M]$) under steady-state conditions enables the determination of the rate coefficient of initiation (k_i) and the ratio of the rate coefficients of propagation and termination ($k_p/k_t^{1/2}$) from equation (21). In order to determine the individual propagation and termination rate coefficients, the average lifetime of an active site must be obtained:

$$\tau = \frac{[M^\bullet]}{2k_t[M^\bullet]^2} = \frac{1}{2k_t[M^\bullet]} = \frac{k_p[M]}{2k_tR_p} \qquad (22)$$

By dividing the concentration of active centers by their rate of consumption, the average time which passes between the formation and termination of an active center may be determined. An accurate measurement of the concentration of propagating radicals is necessary in order to evaluate equation (22). Electron paramagnetic resonance (EPR) is the most commonly used technique for such a task, but sensitivity of this measurement is

often insufficient to accurately determine steady-state concentrations of propagating radicals.

An alternative approach to the determination of individual rate coefficients for propagation and termination involves the use of experimental measurements under non-steady-state conditions through a technique known as the rotating sector method [16]. It involves the exposure of a polymerizable system to alternating 'light' and 'dark' periods of known length in time. The non-steady-state kinetics on which this method is based may be produced by a pulsed electron beam. When a sample is exposed to electron irradiation (this period in time is known as a "light period"), radicals are abruptly generated. When the irradiation is stopped (this period in time is known as a "dark period"), the radical concentration decays as the radicals combine and terminate each other.

The rate of polymerization may be studied as a function of the cycle time of alternating light and dark periods which is applied to the system. The ratio of the length of the dark and light periods is described by:

$$r = \frac{t'}{t} \tag{23}$$

where t' is length of the dark period and t is the length of the light period. If the cycle time is much larger than the average lifetime of an active site under steady-state conditions ($r >> \tau$), then the rate of polymerization during the light period will be equal to that under steady state conditions ($R_p = (R_p)_s$), whereas it will be equal to zero during the dark period ($R_p = 0$). This kinetic pattern is displayed under these conditions because

the system has a relatively long period of time to either reach steady-state (during light period) or decay to zero (during dark period).

If the cycle time is short compared to the average lifetime of an active site under steady-state conditions ($r < \tau$), then the system does not have sufficient time during the light period to reach steady-state, and the radical decay during the dark period is incomplete. If the cycle time is much shorter than the average lifetime of an active site ($r << \tau$), then the radical concentration may be maintained at an approximately constant level, which is also comparable to that which would be induced by continuous irradiation. The ratio of the average rate of polymerization at infinite sector rotation to the rate of polymerization under steady-state conditions is described by:

$$\frac{(\bar{R}_p)_\infty}{(R_p)_s} = \frac{1}{(1+r)^{1/2}} \tag{24}$$

When the cycle time is short ($r << \tau$), the concentration of radicals changes from $[M^\bullet]_1$ at the end of each light period to $[M^\bullet]_2$ at the end of each dark period. The average radical concentration over several light/dark cycles is given by:

$$[\overline{M}^\bullet](t+rt) = \int_0^t [M^\bullet]dt + \int_0^{t'} [M^\bullet]dt' \tag{25}$$

where the first integral, which corresponds to the light period, is described by:

$$\tanh^{-1}\left(\frac{[M^{\bullet}]_1}{[M^{\bullet}]_s}\right) - \tanh^{-1}\left(\frac{[M^{\bullet}]_2}{[M^{\bullet}]_s}\right) = \frac{t}{\tau_s} \tag{26}$$

and the second integral, which corresponds to the dark period, is described by:

$$\frac{[M^{\bullet}]_s}{[M^{\bullet}]_2} - \frac{[M^{\bullet}]_s}{[M^{\bullet}]_1} = \frac{rt}{\tau_s} \tag{27}$$

The integrals in equation (25) may be evaluated to give:

$$\frac{[\overline{M}^{\bullet}]}{[M^{\bullet}]_s} = \frac{1}{r+1}\left[1 + \frac{\tau_s}{t}\ln\left(\frac{[M^{\bullet}]_1/[M^{\bullet}]_2 + [M^{\bullet}]_1/[M^{\bullet}]_s}{1 + [M^{\bullet}]_1/[M^{\bullet}]_s}\right)\right] \tag{28}$$

This expression describes the relationship between $[\overline{M}^{\bullet}]/[M^{\bullet}]_s$ and t/τ_s at a fixed value of r. When τ_s has been experimentally determined, the individual propagation and termination rate coefficients may be calculated through combination of their ratios described by equations (21) and (22).

1.2.2 Ionizing Radiation-Induced Polymerization

Ionizing radiation-induced polymerization is based on the addition mechanism which characterizes chain polymerization reactions, and is usually applied to vinyl-type monomeric compounds with the general structure of $CH_2{=}CR_1R_2$, where R_1 and R_2 are hydrocarbon groups. The primary transient species generated upon exposure of polymerizable substances to ionizing radiation include solvated electrons, radical cations,

radical anions, and neutral free radicals. The ability of ionizing radiation to generate radicals and ions enables it to initiate both free radical and ionic polymerization. However, the type of polymerization mechanism which predominates depends on the yield of each type of transient species temperature, dose rate, and the purity of the monomer.

The free radical mechanism has been found to be the predominant means of polymerization of vinyl-type compounds initiated by ionizing radiation[11]. Ionic polymerization mechanisms have been observed only under certain reaction conditions, including low temperatures and in systems that have been extensively purified. An example of this is the ionizing radiation-induced ionic polymerization of styrene, which has been demonstrated to be enhanced at low temperatures (-78 ºC) and under conditions in which water has been carefully removed from the system [5]. This is due to the fact that water acts as a cation scavenger and thereby suppresses the ionic mechanism of polymerization.

Most acrylate polymerization reactions induced by ionizing radiation have been observed to take place through a free radical mechanism. An expression for the rate of initiation that is more specific to ionizing radiation-induced reactions is given by:

$$R_i = G\rho \dot{D} \tag{29}$$

where G is the radiation yield of acrylate radicals, ρ is the density of the monomer (g cm^{-3}), and $\dot{D}$ is the dose rate (Gy s^{-1}) [3].

Equations (20) and (29) may be combined to derive an expression for the rate of polymerization reactions initiated by ionizing radiation as follows:

$$R_p = k_p \left(\frac{G\rho \dot{D}}{2k_t} \right)^{1/2} [M] \tag{30}$$

Most studies of acrylate polymerization reactions report the bimolecular combination of propagating chains as the predominant termination mechanism [17]. The rate of this step of the reaction is generally agreed to be diffusion-controlled with k_t decreasing as the degree of polymerization increases and produces chains which are less mobile.

The average lifetime of a propagating chain radical in an ionizing radiation-induced polymerization reaction is given by:

$$\tau = \frac{1}{(G\rho \dot{D} 2k_t)^{1/2}} \tag{31}$$

This expression applies under steady-state conditions with a bimolecular termination mechanism.

Equation (28) may be used to derive an alternative expression for the rate of polymerization:

$$R_p = \frac{\overline{R}_p}{\left([\overline{M}^{\bullet}] \Big/ [M^{\bullet}]_s \right)} = k_p \left(\frac{G\rho \dot{D}}{2k_t} \right)^{1/2} [M] \tag{32}$$

This equation may then be used to describe the radical concentrations at the end of each light and dark period as follows:

$$\frac{[M^{\bullet}]_s}{[M^{\bullet}]_1} = \frac{-0.5rt}{\tau_s} + 0.5 \left\{ \left(\frac{rt}{\tau_s} \right)^2 + 4 \left[1 + (e^{2t/\tau_s}) \times \frac{\left(rt \Big/ \tau_s \right)}{(e^{2t/\tau_s})} \right] \right\}^{1/2} \tag{33}$$

$$\frac{[M^{\bullet}]_s}{[M^{\bullet}]_2} = \frac{-0.5rt}{\tau_s} + 0.5 \left\{ \left(\frac{rt}{\tau_s} \right)^2 + 4 \left[1 + (e^{2t/\tau_s}) \times \frac{\left(rt \Big/ \tau_s \right)}{(e^{2t/\tau_s})} \right] \right\}^{1/2} \tag{34}$$

After evaluation of equations (33) and (34), R_p can be determined from equation (32) for a given value of $2k_tG$.

1.2.2.1 Effect of Dose Rate

In general, for radiation-induced bulk radical polymerization at relatively low extents of conversion (≤ 10 mol%), the rate of polymerization has been demonstrated to be proportional to (dose rate)$^{1/2}$, as is consisted with equation (30). This relationship is based on a steady-state assumption in which the rates of radical formation and consumption are equivalent:

$$c\dot{D} = k_t\left[M^{\bullet}\right]^2 \tag{35}$$

$$\left[M^{\bullet}\right] = \left(\frac{c\dot{D}}{k_t}\right)^{\frac{1}{2}} \tag{36}$$

where c is a constant related to the G-value of a particular species and its density. The dependence of the rate of polymerization on the dose rate is thus as follows:

$$\frac{d\left[P\right]}{dt} = k_p[M][M^{\bullet}] = k_p\left(\frac{c}{k_t}\right)^{\frac{1}{2}}[M](\dot{D})^{\frac{1}{2}} \tag{37}$$

where $d[P]/dt$ is the rate of polymer formation as a function of time. The molecular weight of the polymer which forms has been demonstrated to be proportional to (dose rate)$^{-1/2}$, based on the following relationship between the radiation chemical yield of polymer and dose rate:

$$G(P) = \frac{d[P]}{dE} = \frac{d[P]}{dt} \times \frac{dt}{dE} = k_p\left(\frac{c}{k_t}\right)^{\frac{1}{2}}[M](\dot{D})^{\frac{-1}{2}} \tag{38}$$

where $d[P]/dE$ is the rate of polymer formation as a function of energy absorbed and dE/dt is the rate of energy absorption (or absorbed dose rate).

At any particular moment during the irradiation of the sample, the radicals produced will undergo primarily either propagation (addition of monomer) or termination (combination with another radical):

$$\text{Propagation: } M_n^{\bullet} + M \xrightarrow{k_p} M_{n+1}^{\bullet} \tag{39}$$

$$\text{Termination: } M_n^{\bullet} + M_m^{\bullet} \xrightarrow{k_t} M_{n+m} \tag{40}$$

The relative probability of either of these reactions taking place will depend on the concentration of free radicals in the system, which will in turn depend on experimental parameters such as the dose rate.

1.2.2.2 Inhibition

Low levels (ppm) of inhibitors are added to many monomeric materials to prevent polymerization from taking place during transportation and storage. The most commonly used inhibitors for acrylate monomers include hydroquinone (HQ) and hydroquinone monomethyl ether (MEHQ) [18]. Compounds which are capable of initiating free radical polymerization are difficult to eliminate completely from acrylate systems. For example, side reactions which often occur during the manufacture of acrylate monomers may result in the production of hydroperoxides. These substances decompose very easily when exposed to heat or ultraviolet light to form hydroxyl and alkoxy radicals which may then attack the unsaturated sites of an acrylate monomer and thereby initiate polymerization. However, in the presence of HQ or MEHQ, an alkoxy radical may abstract hydrogen

from a hydroxyl group of a quinone molecule to generate a quinone radical. This quinone radical is relatively stable due to the delocalization of electron charge provided by its aromatic structure. It is not capable of initiating polymerization, but it may combine with another radical to form a less reactive compound and terminate propagation reactions which may have otherwise occurred.

Oxygen has been found to considerably inhibit the polymerization of acrylate monomers. Acrylate radicals rapidly react with oxygen to form peroxy radicals, which contain very low reactivity.

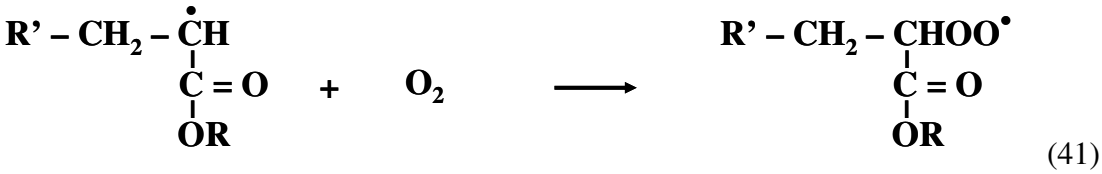

(41)

The synthesis of polyacrylates in the presence of oxygen thus leads to changes in the final polymer composition and reductions in the rate of reaction with monomer and the degree of polymerization. Oxygen has therefore been excluded from all of the reactions studied in the work presented in this dissertation.

1.2.2.3 Autoacceleration

Under conditions of high initial concentration of monomer, a sudden increase in the rate of polymerization has been observed to take place known as autoacceleration. This phenomenon originates from the increased viscosity of a reaction medium as polymer molecules are formed. It becomes more difficult for growing chain radicals to diffuse and combine with one another to terminate the reaction. The rates of initiation

and propagation are not as dramatically affected by increases in viscosity, since they are determined by the mobility of monomer molecules, which is not as significantly reduced even within a viscous medium.

In general, free radical polymerization reactions of acrylate esters are highly exothermic. When autoacceleration occurs, the viscosity of the system makes it difficult for the heat generated by the reaction to be dissipated, thereby causing the reaction to become even farther out of control. In order to prevent this from taking place, lower concentrations of monomer may be used or the reaction may be limited to low extents of conversion. Dilute solutions of monomer usually lead to a greater amount of chain transfer reactions. The main focus of the polymerization experiments performed in this work was on the kinetics of acrylate systems in the absence of solvent, so most measurements were performed on samples which had not been irradiated to complete conversion of monomer into polymer.

1.2.3 Copolymerization

One of the ways of broadening the range of properties available from a particular polymer is by copolymerizing it with another type of monomer. This is commonly done with acrylate ester monomers, since they often polymerize easily with one another. It is therefore of great research interest to study the kinetics of their copolymerization reactions.

The main feature of a copolymerization reaction that distinguishes it from homopolymerization is the additional types of propagation reactions which may take place. There are four types of propagation reactions possible for a polymerization

reaction containing two different types of monomers. In terms of 2-ethylhexyl acrylate and acrylic acid, they are as follows:

2-EHA homopropagation: $\sim\sim\sim\ EHA^{\bullet} + EHA \xrightarrow{k_{11}} \sim\sim\sim\ EHA - EHA^{\bullet}$ (42)

2-EHA coss-propagation: $\sim\sim\sim\ EHA^{\bullet} + AA \xrightarrow{k_{12}} \sim\sim\sim\ EHA - AA^{\bullet}$ (43)

AA homopropagation: $\sim\sim\sim\ AA^{\bullet} + AA \xrightarrow{k_{22}} \sim\sim\sim\ AA - AA^{\bullet}$ (44)

AA cross-propagation: $\sim\sim\sim\ AA^{\bullet} + EHA \xrightarrow{k_{21}} \sim\sim\sim\ AA - EHA^{\bullet}$ (45)

where ~~~EHA$^{\bullet}$ and ~~~AA$^{\bullet}$ are propagating radical chains with 2-EHA and AA radical ends. If the 2-EHA and AA monomeric species being added to the chain during propagation are known as monomers 1 and 2 respectively, then rate coefficients for each type of propagation reaction may be defined. These rate coefficients include k_{11} for 2-EHA homopropagation, k_{12} for 2-EHA cross-propagation, k_{22} for AA homopropagation, and k_{21} for AA cross-propagation. The monomer which is more reactive will be more easily incorporated into the copolymer. The relative preference for addition of each type of repeat unit to a growing chain during a copolymerization reaction is described by what is known as the monomer reactivity ratios:

$$r_1 = \frac{k_{11}}{k_{12}} \quad (46)$$

$$r_2 = \frac{k_{22}}{k_{21}} \tag{47}$$

where r_1 and r_2 are the reactivity ratios for monomers 1 and 2, respectively. These ratios may be estimated theoretically by accounting for the structural effects on the reactivity of a compound by what is known as the Q-e scheme [11]. Q is a parameter used to account for resonance effects (2-EHA: $Q_1 = 0.37$, AA: $Q_2 = 0.83$), and e is a parameter used to account for polarity effects (2-EHA: $e_1 = 0.24$, AA: $e_2 = 0.88$). The reactivity ratios for 2-EHA and AA may be estimated using the Q-e scheme as follows:

$$2-EHA\ monomer: r_1 = \frac{k_{11}}{k_{12}} = \frac{Q_1}{Q_2}\exp\left[-e_1\left(e_1 - e_2\right)\right] = 0.520 \tag{48}$$

$$AA\ monomer: r_2 = \frac{k_{22}}{k_{21}} = \frac{Q_2}{Q_1}\exp\left[-e_2\left(e_2 - e_1\right)\right] = 1.28 \tag{49}$$

According to the Q-e scheme, AA is anticipated to be the more highly reactive compound, since it possesses a higher reactivity ratio.

1.2.3.1 Ionomers

Ionomers are copolymers consisting of a minor component which contains functional groups that are capable of forming ionic interactions. One of the most

commonly employed functional group of this type is the carboxyl group, which is the functional group of carboxylic acids.

The most widely accepted theory of ionomer morphology is the Eisenberg-Hird-Moore (EHM) cluster model [19]. It assumes that there is a region immediately surrounding each ionic cluster in which the chain mobility is reduced, and the mobility then increases with increased distance from the cluster. This region of restricted segmental mobility is considered to be on the order of the persistence length of the polymer, and there is assumed to be a continuous transformation from the rigid, extended structure of the chains closest to the aggregate into a more flexible surrounding chain structure known as the corona. If the ionic content of the system is increased, these areas of restricted mobility begin to overlap with one another to produce continuous regions of restricted segmental mobility. This leads to the formation of a distinct thermal transition associated with their destabilization which is located at a higher temperature than the bulk glass transition.

1.2.4 Polymer Thermodynamics

The work presented in this dissertation on the formation of ionomeric materials is based on polymer thermodynamics, in which microphase separation of the various components of a copolymer is employed as a means of controlling the distribution of the inorganic materials which are incorporated to form a composite. Some basic definitions of major theoretical polymer thermodynamics concepts which are relevant to the work contained in this dissertation are provided below.

The thermodynamics of polymeric materials is an important means of determining under which conditions different types of polymers may become compatible. The change in free energy upon mixing two substances together is given by:

$$\Delta G_m = \Delta H_m - T\Delta S_m \tag{50}$$

where ΔH_m is the enthalpy of mixing, T is the temperature, and ΔS_m is the entropy of mixing. The necessary condition for mixing to take place is a reduction of the free energy of a system (i.e., $\Delta G_m < 0$).

The miscibility two different polymers, one of which contains repeat units of type A while the other of which contains repeat units of type B may be described by what is known as the Flory-Huggins free energy of mixing:

$$\frac{\Delta G_m}{RT} = \frac{\phi_A}{M_A}\ln\phi_A + \frac{\phi_B}{M_B}\ln\phi_B + \phi_A\phi_B\chi \tag{51}$$

where $R =$ 8.31 J k^{-1} mol^{-1} is the ideal gas constant, ϕ_A and ϕ_B, and M_A and M_B are the volume fractions and degrees of polymerization of polymers A and B, respectively. χ is a parameter used to describe the interaction between polymer segments:

$$\chi = \frac{z\Delta\omega_{pp}}{k_B T} \tag{52}$$

where z is the coordination number of a given site (number of nearest neighbors), $\Delta\omega_{pp}$ is an energy parameter associated with the formation of a polymer/polymer segment contact, and $k_B = 1.38 \times 10^{-23}$ J K^{-1} is the Boltzmann constant. The first two terms in equation (51) correspond to the change in entropy of mixing, while the last term corresponds to the change in enthalpy upon mixing two polymers together.

The change in the entropy of mixing two polymers together is small compared to that which would take place upon mixing two compounds of low molecular weight. The chemical linkages between segments of a polymer chain together causes the number of possible arrangements of these segments to be much lower than if they were not bonded to one another. The reduction in entropy which is due to the connectivity of a polymer chain results in most polymers being immiscible with one another.

1.2.4.1 Microphase Separation in Ionomers

One of the most effective means of compatabilizing different types of polymers is to form a copolymer out of two different types of repeat units. Rather than attempting to combine the different properties of homopolymers by physically mixing them together, they can be chemically bonded to one another within the same polymer chain. Different types of repeat units, when chemically connected to one another, are prevented from undergoing full phase separation by the chemical linkages that bond them together. Instead, they undergo what is known as microphase separation. This involves phase separation within localized regions of the system, while the overall phase composition may remain uniform. The morphology which is produced depends on the relative content of each type of repeat unit and their miscibility with one another.

2. Introduction

2.1 Acrylate Ester Polymers

Acrylate ester polymers are a category of materials obtained by the polymerization of monomers derived from acrylic acid, which may be described by a general reaction as follows:

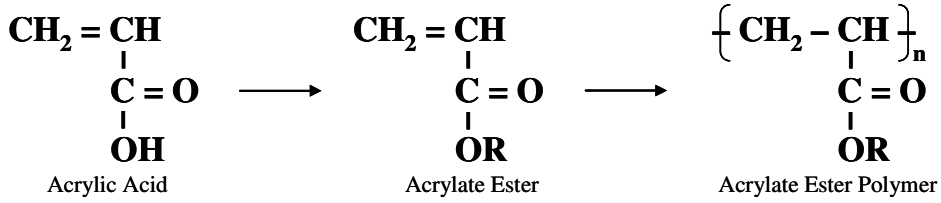

(53)

where n is the number of repeat units in the polymer and R is an organic side group that contributes specific properties to each type of ester (such as hardness flexibility, and gloss level) [20]. Acrylic acid is commonly synthesized through the catalytic oxidation of propylene vapor to form acrolein (CH_2=CHCHO), which is then subsequently oxidized to form the acid. Esterification of acrylic acid is then accomplished through a reaction with alcohol. The polymerization of acrylate esters may be initiated through a variety of methods (chemical, photochemical, radiation), and usually takes place through a free radical mechanism.

2.1.1 Curing of Acrylate Ester Polymers

Curing is a process used to toughen or harden materials through polymerization and/or cross-linking reactions, and is usually initiated by heat, chemical additives, or

radiation. It is employed most commonly for the modification of surfaces, including such materials as coatings (paint, varnish, decorative, laminates), inks, adhesives (pressure-sensistive, construction, and film-to-film laminating adhesives), and sealants [21]. Curing processes usually involve the application of a liquid formulation of ingredients to a substrate, followed by the transformation of the mixture into a solid. Acrylate esters are a class of polymerizable substances that are commonly used for such cured materials applications. They tend to be amorphous, colorless, clear, stable upon aging, and encompass a broad range of properties, from soft, tacky adhesives (such as poly(2-ethylhexyl acrylate)) to hard plastics (such as poly(methyl methacrylate)).

The majority of industrial coatings manufactured up until the early 1970s were "low solids and solvent borne"; i.e., containing 10 – 20 wt% solids and 80 – 90 wt% solvent [21]. This combination of ingredients was used at that time since the solvent and energy used to evaporate it were relatively inexpensive, the use of the more expensive polymer components was minimized, and the product showed excellent application characteristics (flow, leveling) and final properties (gloss, continuity, thinness).

The conventional method of curing acrylate polymer coatings is based on a thermally initiated reaction [21]. The coating mixture employed in this process usually contains polymers, cross-linking agents, catalysts, additives, pigments, fillers, and a solvent. After the reaction mixture has been applied to a substrate and the solvent has been thermally removed, the cross-linking of the polymer takes place. The chemical mechanism which predominates during radiation cross-linking usually involves the abstraction of hydrogen atoms from the backbone to generate polymer radicals which then recombine to form cross-links.

Thermal energy employed for coatings production may function as a means of liquefaction of formulation ingredients as they are applied to a substrate, as a means of evaporative drying, and as a way to initiate a polymerization and/or cross-linking reaction [21]. This method is limited by the fact that it involves an inefficient use of energy and materials. Much of the heat energy applied ends up being absorbed by the substrate, leaving less heat available for curing of the polymer itself. This process also releases large quantities of solvent into the atmosphere as it is evaporated, and is thus a highly polluting technology.

In the effort to reduce the energy consumption and waste materials involved in curing processes, techniques based on electromagnetic radiation have been developed more recently [21]. This has been performed using radiofrequency, microwave, laser, infrared, visible, ultraviolet and ionizing forms of radiation. Electromagnetic radiation is usually employed as a technique to modify the surface of a polymer in order to change such properties as adhesion, wettability, wear, abrasion resistance, and light transmissivity. Radiofrequency techniques of curing are based on the initiation of plasma polymerization (glow discharge) reactions. Microwaves are an alternative means of initiating a thermal cure, through such mechanisms as resistive losses in a conductor or magnetic losses in a magnetic material. Infrared, visible, and ultraviolet curing require the presence of photosensitive molecules to initiate the curing process. These techniques are widely used in the manufacture of photoimaging and photoresist materials, but are generally unable to cure highly pigmented coatings, since the pigment molecules in these systems compete with the photoinitiator molecules for light absorption.

2.1.2 Ionizing Radiation-Induced Polymerization of Acrylate Ester Polymers

The use of ionizing radiation (x-ray, γ-ray, electrons) to initiate acrylate ester polymerization reactions is a well established technique, particularly using electron beam irradiation. It is employed as a method of curing such materials for a wide variety of fields in adhesive, coating, ink and lithographic applications [22]. This method possesses several advantages over the other radiation curing techniques. It requires fewer additives, such as photo-sensitizers and catalysts, which may contaminate the final product and may be difficult to remove. It is also better able to penetrate thicker and opaque materials.

One of the major advantages of using ionizing radiation is that it does not necessitate the use of solvents that would later require removal. This reduces the costs associated with the handling of solvents, including their purchase, storage, evaporation, recovery, and disposal. An alternative to the use of solvents in radiation-cured coatings involves ethylenically unsaturated monomers or oligomers known as 'reactive diluents' [23]. An example of this is bisphenol A (4,4'-dihydroxy-2,2-diphenylpropane), a reactive diluent used in epoxy resins which provides useful application characteristics the way that a solvent does by lowering the viscosity, but unlike a solvent does not evaporate away and instead cross-links to become part of the final cured material. Reactive diluents thus reduce the viscosity of the uncured material as it is applied to a substrate, and they also to promote polymerization and cross-linking upon exposure to radiation. This is a more efficient use of materials since all the ingredients initially included in the uncured mixture remain within the final cured product.

Another advantage of ionizing radiation-induced curing is that it involves relatively lower energy consumption compared to thermal processing methods. The rate

of reaction may be controlled through manipulation of the dose rate, and this approach has been demonstrated to provide more rapid and uniform curing than thermal curing techniques [24]. One of the major operating costs for thermal curing systems is for the power required for ovens used to evaporate away solvents. The ability to cure materials at ambient temperatures along with the elimination of the solvent removal step results in less energy being required to be applied to such systems per amount of coating material ultimately produced. This technology may also be applied to a broader range of substrate materials, including those that are sensitive to heat, such as plastics, paper, and wood.

The use of ionizing radiation for polymerization also possesses several limitations. One of the main drawbacks of ionizing radiation is its lack of selectivity [3]. Unlike most chemical or photoinitiated reactions which may be more easily tailored to react with specific bonds or molecules in a substance, ionizing radiation tends to react somewhat indiscriminately with all bonds or compounds within a material. Another limitation is the fact that the energy of ionizing radiation is often sufficient to induce degradation within materials [25]. Anther limitation is the cost involved with the use of ionizing radiation facilities, which have relatively large power requirements and require shielding [1].

Copolymers of 2-ethylhexyl acrylate (2-EHA) and acrylic acid (AA), the materials of interest in this dissertation, are widely used for pressure sensitive adhesive applications [26]. For these materials, a high tack and peel strength may be attained by the formation of high molecular weight between entanglements [27, 28]. The ability to isolate local sites ("spurs" - nanosize volumes in which primary species are formed) during polymerization reactions initiated using electron beam radiation is a method of achieving these characteristics [29]. In order to do this, spur overlapping must be

minimized - a heterogeneous mechanism may be induced when the system is kept below the threshold dose rate and dose for overlapping of the spurs. (I.e., irradiation conditions may be employed which optimize the heterogeneous nature of energy deposition which takes place, as is shown in figure 1.2)

The homopolymer of 2-EHA is soft and tacky and it possesses low cohesive strength. The cohesive strength may be enhanced through the use of a relatively small concentration of comonomer such as acrylic acid. The ethylhexyl portion of the acrylate segments enables it to act as a plasticizer, thereby generating a soft and tacky surface [30]. The swelling behavior of the material can also be manipulated by adjusting the relative amount of each comonomer, since their polarities are so different [11].

2.2 Motivation

The first section of the experimental results presented in this dissertation involves an investigation of the radiation-induced polymerization of 2-ethylhexyl acrylate and acrylic acid. Ionizing radiation (in the form of electron beam and gamma irradiation) is employed as a tool for initiating the polymerization reaction. The majority of the research that has been reported in this area has been empirical in nature, focused on the evaluation of the materials formed, rather than on the understanding of the underlying processes taking place. Investigations of this type which focus on the practical aspects of synthesizing such materials provide useful information related to specific applications in which acrylate polymers are employed, but are limited in terms of their additions to the comprehension of these materials from a more fundamental perspective. The work presented in this dissertation uses a slightly different approach, with the emphasis on

accumulating knowledge with regards to the chemical mechanism taking place during the radiation-induced bulk polymerization of polymeric acrylate systems. An investigation of the kinetic behavior of such reactions is significant from both practical and theoretical standpoints. One of our goals in this work is to contribute useful data which may give greater insight into such systems on a more basic level.

There are two approaches employed in this study of the kinetics of the radiation-induced polymerization of 2-ethylhexyl acrylate and acrylic acid. One involves the characterization of the final polymeric materials formed, whereas the other focuses on the role of intermediate species in the reactions taking place. The former approach has been pursued in this project through the ^{1}H NMR analysis of residual monomer remaining in samples after subjection to different total doses, dose rates, and acrylic acid concentrations. The latter approach has been pursued through pulse radiolysis investigations. This technique is based on time-resolved spectrophotometric measurements which are employed to observe short-lived transient species that are generated upon radiolysis of the materials investigated.

The final section of this dissertation involves an investigation of the use of a radiation-synthesized copolymer as the basis for an ionomeric material. This is done with the intent of exploring whether the properties available to these radiation-synthesized materials may be potentially extended into the category of composite materials. Several parameters associated with the formation of these ionomers have been explored, including the effect of the type and concentration of metal salt. Characterization of the final material synthesized has been performed by FTIR, XPS, EDS, and TEM.

2.3 Overview of Dissertation

The theoretical background relevant to the work presented in this dissertation has been described in chapter 1. This includes an overview of basic concepts related to ionizing radiation and polymerization. Chapter 2 consists of a more specific introduction to the area of research reported in this dissertation, including the polymerization of acrylate esters, ionomers, and motivation for the project. The materials, equipment, and analysis techniques employed are described in chapter 3. The results and discussion of experiments related to the kinetics of ionizing radiation-induced polymerization of 2-EHA and AA, pulse radiolysis, and ionomer formation are reported in chapters 4, 5, and 6, respectively. The conclusions and recommendations for future work are presented in chapter 7.

3. Experimental

3.1 Materials

2-Ethylhexyl acrylate (2-EHA, Aldrich, stabilized with 10 ppm hydroquinone monomethyl ether (MEHQ) inhibitor was purified using a chromatographic column filled with poly(styrene-co-vinylbenzene) beads (Aldrich) [31]. Acrylic acid (AA, Aldrich) was used as received. Each monomer sample was deaerated by flushing with argon (Airgas, research grade) [32] prior to irradiation. Each sample was irradiated in glass vial (2 or 10 mL, Wheaton) capped with a rubber septum (Wheaton), and crimped with an aluminum cap [33].

Ferric chloride ($FeCl_3$, 98 %, anhydrous, Alfa Aesar) [34] and iron (II) acetate ($Fe(CO_2CH_3)_2$ or $FeAc_2$, Aldrich) were used as received. Tetrahydrofuran (THF, Fisher Scientific) [35] solvent was used for preparation of polymer/metal salt solutions, and was used as received.

Dialysis was performed using a cellulose membrane (12,000 molecular weight cutoff, Aldrich) in order to remove unassociated ions from the copolymer (see section 3.4). Chloroform and methanol (Fisher Scientific) solvents were employed for dialysis.

3.2 Ionizing Radiation Techniques

3.2.1 Electron Linear Accelerator (LINAC)

The UMCP electron linear accelerator is a Varian Model 5V-7715 instrument capable of producing electron beams within the 1-8 MeV energy range [5]. A schematic of this instrument is shown in figure 3.1 [2]. Electrons are initially produced by the

source are transferred from ground to a capacitor in which a high potential is built. A cathode at 80 kV emits a pulsed electron stream which is then chopped and compressed into a train of electron bunches. These electrons are then accelerated by parallel pulsing of the electron gun and magnetron microwave RF source. A series of electrodes are positioned along the length of the accelerator tube, with the voltage difference maximized at the gaps between the electrodes by the frequency of the driving signal and the gap spacing. After the electron velocity has nominally surpassed the speed of light, the energy imparted to them as they cross each gap is introduced as a relativistic change in mass, rather than velocity. The energy of the beam may then be adjusted by changing the RF frequency.

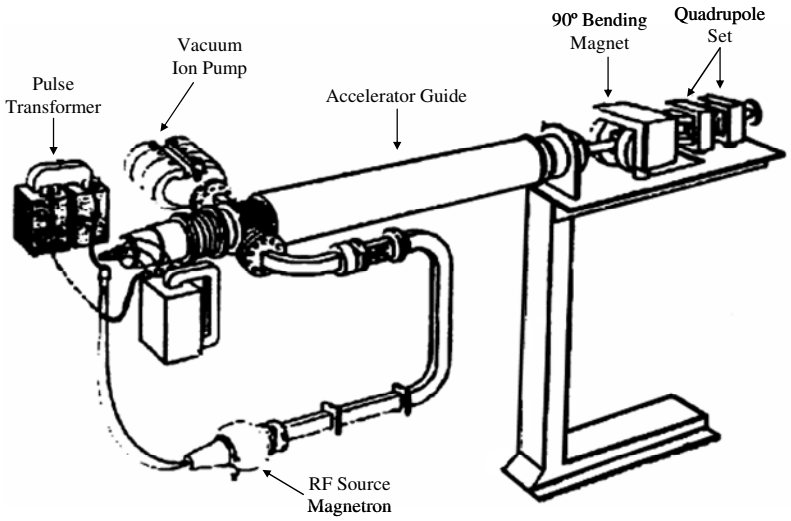

Figure 3.1. Schematic of the UMCP Linear electron accelerator (LINAC) [2].

As the electrons travel along the length of the acceleration tube, they are focused into a high energy beam. At the end of the acceleration tube, the beam travels through a titanium window into air, and subsequently into the sample. Interaction of the beam with

the window and air as it leaves the instrument generates a Gaussian distribution of electron energies as they approach the sample.

3.2.2 ^{60}Co Gamma Facility

The UMCP gamma irradiation facility consists of ten Neutron Products Model 200324 cobalt-60 source pencils arranged in an annular array with an 8.26 cm outer diameter to produce a highly uniform internal dose rate. A schematic of this facility is shown in figure 3.2 [2]. The total activity of the source as of May 23, 2006 was 7.5×10^{13} Bq and delivered a dose rate of 56.9 Gy/min (in water) in the center position of the source. Each pencil has a 1.27 cm diameter and a 30.5 cm active length, and contains mini-pellets of ^{60}Co encapsulated in two welded stainless steel cylinders with 0.064 cm thick walls.

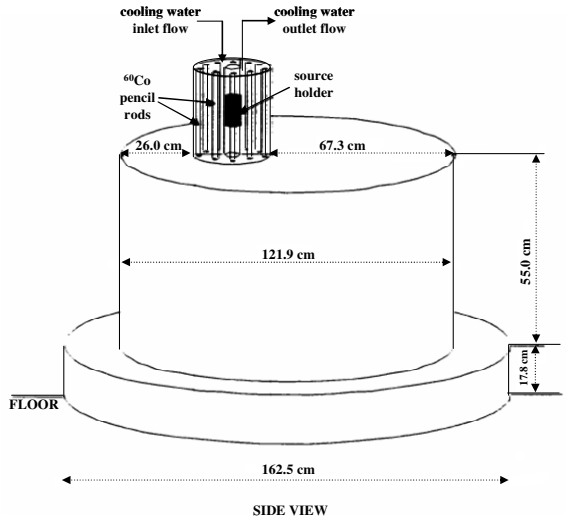

Figure 3.2. Schematic of the UMCP ^{60}Co irradiation facility [2].

The source in its storage position is located at the bottom of a pool of water in a stainless steel tank (1.2 m diameter, 4.3 m deep). The water purity is maintained by an ion exchange unit operating at a flow rate of 7.6 L min^{-1}. The source is raised above the pool through a hole in the aluminum lid that covers the tank to 0.76 m above floor level during operation into a cylindrical aluminum irradiation cell (4.6 m × 4.6 m × 3.05 m high).

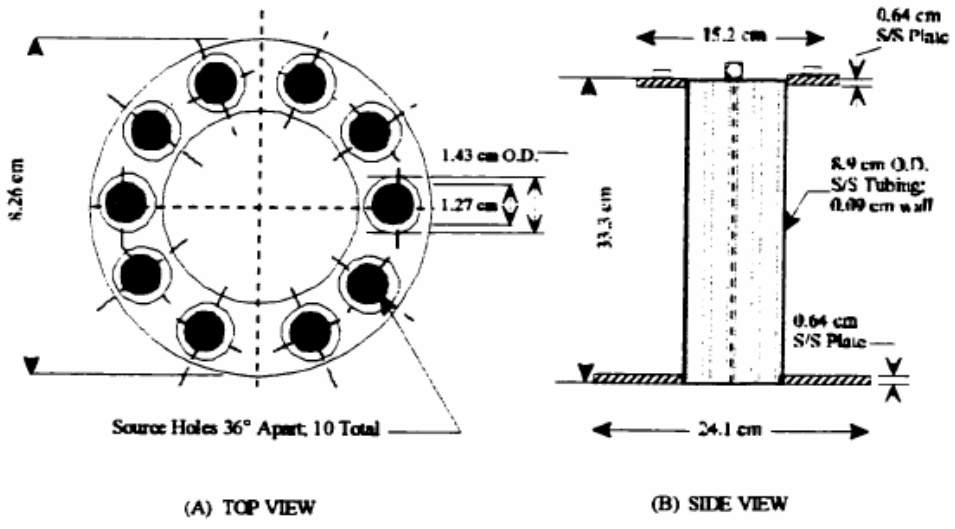

Figure 3.3. Schematic of the UMCP ^{60}Co gamma source pencils and housing (a) top view and (b) side view [2].

Pictures of the UMCP ^{60}Co gamma source facility and pencils in the lowered position at the bottom of the pool are shown in figure 3.4.

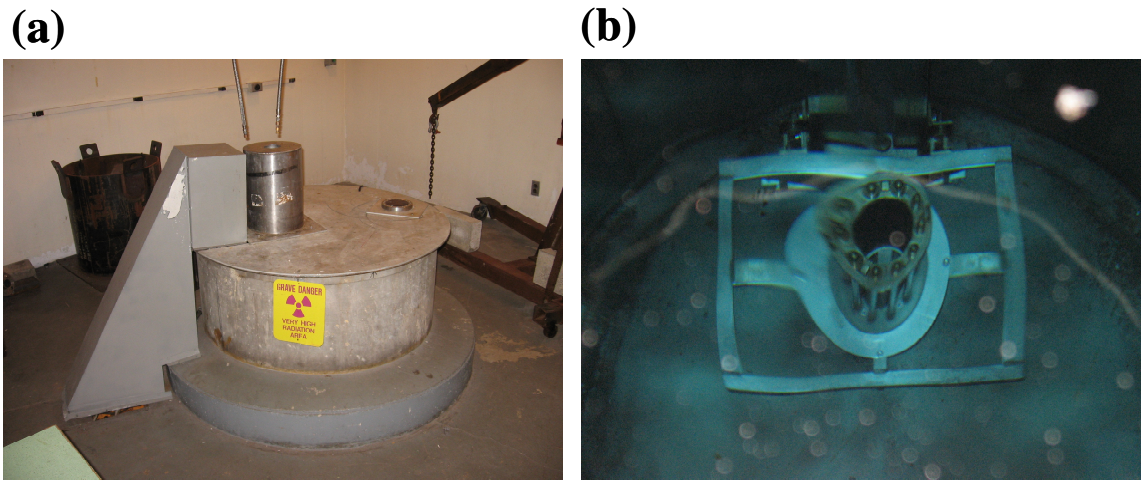

Figure 3.4. UMCP ^{60}Co gamma source (a) facility and (b) pencils (in lowered position at the bottom of the pool.

3.2.3 Radiation Dosimetry

In order to determine the amount of energy transferred from the ionizing radiation to the sample (absorbed dose), calibration of the radiation sources was performed by radiochromic film, Fricke, and potassium thiocyanate dosimetry.

3.2.3.1 Radiochromic Film Dosimetry

FWT-60 series radiochromic films (Far West Technology Inc., 1 × 1 cm, 43.5 - 45 μm average thickness) were employed to determine the absorbed dose for electron beam irradiation. These films are made of nylon and may be used in the 0.5 - 200 kGy dose range in which they are independent of dose rate up to 10^{12} Gy s^{-1}. Irradiation causes them to change from clear to a deep blue color, which is visible due to a hexa(hydroxyethyl) aminotriphenylacetonitrile (HHEVC) dye. The absorbed dose is measured by visible spectroscopy, in which the films exhibit radiation-induced absorption at wavelengths of 510 and 605 nm.

3.2.3.2 Fricke Dosimetry

Fricke dosimetry is a widely used calibration technique which employs aqueous acidic solutions of ferrous sulfate [6]. A standard Fricke dosimetry solution consists of 10^{-3} mol dm^{-3} ferrous sulfate, 10^{-3} mol dm^{-3} sodium chloride, and 0.4 mol dm^{-3} sulfuric acid in air-saturated deionized water. It exhibits a linear response within the 0.04 - 0.4 kGy dose range, and is independent of dose rate in the 0.2 - 2 × 10^{6} Gy s^{-1} range. Sulfuric acid functions to facilitate the conversion of solvated electrons to hydrogen radicals, while sodium chloride prevents the oxidation of ferrous to ferric ions by organic impurities. Chloride ions tend to undergo a reaction with hydroxyl radicals ($^{\bullet}$OH) which generates a radical that reacts preferentially with the ferrous ion rather than with organic species. Irradiation of the Fricke solution causes ferrous ions to oxidize to ferric ions, and the extent of this change is measured by UV spectroscopy at 304 nm. The absorbed dose is then calculated as follows [6]:

$$D = \frac{100 \times \Delta A_{304} \times N_A}{1000 \times \varepsilon_{304} \times \rho \times G(Fe^{3+}) \times l} \tag{54}$$

where N_A is Avogadro's number (6.02 × 10^{23} molecules mol^{-1}), ΔA_{304} is the change in absorbance at 304 nm before and after irradiation, ε_{304} is the decadic molar absorptivity (2205 mol^{-1} dm^{3} cm^{-1}, at T_1 = 25°C, λ = 304 nm), ρ is the specific gravity of the dosimeter solution (1.024 g cm^{-3} for 0.4 mol dm^{-3} H_2SO_4), $G(Fe^{3+})$ is the number of ferric ions produced per 100 V of absorbed energy, and l (cm) is the optical path length.

3.2.3.3 Potassium Thiocyanate Dosimetry

Potassium thiocyanate (KSCN) dosimetry was employed for the determination of dose per pulse for pulse radiolysis experiments [36]. This type of dosimeter consisted of a 0.02 mol dm^{-3} solution of KSCN in water (aerated). Upon irradiation of this solution, thiocyanate anions react with hydroxyl radicals to produce thiocyanate radicals. These thiocyanate radicals then react with other thiocyanate anions to produce a radical anion dimer, whose absorbance is measured at 480 nm. The absorbed dose is calculated as follows:

$$D = \frac{\Delta A_{480} \times N_A}{\varepsilon_{480} \times 10 \times (6.23 \times 10^{13}) \times G((CNS)_2^{\bullet -}) \times l} \tag{55}$$

where ε_{480} = 7600 mol^{-1} dm^3 cm^{-1} is the molar absorptivity of the thiocyanate dimer at 480 nm, and $G((CNS)_2^{\bullet -}$ = 2.9 μmol J^{-1} is the radiation chemical yield of thiocyanate dimers.

3.3 Copolymer Synthesis

A stock solution of 2-ethyhexyl acrylate (75 - 100 mol%) and acrylic acid (0 – 25 mol%) was placed in a conical flask which was sealed with a rubber septum and purged of oxygen by bubbling with argon gas. Aliquots of the deaerated mixture were transferred to individual glass vials in a glove box, sealed with rubber septa, and crimped

with aluminum caps. Copolymer synthesis was performed through either electron beam or gamma irradiation of the monomer mixture.

3.4 Ionomer Synthesis

The irradiated sample was dissolved in THF and a metal salt (ferrous acetate ($FeAc_2$) or ferric chloride ($FeCl_3$)) was mixed with the solution. Two different formulated compositions of metal salt were applied for each type of system: a 1:2 or 2:1 mole ratio of $FeAc_2$ to AA, and a 1:3 or 3:1 mole ratio of $FeCl_3$ to AA. All of these formulated compositions were calculated based on the initial concentration of acrylic acid in the sample before irradiation. Dialysis was used to remove ions that were not strongly associated with the acrylic acid units after mixture of the metal salt with the copolymer. This involved the placement of the sample into a cellulose membrane which was then placed into a mixture of 1:1 ratio of chloroform to methanol by volume.

3.5 Characterization Techniques

3.5.1 ^{1}H Nuclear Magnetic Resonance (NMR) Spectroscopy

The chemical structure and extent of conversion of monomer into polymer were determined by nuclear magnetic resonance spectroscopy. ^{1}H NMR measurements were performed using a 400 MHz Bruker DRX400 spectrometer [37] with samples in deuterated acetone (Cambridge Isotope Laboratories, Inc.) [38]. A delay time of 4 seconds was applied between each radiofrequency pulse, and the final spectrum was based on 32 repeat scans.

3.5.2 Fourier Transform Infrared (FTIR) Spectroscopy

Reaction of the polymers synthesized with various metal salts was investigated using FTIR spectroscopy. FTIR spectra were measured with a Nicolet Nexus 670 spectrometer [39]. The spectra were collected from samples by coating the sample on a zinc selenide crystal (for attenuated total reflection (ATR) mode). Spectra were measured in the 650 – 4000 cm^{-1} region with 32 scans and a resolution of 4 cm^{-1}. The ATR measurement system employed involved an 8 mm spot size and 45° angle of incident light, and was a single reflection instrument.

3.5.3 Ultraviolet-Visible (UV-VIS) Spectroscopy

UV-VIS spectrophotometry was used for the measurement of absorbed dose by radiochromic film and Fricke dosimetry. UV-VIS spectral measurements were performed using a Beckman DU Series 7000 spectrophotometer. A quartz sample cell with a 1 cm path length was employed.

3.5.4 X-ray Photoelectron Spectroscopy (XPS)

X-ray photoelectron spectroscopy was employed to study the ionomeric materials synthesized in this work. XPS measurements are performed using a Kratos AXIS 165 spectrometer [40] operated at 4×10^{-10} Torr non-monochromatic Mg K_α radiation. All measurements are done using an x-ray power of 150 W using electrostatic and magnetic lenses with a step size of 0.1 eV and a sweep time of 60 s. Survey spectra are measured a pass energy of 160 eV. Individual region spectra are obtained with a pass energy of 20 eV. All binding energies are calibrated with respect to C 1s 284.6 eV.

3.5.5 Transmission Electron Microscopy (TEM)

A JEOL JEM-2100 LaB_6 TEM [41] was used to measure images of the ionomeric materials synthesized in this work. A beam energy of 100 keV was employed for these measurements. A copper grid (150 mesh, Electron Microscopy Sciences) [42] coated with a Formvar™ (Monsanto Corp.; polyvinylformal) support film was used as a substrate for the samples.

3.5.6 Energy Dispersive X-ray Spectroscopy (EDS)

EDS was performed using the JEOL JEM-2100 LaB_6 TEM for the quantitative elemental analysis of the ionomers formed in this work. These measurements were performed directly on the TEM films of the ionomer after solvent evaporation without adding any fixative medium (such as epoxy).

3.5.7 Pulse Radiolysis

Pulse radiolysis measurements were employed to investigate the fast kinetics and structure of radiation-induced ions and free radicals during the synthesis of the polymers. Figure 3.5 shows a schematic of the UMCP pulse radiolysis facility, the major components of which include a pulsed irradiation source (LINAC) and an optical measurement system (xenon lamp, sample cell, shutter, monochromator, photomultiplier, oscilloscope, and lenses). The xenon lamp (Hamamatsu, model: C2577 power supply, 200 – 2000 nm output) was employed as a light source for observation of transient species. A cylindrically shaped quartz cell (1 or 3 cm optical pathlength) was used to

hold the sample during pulse radiolysis measurements, and contains two openings – one at the bottom for flowing sample into the cell, and another at the top for flowing irradiated sample out of the cell. The monochromator (Kratos Analytical, model: GM 252, grating: 1180 gr/mm/std, blaze: multiple, dispersion: 3.3 nm/mm/std, range: 180 – 800 nm/std) was employed to select light of a particular wavelength which was transmitted by the sample after irradiation. The oscilloscope (Agilent Infiniium, model: 54820A, 500 MHz, maximum real-time sampling rate: 2 GSa s^{-1}) was operated in real-time sampling mode for single shot acquisitions.

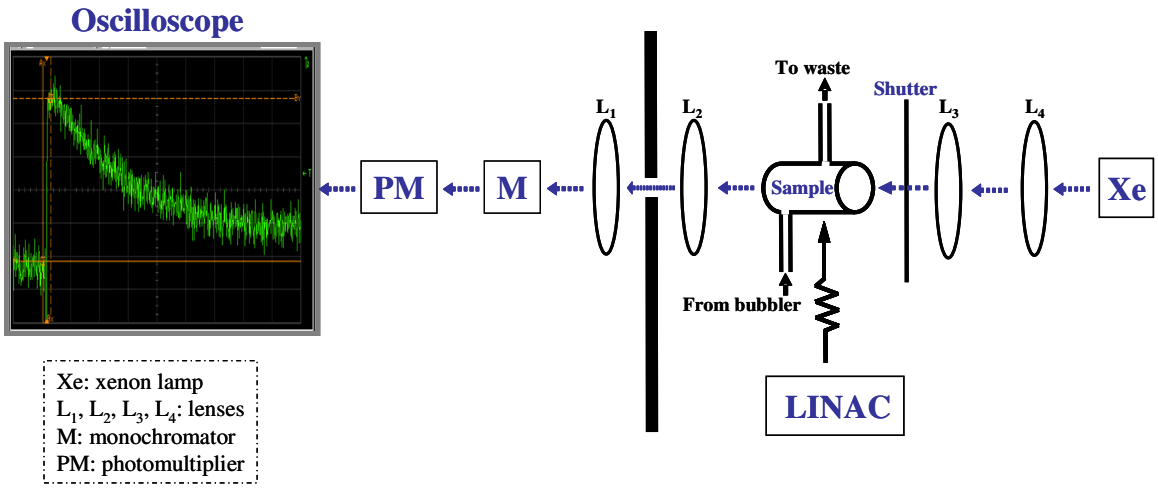

Figure 3.5. Schematic of the UMCP Pulse radiolysis facility.

The electron beam emerging from the LINAC is directed along the width of the sample cell, and functions as a means of initiating the polymerization reactions under investigation. Light from a xenon lamp is directed along the length of the cell, and is employed to observe the formation of transient species and products. A shutter located between the optical cell and the xenon lamp serves to protect the sample and the photomultiplier from excessive exposure to the xenon light. A series of four lenses along

the optical path are positioned in order to focus the xenon light towards the center of the cell, and subsequently onto the slit of the monochromator. Tygon® tubing (6.4 mm I.D., 7.9 mm O.D., wall thickness: 0.8 mm) with glass connectors (Quark Glass, 12/5 size socket joints) at either end was used to transport sample through the system. A picture of the experimental setup used in this work is shown in figure 3.6.

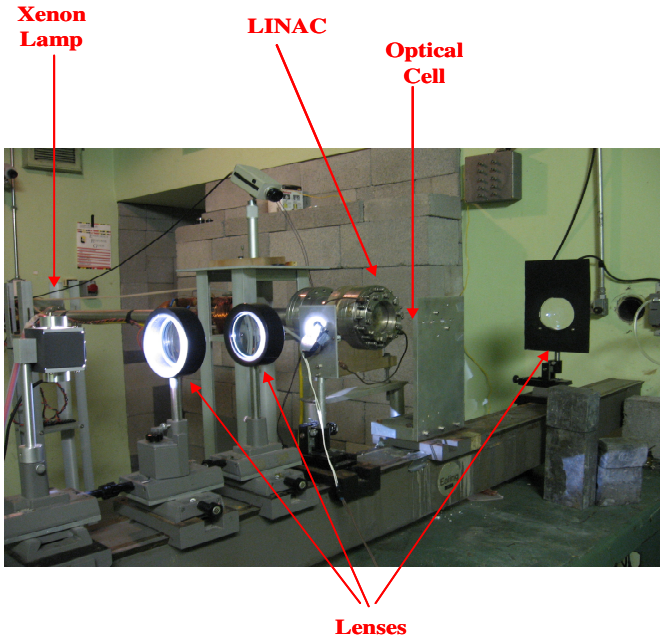

Figure 3.6. Picture of theUMCP pulse radiolysis facility.

The procedure began with the removal of inhibitor from the monomer using a chromatographic column. A stock solution of the monomer was placed into a graduated cylinder which contained three openings: (i) an inlet for argon bubbling in order to purge oxygen from the sample, (ii) an outlet for the removal of oxygen from the sample, and (iii) an outlet for the flow of purified sample from the bubbler into the bottom opening of the optical cell. After filling the cell with sample, the shutter was opened to expose it to

xenon light and it was then given a single pulse of electrons from the LINAC. Any changes in the transmittance of the xenon light by the sample upon irradiation at the wavelength being selected by the monochromator are detected by the photomultiplier detector. The photomultiplier then transforms the optical signal into a voltage output which is displayed on the oscilloscope.

Figure 3.7 shows a typical oscilloscope trace obtained from the irradiation of 2-ethylhexyl acrylate monomer. It represents an example of the raw data that are seen immediately after pulsing the sample. The method employed for pulse radiolysis measurement begins with the opening of the shutter which exposes the sample to the analysis light from the xenon lamp. The voltage signal measures the intensity of the light reaching the detector. The voltage that is recorded before the electron pulse corresponds to the baseline transmittance of xenon light by the unirradiated sample. The sample is then irradiated with a single electron pulse. At the beginning of the pulse, there is a sudden increase in the amount of light reaching the detector due to the onset of Čerenkov radiation. This amount of light is maintained throughout the duration of the pulse (all of the measurements performed in this work were obtained using a 3 μs pulse width). The increased amount of light translates into 'negative absorbance' when the detector signal is converted into an absorbance vs. time plot (see figure 3.7). After the electron pulse has stopped, the absorbance builds up to a maximum which corresponds to the generation of transient species. This build-up is more gradual than the drop into the Čerenkov 'trench' since it is a mixture of Čerenkov radiation and various chemical intermediates that are quickly forming and decaying. For the materials studied in this work, the build-up

reached a maximum within the first 0.7 – 2 μs after the pulse. The absorbance then more gradually decreases as the transients produced are transformed into products.

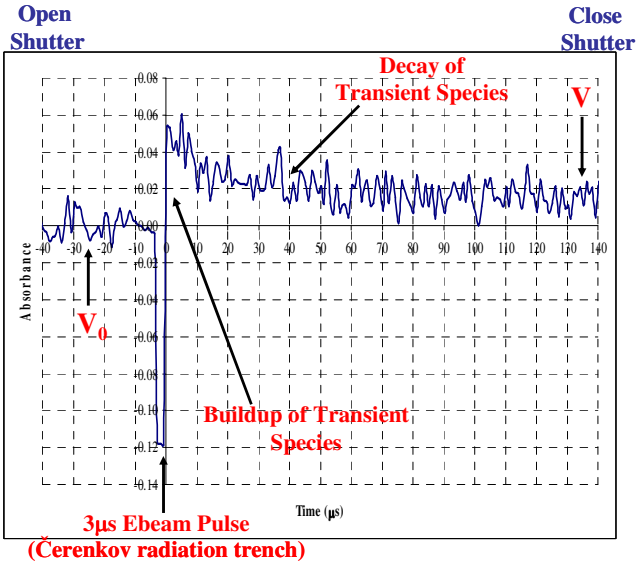

Figure 3.7. Typical oscilloscope trace obtained from the irradiation of 2-ethylhexyl acrylate monomer after a single pulse of electrons.

Beer's law is used to calculate the change in absorbance of xenon light by the system produced by the electron pulse:

$$Absorbance: \Delta A = \log\left(\frac{V_0}{V}\right) = \varepsilon c l \qquad (56)$$

where V_0 is the voltage recorded before the electron beam pulse, V is the voltage after the pulse, ε (mol^{-1} dm^3 cm^{-1}) is the molar absorptivity of the compound of interest, c (mol dm^{-3}) is the concentration of the compound, and l (cm) is the optical path length. This oscilloscope trace thus allows us to follow the formation and transformation of transient species into products through measurement of the build-up and decay in their absorbance

of the analysis light. Measurement of absorbance-time profiles of intermediates at different wavelengths at a constant time after pulse can then be used to obtain the transient absorption spectra of these species. Any change in the shape of this spectrum with time following the pulse is indicative of a change in the chemical structure of the intermediates under investigation.

4. Radiation-Induced Copolymerization of 2-Ethylhexyl Acrylate and Acrylic Acid

The composition of the 2-EHA/AA copolymers produced through electron beam and ^{60}Co gamma irradiation is an important characteristic which reflects the relative selectivity of the various types of free radical active sites consuming monomer during the polymerization reaction. This chapter presents a ^{1}H NMR spectroscopic method of determining the mole fraction of 2-EHA and AA repeat units in the polymeric materials synthesized. It is intended to determine the individual conversion profiles for each monomer as a function of dose. ^{1}H NMR is an appropriate technique for determination of this information since the signal intensities give a quantitative measure of the number of protons which they represent and the resolution is high enough that each chemically distinct type of ^{1}H nucleus is resolved.

There are various experimental parameters which have been investigated in this work, including the effect of dose rate and acrylic acid concentration. The effect of dose rate is determined through comparison of conversion data measured for samples irradiated using electron beam irradiation (high dose rate) with those irradiated using gamma irradiation (low dose rate). The effect of the acrylic acid concentration in the starting composition of monomers is also studied. Information regarding the chemical composition of the 2-EHA/AA copolymers produced under different experimental conditions is significant for the optimization of this material as a matrix for a composite, as will be discussed in more detail in chapter 6.

4.1 Copolymer Structure

The structure and ^{1}H NMR spectrum of 2-ethylhexyl acrylate monomer is shown in figure 4.1. The peak assignments in this figure are based on comparison to a reference spectrum of 2-EHA monomer [43]. The peaks located in the 0 - 2 ppm region are associated with protons adjacent to saturated carbons. The chemical shifts for these peaks are distinguished according to the type of saturated carbon center to which each type of proton is bonded, including protons bonded to primary (1.00 ppm), secondary (1.41 ppm), and tertiary (1.69 ppm) carbons. The resonance at 2.15 ppm corresponds to protons from residual undeuterated acetone solvent, and the signal at 4.14 ppm corresponds to the proton bonded to a carbon adjacent to the alkoxy oxygen. Both the acetone and alkoxy group protons are shifted farther downfield than the signals from the other protons bonded to secondary carbons due to the deshielding effect of the electronegative oxygen.

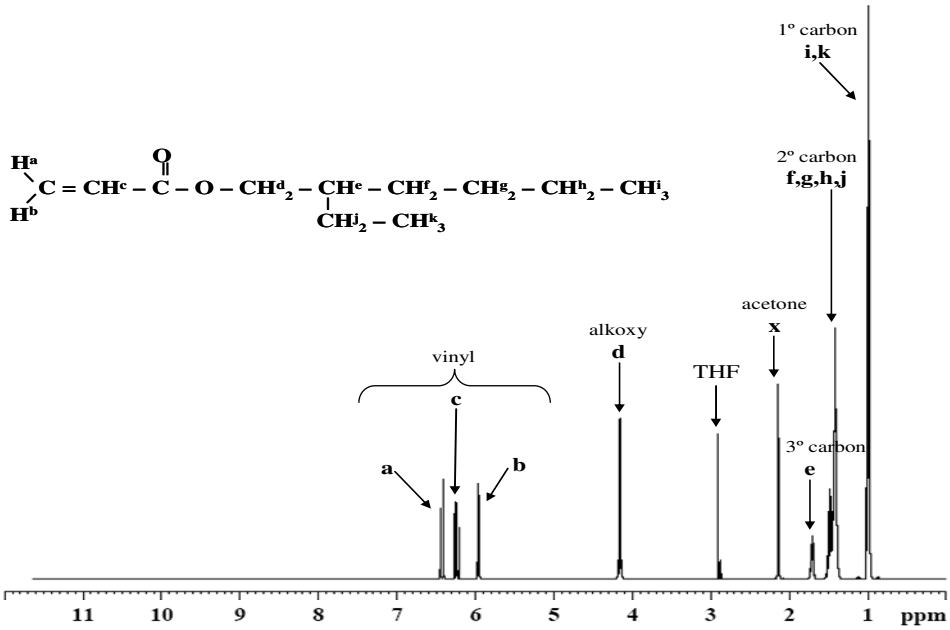

Figure 4.1. ^{1}H NMR spectrum of 2-ethylhexyl acrylate monomer.

The peaks located in the 5 - 7 ppm region of the spectrum are associated with the vinylic protons of the 2-EHA monomer. The Tobey-Simon rule for prediction of chemical shifts of protons on double bonds was used to verify which vinyl resonance corresponded to which vinyl proton [44]. This is based on the substituent parameters of each proton and is calculated using the following equation:

$$\delta = 5.28 + Z_{gem} + Z_{cis} + Z_{trans} \tag{57}$$

where δ is the chemical shift of the proton of interest, 5.28 ppm is the chemical shift of ethane, and Z_{gem}, Z_{cis}, and Z_{trans} are the substituent parameters for the groups geminal, cis, and trans to this proton. Table 4.1 shows the ^{1}H NMR spectral assignments for vinylic protons in 2-ethylhexyl acrylate monomer.

Table 4.1. ^{1}H NMR spectral assignments for vinylic protons in 2-ethylhexyl acrylate monomer.

Proton	Z_{gem}	Z_{cis}	Z_{trans}	$\delta_{predicted}$ (ppm)	$\delta_{experimental}$ (ppm)
a	H^b: 0	COOR: 1.15	H^c: 0	6.43	6.41
b	H^a: 0	H^c: 0	COOR: 0.56	5.84	6.24
c	COOR: 0.84	H^b: 0	H^a: 0	6.12	5.98

There is a resonance near 2.90 ppm in the spectrum shown in figure 4.1 which has been assigned to THF. All of the irradiated samples on which quantitative ^{1}H NMR analysis was performed and reported in this work involved the use of THF as a solvent. Most of the samples were viscous and sticky after irradiation, so they were placed into THF in order to more easily transfer them into the NMR tubes. THF was also added to the unirradiated monomer samples for comparison to samples after irradiation, which is why it appears in the spectrum shown in figure 4.1. However, it does not appear in the spectra shown in figures 4.2 and 4.3, since these are presented just for qualitative identification of the peak assignments, and were not used for quantitative analysis.

The structure and ^{1}H NMR spectrum of acrylic acid monomer are shown in figure 4.2. The spectrum contains signals associated with three types of protons - vinylic, hydroxyl, and those from residual undeuterated acetone solvent.

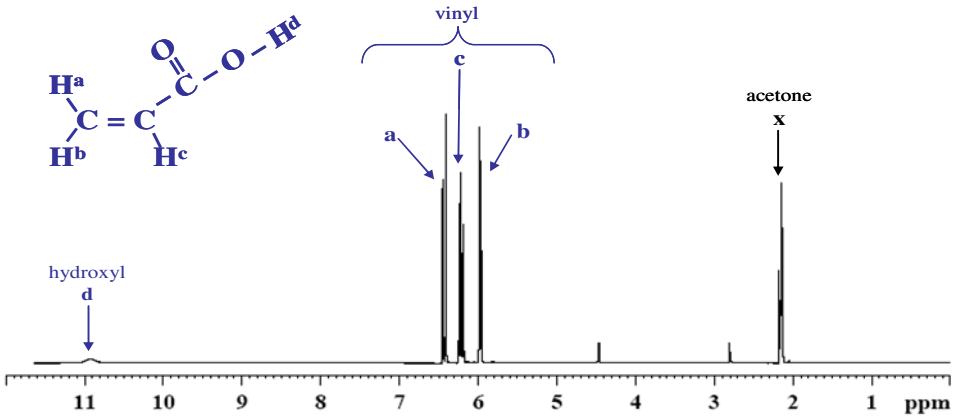

Figure 4.2. ^{1}H NMR spectrum of acrylic acid monomer.

Table 4.2 shows the ^{1}H NMR spectral assignments for vinylic protons in acrylic acid monomer. The expected vinylic proton chemical shifts were determined by the Tobey-Simon rule, which was used to distinguish each type of vinylic proton resonance. This region of the spectrum contains similar chemical shifts and splitting pattern to that displayed in the ^{1}H NMR spectrum of 2-ethylhexyl acrylate.

Table 4.2. ^{1}H NMR spectral assigments for vinylic protons in acrylic acid monomer.

Proton	Z_{gem}	Z_{cis}	Z_{trans}	$\delta_{predicted}$ (ppm)	$\delta_{experimental}$ (ppm)
a	H^b: 0	COOH: 1.35	H^c: 0	6.63	6.41
b	H^a: 0	H^c: 0	COOH: 0.74	6.02	5.98
c	COOH: 1.00	H^b: 0	H^a: 0	6.28	6.22

Figure 4.3 shows the ^{1}H NMR structure of poly(2-ethylhexyl acrylate-co-acrylic acid) and suggested peak assignments. This copolymer was synthesized from a starting comonomer mixture of 90% 2-EHA and 10% AA by weight which was irradiated with a 100 Gy dose of gamma irradiation. (Note: the residual monomer was not removed from this sample before measurement of the NMR spectrum.)

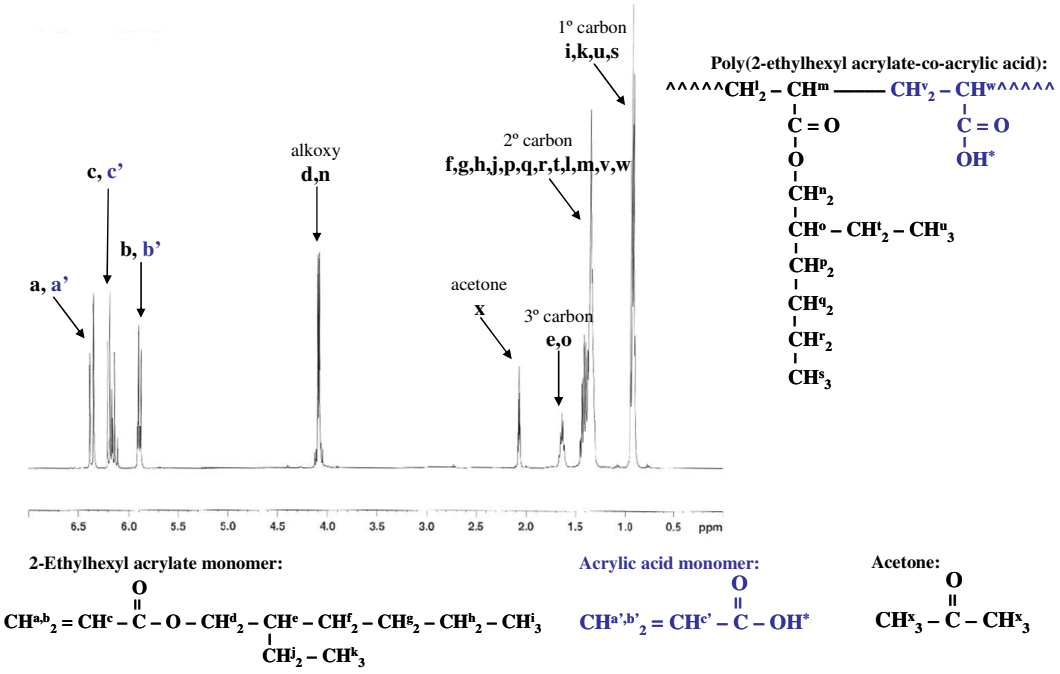

Figure 4.3. ^{1}H NMR spectrum of poly(2-ethylhexyl acrylate-co-acrylic acid).

The peak assignments in figure 4.3 are based on comparison to reference spectra of 2-EHA and AA monomers [43]. The peaks located in the 0 - 2 ppm region are associated with protons adjacent to saturated carbons in the alkyl chain of 2-ethylhexyl acrylate. The resonance at 2.07 ppm corresponds to protons from residual undeuterated acetone solvent, and the signal at 4.04 ppm corresponds to the proton bonded to a carbon adjacent to the alkoxy oxygen. The peaks bonded to saturated carbons contain contributions from both the monomeric and polymeric forms of 2-EHA.

The peaks located in the 5 - 7 ppm region of the spectrum are associated with the vinylic protons of both the 2-EHA and AA monomers. Based on comparison to experimentally measured ^{1}H NMR spectra of the individual 2-EHA and AA monomers, it has been deduced that the signals near 5.78 and 6.35 ppm correspond to the protons

bonded to the unsubstituted carbon of the 2-EHA vinyl group, while the signals near 5.92 and 6.47 ppm correspond to protons of the same type in AA. The peak near 6.10 ppm contains overlapping peaks from the proton bonded to the monosubstituted carbon of the vinyl groups of both the 2-EHA and AA monomers.

4.2 Conversion vs. Dose

Figure 4.4 shows an overlay of the vinyl region of the ^{1}H NMR spectra of pure 2-EHA and AA monomers, and the same region of the spectrum for a starting mixture containing 4.32 mol dm^{-3} (74.7 mol%) 2-EHA and 1.46 mol dm^{-3} (25.3 mol%) AA after a 20 Gy dose of γ-irradiation. Comparison of these spectra shows more clearly from which comonomer each signal in this region originates. This enables us to distinguish which peaks in the copolymer spectrum are associated with which type of repeat unit. The vinyl signals located at 6.26 ppm (2-EHA) and 6.18 ppm (AA) were used to determine the individual conversion profiles for each type of monomer.

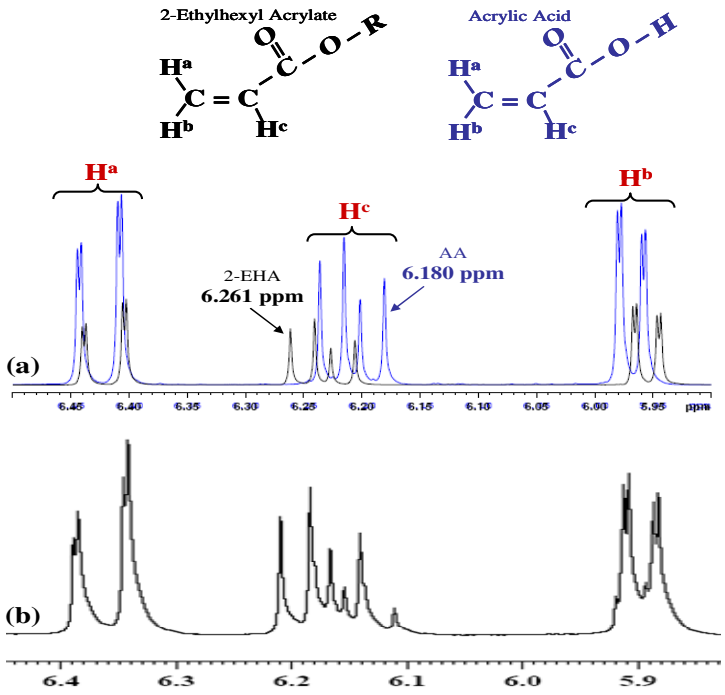

Figure 4.4. (a) Overlay of vinyl region 2-ethylhexyl acrylate monomer and acrylic acid monomer spectra, (b) vinyl region of poly(2-EHA-co-AA) after a 20 Gy dose of γ-irradiation (starting monomer mixture composition: [2-EHA] = 4.32 mol dm^{-3} (74.7 mol%), [AA] = 1.46 mol dm^{-3} (25.3 mol%).

An assessment of whether this method was appropriate for the determination of the content of each type of monomer was performed by measurement of the peak areas of monomer across a series of concentrations. Figure 4.5 shows a plot of the peak areas of 2-EHA monomer and AA monomer as a function of the concentrations of these compounds (mol dm^{-3}) in each solution in deuterated acetone. These calibration curves are used to determine the concentration of each type of residual monomer that remains in a sample after a particular dose of irradiation. Notice that although both 2-EHA and AA monomers contain the same number of vinylic protons (three), the peak areas obtained from 2-EHA are greater than those obtained from AA. This is perhaps due to differences in the chemical structure of 2-EHA and AA which lead to differences in the extent to which these protons are shielded from the magnetic field applied during NMR analysis.

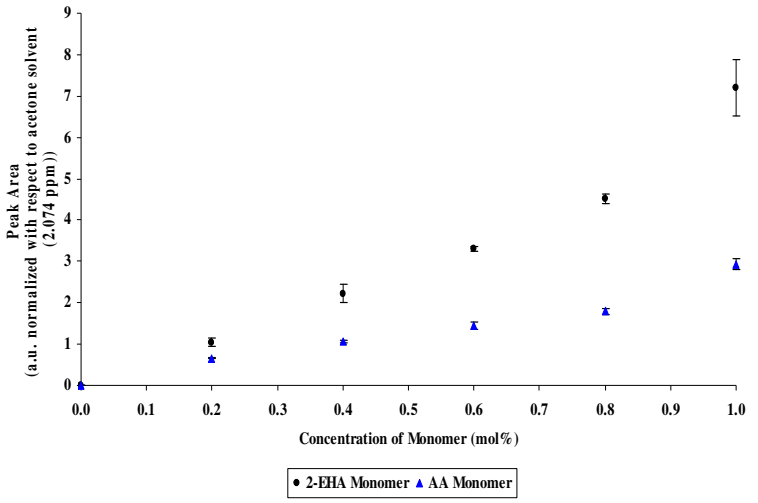

Figure 4.5. Comparison of the ^{1}H NMR peak areas of 2-EHA monomer (δ = 6.211 ppm) and AA monomer (δ = 6.116 ppm) to the concentration (mol dm^{-3}) of each compound in deuterated acetone.

Another type of assessment of whether this method was appropriate for the determination of the content of each type of monomer was performed by measurement of the peak area ratios of 2-EHA and AA in mixtures containing variations in the content of each monomer. The results of this evaluation are shown in figure 4.6, which includes a comparison of the experimentally determined ratio of AA monomer (δ = 6.180 ppm) and 2-EHA monomer (δ = 6.261 ppm) to the expected ratio of these two compounds in a mixture based on the formula that was used to make each sample. The ratios that were obtained experimentally were all lower than those expected, due to the difference in the magnitude of the NMR response of each of these monomers. However, the ratios fit very well to a straight line trend relative to one another.

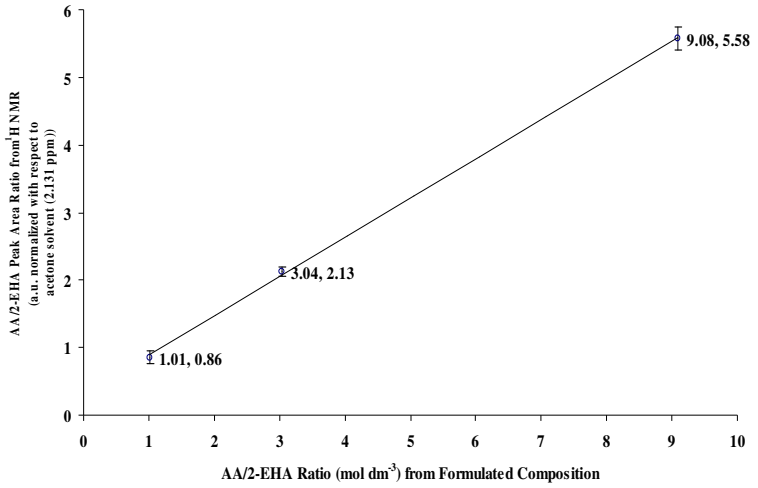

Figure 4.6. Comparison of the ratio of AA monomer (δ = 6.180 ppm) to 2-EHA monomer (δ = 6.261 ppm) determined from ^{1}H NMR peak areas and the expected ratio based on formulated composition.

The concentration of residual monomer remaining in each sample after a given dose of irradiation was calculated based on the trend lines obtained from the calibration curves shown in figure 4.5. The equation for the trend line obtained from the 2-EHA monomer data is y = 49.9x – 0.35, and that obtained from the AA monomer data is y = 19.35x – 0.0034. In each of these equations, x corresponds to the concentration (mol dm^{-3}) of the monomer of interest based on the formulated composition which was used for each solution, and y corresponds to the peak area of the ^{1}H NMR resonance (arbitrary units normalized with respect to the peak area of undeuterated acetone at 2.074 ppm).

The conversion (mol%) of monomer into polymer for each type of repeat unit as a function of irradiation dose was determined from the change in concentration of monomer as a function of dose, and is calculated as follows:

$$\%Conversion\ 2-EHA = \frac{[EHA]^{\nu}_{D=0} - [EHA]^{\nu}_{D}}{[EHA]^{\nu}_{D=0}} \times 100 = \left(1 - \frac{[EHA]^{\nu}_{D}}{[EHA]^{\nu}_{D=0}}\right) \times 100 \qquad (58)$$

$$\%Conversion\ AA = \frac{[AA]^{\nu}_{D=0} - [AA]^{\nu}_{D}}{[AA]^{\nu}_{D=0}} \times 100 = \left(1 - \frac{[AA]^{\nu}_{D}}{[AA]^{\nu}_{D=0}}\right) \times 100 \quad (59)$$

where $[EHA]^{\nu}_{D=0}$ and $[AA]^{\nu}_{D=0}$ are the peak areas of the vinyl resonances (at frequency ν (ppm)) before irradiation (dose: D = 0 Gy) and $[EHA]^{\nu}_{D}$ and $[AA]^{\nu}_{D}$ are the peak areas after irradiation at dose D (in Gy).

4.2.1 Electron Beam Synthesis of Poly(2-EHA-co-AA)

Figure 4.7 shows the conversion (mol%) as a function of dose calculated from the peak areas of residual monomer remaining in the sample after a series of doses of electron beam irradiation. These values were based on samples irradiated within a total dose range of 18.9 – 56.7 Gy. An average dose rate of 18.9 Gy per 3 μs pulse (1.2 kGy s^{-1}) and a pulse frequency of 60 Hz were employed. The composition of the monomer mixture before irradiation was $[2\text{-EHA}]_0$ = 4.56 mol dm^{-3} (88.3 mol%) and $[AA]_0$ = 0.614 mol dm^{-3} (11.7 mol%).

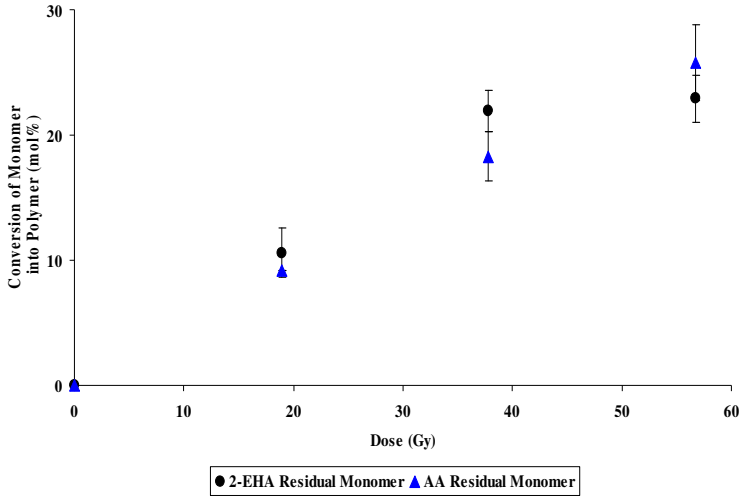

Figure 4.7. Conversion (mol%) of 2-EHA (6.209 ppm) and AA (6.107 ppm) as a function of dose of electron beam irradiation (1.2 kGy s^{-1}) determined by ^{1}H NMR spectroscopy (starting monomer mixture composition: [2-EHA] = 4.56 mol dm^{-3} (88.3 mol%), [AA] = 0.614 mol dm^{-3} (11.7 mol%).

Table 4.3 shows the experimentally determined peak areas for residual 2-EHA and AA monomer in these samples and the mol% conversion of each monomer into polymer as a function of electron irradiation dose.

Table 4.3. ^{1}H NMR peak areas, concentrations, and conversions of 2-EHA and AA monomer as a function of dose of electron beam irradiation.

Dose (Gy)	Peak Area 2-EHA	[2-EHA] (mol dm^{-3})	Conversion 2-EHA (mol%)	Peak Area AA	[AA] (mol dm^{-3})	Conversion AA (mol%)
0	2.69	0.061	0	0.638	0.033	0
0	1.98	0.047	0	0.296	0.015	0
0	2.12	0.049	0	0.220	0.012	0
18.9	1.93	0.046	12.8	0.349	0.018	9.19
18.9	2.00	0.047	10.1	0.371	0.019	3.52
18.9	2.03	0.048	8.93	0.349	0.018	9.19
37.8	1.72	0.041	20.8	0.316	0.017	17.7
37.8	1.71	0.041	21.2	0.320	0.017	16.7
37.8	1.64	0.040	23.9	0.305	0.016	20.5
56.7	1.63	0.040	24.2	0.280	0.015	27.0
56.7	1.70	0.041	21.6	0.298	0.016	22.3
56.7	1.97	0.046	11.2	0.276	0.014	28.0

For the 0 – 56.7 Gy dose range shown in figure 4.7, maximum conversions of 23 mol% 2-EHA and 26 mol% AA monomer into polymer were determined through quantitative analysis using the vinylic ^{1}H NMR resonances. For the 18.9 and 37.8 Gy doses, 2-EHA shows a greater extent of conversion than AA, this pattern is reversed at 56.7 Gy. Although the AA monomer is expected to display higher reactivity (according to the Q-e scheme estimation described by equations (48) and (49)), it does not undergo a greater extent of conversion until a total dose of 56.7 Gy is applied, according to the results shown in figure 4.7. This could be due to the fact that the AA monomer ($[AA]_0 = 0.614$ mol dm^{-3} (11.7 mol%) is much lower in concentration in the initial monomer mixture than the 2-EHA monomer ($[2\text{-EHA}]_0 = 4.56$ mol dm^{-3} (88.3 mol%).

4.2.2 Gamma Irradiation Synthesis of Poly(2-EHA-co-AA)

Figure 4.8 shows the conversion (mol%) as a function of dose calculated from the peak areas of the residual monomer remaining in the sample after a series of doses of γ-irradiation (0.833 Gy s^{-1}). These values were based on samples irradiated within a total dose range of 20 - 60 Gy. The composition of the monomer mixture before irradiation was $[2\text{-EHA}]_0 = 4.32$ mol dm^{-3} (74.7 mol%) and $[AA]_0 = 1.46$ mol dm^{-3} (25.3 mol%).

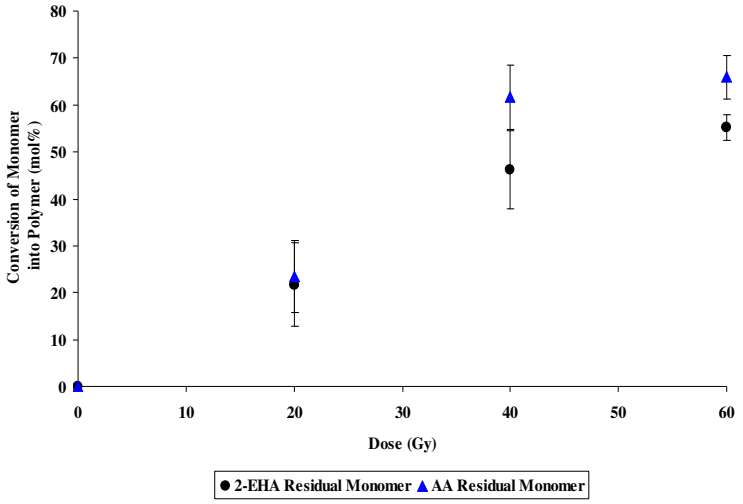

Figure 4.8. Conversion (mol%) of 2-EHA (6.210 ppm) and AA (6.110 ppm) as a function of dose of gamma irradiation (0.833 Gy s^{-1}) determined by ^{1}H NMR spectroscopy (starting monomer mixture composition: [2-EHA] = 4.32 mol dm^{-3} (74.7 mol%), [AA] = 1.46 mol dm^{-3} (25.3 mol%).

Table 4.4 shows the experimentally determined peak areas for residual 2-EHA and AA monomer in these samples and the mol% conversion of each monomer into polymer as a function of gamma irradiation dose.

Table 4.4. ^{1}H NMR peak areas, concentrations, and conversions of 2-EHA and AA monomer as a function of dose of gamma irradiation.

Dose (Gy)	Peak Area 2-EHA	[2-EHA] (mol dm^{-3})	Conversion 2-EHA (mol%)	Peak Area AA	[AA] (mol dm^{-3})	Conversion AA (mol%)
0	2.62	0.060	0	0.847	0.044	0
20	1.91	0.045	23.9	0.699	0.036	17.4
20	2.19	0.051	14.5	0.615	0.032	27.3
20	2.31	0.053	10.4	0.560	0.029	33.7
20	2.51	0.057	3.71	0.722	0.037	14.7
20	2.57	0.059	1.68	0.638	0.033	24.6
40	1.05	0.028	52.9	0.285	0.015	66.1
40	0.923	0.025	57.2	0.242	0.013	77.1
40	1.45	0.036	39.4	0.385	0.020	54.3
40	1.35	0.034	42.8	0.361	0.019	57.2
40	1.47	0.036	38.7	0.339	0.018	59.7
60	1.07	0.028	52.2	0.265	0.014	68.4
60	0.979	0.027	55.3	0.258	0.014	69.3
60	1.01	0.027	54.2	0.354	0.018	58.0
60	1.00	0.027	54.6	0.284	0.015	66.2
60	0.849	0.024	59.6	0.270	0.014	67.9

For the 0 – 60 Gy dose range shown in figure 4.8, maximum conversion of 55 mol% 2-EHA and 66 mol% AA monomer were determined through quantitative analysis of the ^{1}H NMR vinylic resonances. AA displayed a greater extent of conversion than 2-EHA at each dose which was applied to this composition. This could be due to the fact that a larger mole fraction of the unirradiated monomer mixture ($[2\text{-EHA}]_0$ = 4.32 mol dm^{-3} (74.7 mol%), $[AA]_0$ = 1.46 mol dm^{-3} (25.3 mol%)) was employed for these gamma irradiated samples than for the electron beam irradiated samples. The conversion of both of these monomers was higher at each dose of gamma irradiation than that observed in the electron beam irradiated samples shown in figure 4.7. It is thus shown that at lower dose rates and higher initial concentrations of acrylic acid monomer, a greater amount of conversion of both the 2-EHA and AA monomers into polymer is produced.

4.3 Summary of Results and Conclusions

(1) ^{1}H NMR measurements were conducted using a 400 MHz instrument (see section 3.5.1) with a delay time of four seconds. The samples were measured after dissolving them in deuterated acetone. The most clearly resolved vinyl ^{1}H NMR resonances were located at 6.261 (2-EHA monomer) and 6.180 ppm (AA monomer).

(2) These resonances were shown to provide a linear response in the peak area integration for individual solutions of each monomer within the 0.02 – 0.14 mol dm^{-3} range of concentration in deuterated acetone. The magnitude of the peak areas calculated from 2-EHA monomer were greater than those observed for AA monomer at any given concentration within this range. 2-EHA monomer also displayed a greater rate of increase in the peak area as a function of concentration, compared to that shown by AA monomer. A similar pattern was observed in the ratio of peak areas of AA and 2-EHA monomers in samples containing mixtures of these monomers across a range of concentration ratios of 1 – 9 mol dm^{-3}. The deviation in the experimentally observed peak area ratio increased as the AA:2-EHA mole ratio increased, which corresponds to the greater increase in peak area associated with 2-EHA monomer as its concentration is increased.

(3) These resonances were demonstrated to be used successfully for the quantitative determination of the mol% conversion of monomer into polymer as a function of dose. This includes samples irradiated with an electron beam (1.2 kGy s^{-1}) and γ-rays (0.833 Gy s^{-1}) for total doses of 60 Gy and below. Conversions of 23 and 26 mol% of 2-EHA

and AA monomer into polymer were observed under conditions of high dose rate electron beam irradiation at a total dose of 56.7 Gy. Conversions of 55 and 66 mol% of 2-EHA and AA monomer into polymer were observed under conditions of low dose rate gamma irradiation at a total dose of 60 Gy. The conversion of both monomers into polymer was demonstrated to be enhanced under conditions of low dose rate and higher concentrations of acrylic acid. These phenomena are attributed to the enhancement of the propagation step of the reaction due to the generation of a lower concentration of initiating monomer radicals at lower dose rates, along with a diffusion-controlled bimolecular termination step of the reaction.

5. Pulse Radiolysis

High energy initiated polymerization reactions (such as those induced by ionizing radiation) tend to take place at a rapid rate [17], due to the fact that they are often proceeding through a free radical mechanism. Some of the most widely used techniques for the investigation of free radical polymerization reaction mechanisms and kinetics include electron paramagnetic resonance spectrosocopy (EPR), pulsed laser polymerization with molecular weight detection (PLP-MWD), and pulse radiolysis with kinetic spectrosocopic detection (PR-KSD). EPR and PR-KSD are analysis methods which emphasize the role of chemical intermediates in the mechanisms and rates of reactions, while PLP-MWD is a method of determining rate coefficients through the analysis of the products of polymerization reactions [45].

EPR spectroscopy is a technique used to study compounds containing unpaired electrons (paramagnetic), the most common example of which are free radicals. It is based on the excitation of electron spins of a compound that is placed in a strong magnetic field and irradiated with microwaves. The EPR spectrum that results can give information about radical structure and geometry, which may be used to obtain mechanistic information that is helpful in understanding the reactions which lead to the formation of these radicals. EPR is frequently employed in conjunction with PLP-MWD or PR-KSD as a means of verifying the structure of the radical species produced during a reaction. It is relatively difficult to quantitatively determine radical concentrations accurately by EPR, and is thus not used as extensively as PLP-MWD and PR-KSD for the determination of rate coefficients for free radical polymerization reactions.

PLP-MWD is an indirect method of estimating rate parameters from the molecular weight distribution of the materials produced during a polymerization reaction. It involves the application of a series of laser pulses to a monomer sample which periodically creates a population of propagating radicals. This method has been demonstrated to provide highly consistent data when the pulse frequency is timed in relation to the rate of reaction under investigation so that the pulse is the major chain-starting and chain-stopping event [45]. This technique is considered by the IUPAC Working Party on Modeling of Free Radical Polymerization Kinetics [45] to be the most reliable method of determining propagation rate coefficients. However, the usefulness of this technique of determination of termination rate coefficients (particularly the chain length dependence of k_t) has not yet been as thoroughly explored [46].

PLP-KSD is a technique of measuring instantaneous concentrations of chemical intermediates. The time window of detection employed may be generally varied from the nanosecond to the microsecond time scale. The size of the time window applied can then be used to distinguish various steps in the reaction, such as the initiation and onset of polymerization. (It may thus be employed to monitor the formation of radical ion precursors, initiating radicals, and propagating oligomer radicals.) It involves the deposition of energy into the system in the form of accelerated electrons in order to initiate the reaction, while the transient concentration generated is observed through UV-VIS absorption measurements. This time-resolved technique thus enables the direct observation of the change in radical concentration produced by a single pulse of electrons [47].

There is large variance in the kinetic parameters reported in the literature for free radical polymerization. Rate coefficients determined using the same measurement techniques for the same monomer have been published with widely diverging values [11]. There are several factors contributing the challenging nature of kinetic investigations of such systems. One is the rapid rate at which these types of reactions tend to take place (μs time scale). Acrylate polymerization is a particularly fast system which is difficult to determine rate coefficients for unless the reaction is carried out at low temperatures [48, 49]. Another is the high sensitivity of most chain reactions to low levels of inhibitors and impurities. The direct optical observation of radicals is complicated by the fact that these absorption bands of interest are usually located close to or below 300 nm, and they often overlap other species which absorb in the UV region of the spectrum.

The types of systems studied in this work may be divided into four main categories: neat 2-EHA, mixtures of 2-EHA and AA, 2-EHA in methanol, and mixtures of 2-EHA and AA in methanol. Experiments have been conducted at various concentrations of all of these components using pulsed electron beam radiation.

5.1 Neat 2-Ethylhexyl Acrylate

Most of the pulse radiolysis investigations of acrylate polymerization reactions published have been performed in dilute solutions. The majority of the energy deposited into the system by the electron beam in the earliest stages of the irradiation is absorbed by the solvent, which usually undergoes radiolysis to form a radical species that then adds to the double bond of the acrylate monomer. The solvent chosen may be known to radiolytically decompose into radical anionic or cationic species, and then this helps to

distinguish between radical anionic or cationic initiating species produced from the monomer. As long as the transients produced by radiolysis of the solvent do not contain absorbance bands overlapping with those of the solvent-acrylate monomer radical, then the initiation of the polymerization reaction can be clearly identified. This radical then adds to other monomer molecules to form oligomers (dimers, trimers, etc.) and eventually a growing polymer radical. The reaction eventually undergoes termination, the mechanism (termination through combination with solvent radical, monomer radical, or polymer radical) of which depends on the concentration of the acrylate and the dose rate applied to the system.

Most of the pulse radiolysis studies published on the polymerization kinetics of 2-ethylhexyl acrylate in solution have employed cyclohexane as the solvent [50]. In a study by Takács *et al.*, cyclohexane was observed to undergo radiolysis to produce cyclohexyl radicals which have an absorption maximum at 280 nm [46]. A solvent-monomer radical adduct was observed at 290 nm, and oligomer radicals were then observed at 330 nm. The propagation ($k_p = 1.8 \times 10^4$ mol^{-1} dm^3 s^{-1}) and termination ($2k_t = 5 \times 10^7$ mol^{-1} dm^3 s^{-1}) coefficients were reported in this work. This particular study emphasized the use of PR-KSD for the determination of the termination rate coefficient from the slope of a plot of the reciprocal radical concentration as a function of time. In order to distinguish monomer decay termination from oligomer termination, this slope may be measured at different times after the pulse. The different termination mechanisms and the chain-length dependence of the rate of termination can thus be studied using PR-KSD.

Fewer investigations of 2-ethylhexyl acrylate polymerization in the neat have been published [51, 52]. This is due to the fact that such systems are difficult to handle experimentally, since they have a tendency to become viscous upon irradiation. To our knowledge, there are only two publications in the literature which report rate coefficients for the polymerization of neat 2-EHA. One of them is a study by Beuermann *et al.* which involved PLP-MWD to determine propagation rate coefficients in the range of 12 243 - 18 096 mol^{-1} dm^3 s^{-1}. In a study reported by Feng *et al.*, PR-KSD has been used to determine a propagation rate coefficient of 280 mol^{-1} dm^3 s^{-1}. Although this value is two orders of magnitude below that reported for 2-EHA in dilute cyclohexane, it is consistent with studies which demonstrate a reduction in the rate of termination with increasing concentration of acrylate [23].

The homopolymerization of neat 2-ethylhexyl acrylate is expected to proceed in the manner shown in figure 5.1. After the formation of the primary ions and excited species within the first 10^{-15} - 10^{-6} seconds of irradiation (which is not observable in these experiments, the 2-EHA monomer is expected to scavenge a thermal electron to form a radical anion [51]. This radical anion is then anticipated to react with a proton to form a neutral α-carboxyalkyl free radical, which is the initiating species of the free radical polymerization reaction. This step of the reactions proceeds on the millisecond timescale. A 2-EHA monomer adds to this free radical (in a head-to-tail manner) during the propagation step to form a dimer radical, and this reaction repeats itself many times to produce a growing chain radical. The termination step of the reaction is expected to take place through the combination of two polymer chain radicals [26].

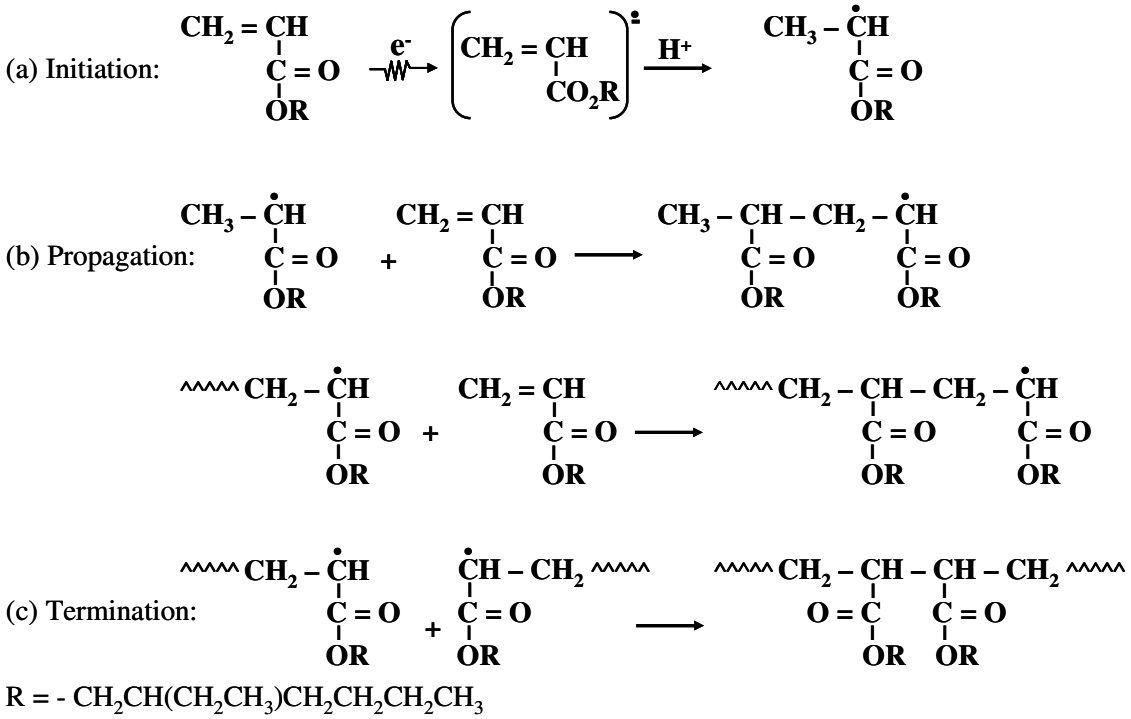

Figure 5.1. Homopolymerization of neat 2-ethylhexyl acrylate (a) initiation, (b) propagation, (c) termination.

In order to distinguish the transient species produced in 2-EHA from absorbance by the unirradiated material, all absorbances of the sample after irradiation were determined with respect to the absorbance of the unirradiated compound, which is used as a baseline measurement for the absorption spectra of the transients. 2-Ethylhexyl acrylate is an α,β-unsaturated ester with high intensity π-π* UV absorption band. The absorbance of neat 2-EHA below 300 nm is so intense that transient absorptions during pulse radiolysis measurements could not be measured below this wavelength.

According to the expected reaction mechanism shown in figure 5.1, the major transient species produced in neat 2-EHA include the radical anions, neutral free radical monomers, propagating free radicals of this compound. Each of these transients corresponds to a different stage in the polymerization reaction, and they may be

distinguished from one another by measuring their build-up and decay curves - i.e., by measuring their absorbance on different time scales. Then by measuring the rate at which they form and are consumed, the rate coefficients of the reactions that they participate in may be determined.

5.1.1 Build-up

When the absorbance of transient species generated by electron irradiation of a sample is measured on a relatively short time scale, the formation ('build-up') of these transients may be observed. For example, the build-up curves presented in this section of the dissertation are based on data obtained from oscilloscope traces measured on a 1 μs per division time scale which extends for a total measurement time of 10 μs. The build-up of transients generated in neat 2-EHA corresponds to the early stages of the reaction, which involves initiation. The initiation of the reaction consists of two steps, according to the expected reaction scheme shown in figure 5.1 - (i) formation of the 2-EHA radical anion, and (ii) formation of the 2-EHA neutral free radical. These are thus the two major transient species which are expected to predominate and contribute to the polymerization of 2-EHA.

A typical oscilloscope trace for the build-up of transient species in neat 2-EHA is shown in figure 5.2. It shows the same general shape as that presented in figure 3.7, including a baseline signal, a Čerenkov trench during the pulse, a build-up and then a decay of transient species. The baseline signal corresponds to the absorbance of the 2-EHA monomer before it has been exposed to radiation. The onset of the electron pulse is displayed as a sudden downward step in the signal to a minimum value which is

maintained through the 3 μs length of the irradiation. The 2-EHA radical anions are anticipated to be among the first generation of radiolytic transient species produced from the acrylate. This expectation is based on the fact that most publications of pulse radiolysis of acrylates which involve the identification of radical ions employ a pulse width below 1 μs. For example, a study by Knolle *et al.* on the polymerization of tripropyleneglycol diacrylate (TPGDA) involved the use of 5 or 15 ns pulses in order to observe radical anions and cations immediately after the pulse [53]. These measurements were performed on dilute solutions of TPGDA in n-butylchloride or tetrahydrofuran solvent, in which most of the electron beam energy is deposited in the solvent to produce transients which then react with the acrylate to generate radical ions. Pulse radiolysis measurements of these compounds in their neat state would be expected to generate these ionic transients at an even faster rate than they would be produced in solution, since most of the electron beam energy would be deposited directly on the acrylate.

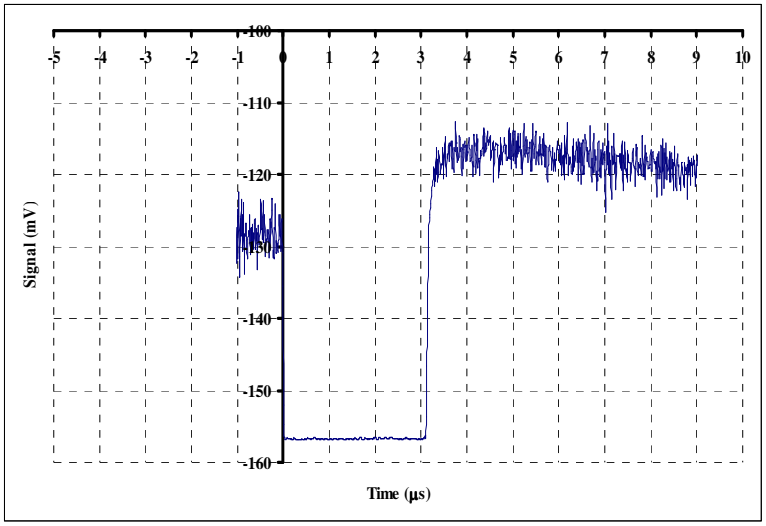

Figure 5.2. Ocilloscope trace for the build-up of transient species in neat 2-ethylhexyl acrylate ([2-EHA] = 4.80 mol dm^{-3}, argon saturated, 330 nm, 85 Gy/pulse, 3 μs pulse width).

After the electron pulse has ceased, the signal rapidly rises to a value which is greater than that of the baseline. This part of the signal profile corresponds to the generation of neutral 2-EHA free radicals through the reaction of the 2-EHA radical anions with H^+ ions in the system [23]. Another reason for assigning the post-pulse absorption to neutral radicals is that the polymerization reaction takes place mainly through a free radical mechanism. The signal due to 2-EHA radicals reaches a plateau at approximately 2 μs after the pulse, after which it begins to undergo decay.

The absorption spectrum for transient species produced in neat 2-ethylhexyl acrylate based on the absorption 2 μs after the pulse is shown in figure 5.3. It was determined from build-up curves measured at a series of wavelengths, and each value shown in this spectrum is based on three measurements which were averaged. The absorption maximum for the build-up of transient species in neat 2-EHA was found to be located in the 310 - 330 nm wavelength region. We propose that the absorption in this wavelength range corresponds to the neutral 2-EHA free radical formed during the initiation step of the reaction, since the formation of the radical anion is expected to take place so quickly that its absorbance would not be as long-lived as that of the neutral radical.

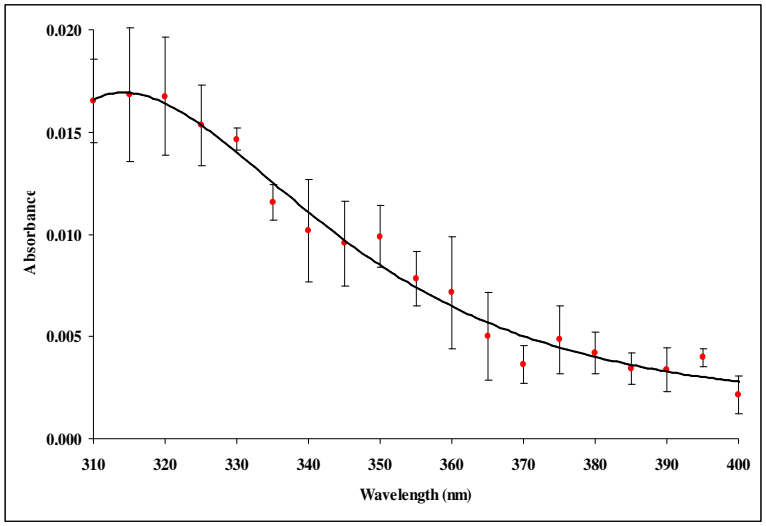

Figure 5.3. Absorption spectrum for transient species produced in neat 2-ethylhexyl acrylate based on the absorption 2 μs after a 3 μs pulse and a dose of 85 Gy/pulse ([2-EHA] = 4.80 mol dm^{-3}, argon saturated).

A typical absorbance build-up curve of transient species in neat 2-ethylhexyl acrylate is shown in figure 5.4. The extent of this build-up (represented by the absorbance) should be proportional to the concentration of neutral 2-EHA radicals formed in the early stages of the polymerization reaction, according to the following equation:

$$A = \log\left(\frac{V_0}{V}\right) = \varepsilon_{EHA\bullet}.[EHA^{\bullet}]l \qquad (60)$$

where V_0 is the baseline voltage (baseline transmittance) of the sample before electron irradiation, V is the voltage (transmittance) of the sample at time t, $\varepsilon_{EHA\bullet}$ is molar absorptivity of the neutral 2-EHA radical, and l is the path length of the xenon light through the optical cell. We propose that the build-up observed at 330 nm corresponds to the reaction between the 2-EHA radical anion and an H^+ ion to produce a neutral 2-EHA

radical. The concentration of both the 2-EHA radical anion and the H^+ ion that it reacts with are expected to be comparable enough that this reaction should follow a second order rate law [54].

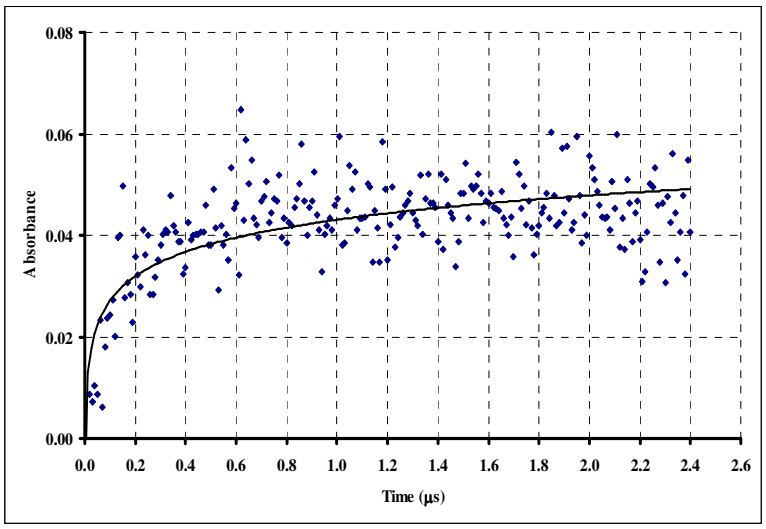

Figure 5.4. Build-up of transients in neat 2-ethylhexyl acrylate ([2-EHA] = 4.80 mol dm^{-3}, argon saturated, 330 nm, 85 Gy/pulse, 3 μs pulse width).

The rate coefficient for the build-up of transients in neat 2-EHA was calculated according to the following equation for a second order rate law:

$$\frac{1}{(A_\infty - A_t)} = \frac{2kt}{\varepsilon_{EHA\bullet}.l} \qquad (61)$$

where A_∞ is the absorbance 2 μs after the pulse, A_t is the absorbance at time t, k is the rate coefficient for the build-up, $\varepsilon_{EHA\bullet}$ is the molar absorptivity of the neutral 2-EHA radical, and l is the path length of xenon light traveling through the optical cell.

The rate coefficient associated with the build-up of neutral 2-EHA free radicals may be determined from a plot of $1/(A_\infty - A_t)$ vs. t. Figure 5.5 shows a straight line fitted to data for the build-up within the first μs after the pulse.

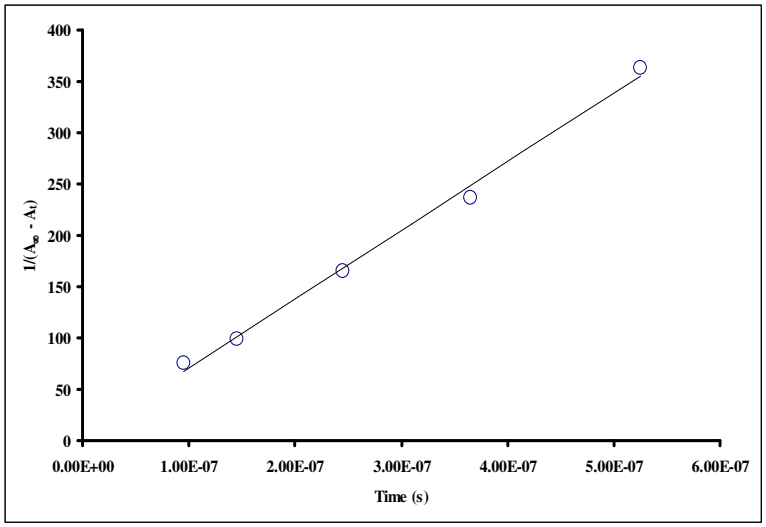

Figure 5.5. Straight line fitted to data for the build-up of transient species in neat 2-ethylhexyl acrylate to a second order rate law ([2-EHA] = 4.80 mol dm^{-3}, argon saturated, 330 nm, 85 Gy/pulse, 3 μs pulse width).

The slope of the trend line from this plot is proportional to the rate coefficient which corresponds to this build-up (slope = $2k / \varepsilon_{EHA}.l$). Table 5.1 shows the results of three repeat calculations of the rate coefficient for build-up in neat 2-EHA.

Table 5.1. Rate coefficients for the build-up of transients in neat 2-EHA.

[2-EHA] (mol dm^{-3})	Dose/pulse (Gy)	Wavelength (nm)	Path length (cm)	$2k / \varepsilon_{EHA}.l$ (s^{-1})	$k_{obs}\varepsilon_{EHA\bullet}$
4.80	85	330	3	6.69×10^8	1.0×10^9
4.80	85	330	3	2.65×10^8	3.98×10^8
4.80	85	330	3	4.37×10^8	6.56×10^8

An average of these results gave a observed rate coefficient for build-up of transients in neat 2-EHA as $k_{obs} = ((7 \pm 2) \times 10^8)\varepsilon_{EHA\bullet}$. This rate coefficient is reported in terms of the molar absorptivity of the neutral 2-EHA radical since the value for this property could not be found in any published reports on the chemistry of 2-EHA.

5.1.2 Decay

When the absorbance of transient species generated by electron irradiation of a sample is measured on a relatively long time scale, the consumption ('decay') of these transients may be observed. For example, the decay curves presented in this section of the dissertation are based on data obtained from oscilloscope traces measured on a 100 - 200 μs per division time scale which extends for a total measurement time of 1000 - 2000 μs. There are several reactions superimposed on one another that are taking place during the course of the transient decay measured in neat 2-EHA, the most prominent of which include propagation and termination. Figure 5.6 shows these two reaction paths. The relative significance of propagation versus termination depends on a combination of mainly three factors: (i) time after the pulse (ii) dose rate, and (iii) concentration of monomer. The expected effect of each of these factors is discussed below.

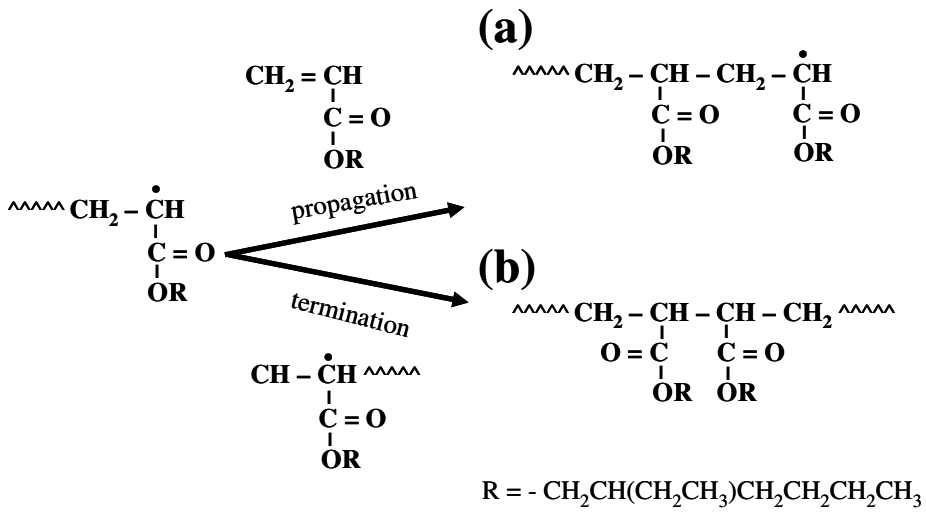

Figure 5.6. Reaction pathways for a 2-EHA chain radical (a) propagation, (b) termination.

First we consider the effect of time after the pulse, when the dose rate and monomer concentration are held constant. When a single pulse of electrons is applied to a sample of 2-EHA in the neat, monomer radicals are the first generation of reactive species which may be observed with the experimental setup employed in this work (3 μs pulse width, ≤ 100 Gy/pulse). These monomer radicals may then undergo either propagation or termination. During the early stages after the pulse for the neat 2-EHA system, the unreacted acrylate monomer concentration is expected to be so large in comparison with that of the acrylate monomer radicals produced by irradiation, that the propagation reaction is anticipated to predominate. As the concentration of monomer is subsequently reduced by its consumption through successive propagation steps, the bimolecular radical combination termination step of the reaction will become more significant later in time after the pulse.

Next we consider the effect of dose rate when the time after pulse and monomer concentration are held constant. The dose rate applied to irradiate a polymerizable

material will determine the number of monomeric radicals which form, and thus influence the rate of the initiation step of the reaction. A low dose rate will generate lower concentrations of monomer radicals, which will tend to favor the propagation step since these monomer radicals are separated from one another by relatively large distances. Application of a high dose rate, in contrast, will generate higher concentrations of monomer radicals which can diffuse and recombine with one another more easily, thereby enhancing the termination step of the reaction.

Finally, we consider the effect of monomer concentration when the time after pulse and dose rate are held constant. In general, the fraction of the electron beam energy which is deposited in each component of a system will be determined by the concentration of each of those components. When a dilute solution of monomer in a solvent is irradiated with a single pulse of electrons, most of the radiation energy is deposited on the solvent to produce solvent radicals. These solvent radicals then react with monomers to generate monomer radicals capable of initiating the polymerization reaction. The propagation step of the reaction proceeds until a large fraction of the monomer is depleted and recombination of radicals becomes competitive with chain propagation and the reaction is terminated. When a more highly concentrated solution of monomer is irradiated, the same indirect process of producing monomer radicals takes place. However, a greater concentration of monomer in the system leads to faster propagation and termination steps. When a monomer in the neat is irradiated, all of the electron beam energy is deposited directly on the monomer to produce a relatively high concentration of monomer radicals (compared to that which would be produced in solution). The system will also contain a high concentration of unreacted monomer after

a single pulse of electrons, which will cause the propagation step of the reaction to predominate. Thus it is only under conditions of extremely high dose rate when the termination step of the reaction will predominate after a single electron pulse.

Now we consider the expected signal profile of the decay obtained under the experimental conditions employed in the work presented in this dissertation. Figure 5.7 shows a typical oscilloscope trace for the decay of transient species in neat 2-EHA. It contains the same basic components as the trace shown in figure 3.7 for the build-up (baseline, Čerenkov trench, build-up, decay), except that it is measured on a longer time scale so that a greater amount of data corresponding to the decay of transients may be obtained. The measurement of transient concentrations on a longer time scale causes the Čerenkov trench to appear less prominently ('compressed') - so the 3 μs electron pulse is not as easily seen. Rather, this longer time scale is chosen in order to emphasize the decay of 2-EHA free radicals as they are consumed by the propagation and termination steps of the reaction. The decaying signal profile shown in figure 5.7 corresponds to the consumption of monomeric, oligomeric, and polymeric 2-EHA free radicals through propagation and termination.

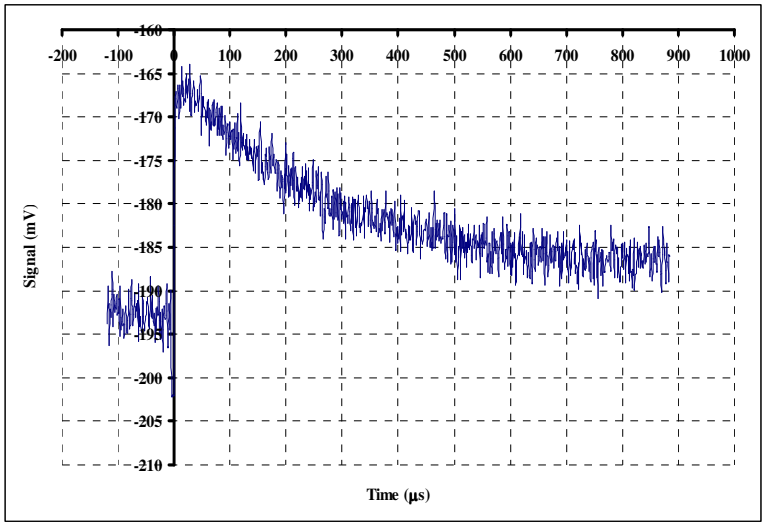

Figure 5.7. Ocilloscope trace for the decay of transient species in neat 2-ethylhexyl acrylate ([2-EHA] = 4.80 mol dm^{-3}, argon saturated, 330 nm, 100 Gy/pulse, 3 µs pulse width).

Notice that the signal decays to a plateau and retains a permanent absorption, rather than returning all the way to the level of the unirradiated material. This indicates that some type of irreversible chemical change has taken place. It is a reflection of the difference in chemical structure of the polymeric products and the monomeric reactants, in which the breaking of C=C double bonds and formation of C—C single bonds would lead to a difference in UV absorbance.

Figure 5.8 shows a typical absorbance decay curve for transients produced after a single pulse of electron irradiation in neat 2-EHA. The measured absorbance is proportional to the concentration of 2-EHA chain radicals, according to the following equation:

$$A = \log \frac{V_0}{V} = \varepsilon_{R^\bullet} [R^\bullet] l \qquad (62)$$

where $\varepsilon_{R^\bullet}$ is the molar absorptivity of the 2-EHA chain radicals, and $[R^\bullet]$ is the sum of the growing chain radical concentrations of different lengths:

$$[R^\bullet] = \sum_i [R_i^\bullet] \tag{63}$$

where $[R_i^\bullet]$ is the concentration of 2-EHA chain radicals containing *i* repeat units.

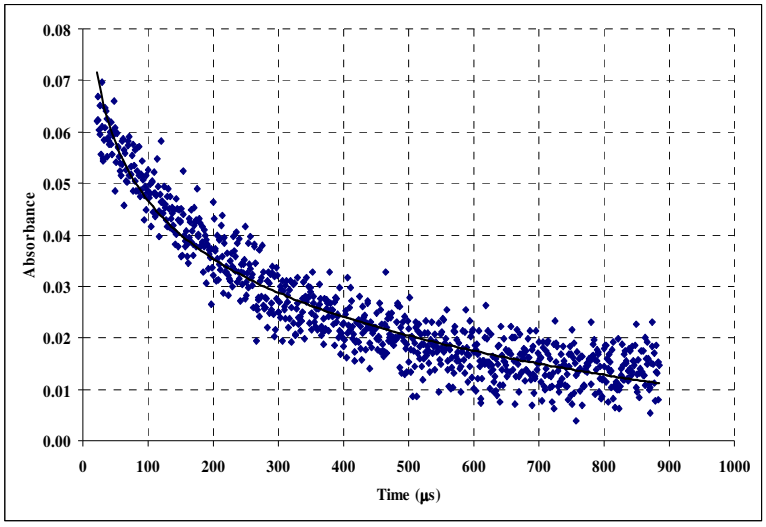

Figure 5.8. Decay of transients in neat 2-ethylhexyl acrylate ([2-EHA] = 4.80 mol dm^{-3}, argon saturated, 330 nm, 100 Gy/pulse, 3 μs pulse width).

As was previously stated, the decay in absorbance represents a mixture of propagation and termination steps of the reaction. We propose that the decay shown in figure 5.8 corresponds primarily to the propagation reaction between 2-EHA chain radicals and 2-EHA monomers. This assignment is based on the fact that during the time range of measurement shown in this figure, the half-life ($t_{1/2}$) of the transient species which is undergoing decay remains constant.

The concentration of unreacted 2-EHA monomer during this time should be so large compared to the concentration of radicals produced ($[EHA]_0 >> [EHA^{\bullet}]$) that it may be considered to remain 'constant'. The propagation reaction is therefore expected to follow a pseudo-first order rate law, which is described by the following equation:

$$\ln(A_t) - \ln(A_0) = -k_p [EHA]_0 t \qquad (64)$$

where A_o is the absorbance at 0 μs after the pulse, k_p is the rate coefficient for propagation, and $[EHA]_0$ = 4.80 mol dm^{-3} is the initial concentration of 2-EHA monomer.

The rate coefficient associated with the decay of 2-EHA chain radicals within the first 400 μs after the pulse may be determined from a plot of ln (A_t) vs. t. Figure 5.9 shows a straight line fit to this part of the decay curve.

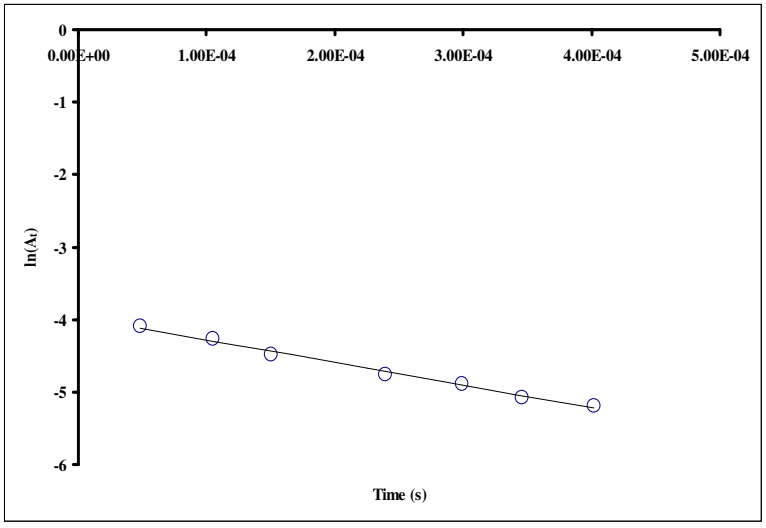

Figure 5.9. Straight line fitted to data for the decay of transient species in neat 2-ethylhexyl acrylate to a pseudo-first order rate law within the first 400 μs after the pulse ([2-EHA] = 4.80 mol dm^{-3}, argon saturated, 330 nm, 85 Gy/pulse, 3 μs pulse width).

The slope of the trend line from this plot is proportional to the rate coefficient which corresponds to the decay (slope = $k_p[EHA]_0$). Thus since the 2-EHA monomer concentration is assumed to remain 'constant' throughout this time period, the experimentally determined slope must be divided by this concentration in order to obtain the actual rate coefficient of propagation. For example, the slope of the fitted trend line which is shown in figure 5.9 may be used to calculate the rate coefficient of propagation as follows:

$$k_p = \frac{3.11\times10^3}{[EHA]_0} = \frac{3.11\times10^3}{4.80} = 6.48\times10^2\ mol^{-1}dm^3s^{-1} \qquad (65)$$

where k_p is the rate coefficient of propagation and $[EHA]_0 = 4.80$ mol dm^{-3} is the initial concentration of the 2-EHA monomer. Table 5.2 shows the results of three repeat calculations of this type for the rate coefficient associated with the decay in the first 400 μs after the pulse.

Table 5.2. Rate coefficients for the decay of transients in neat 2-EHA.

[2-EHA] (mol dm^{-3})	Dose/pulse (Gy)	Wavelength (nm)	Path length (cm)	$k_p[EHA]_0$ (s^{-1})	k_p (mol^{-1} dm^3 s^{-1})
4.80	85	330	3	1.41×10^3	2.93×10^2
4.80	85	330	3	2.37×10^3	4.94×10^2
4.80	85	330	3	3.11×10^3	6.48×10^2

An average of these results gave a rate coefficient for decay of transients in neat 2-EHA within the first 400 μs after the pulse as $k_p = (5 \pm 1) \times 10^2$ mol^{-1} dm^3 s^{-1}. This value is of the same order of magnitude as that reported by Feng *et al* ($k_p = 280$ mol^{-1} dm^3 s^{-1}).

The decay in the absorbance of transients at 330 nm in neat 2-EHA corresponds to a mixture of propagation of termination reactions, as was previously stated. We have proposed that the change in slope during the 400 - 800 μs time range after the pulse corresponds to a time during which the termination step of the reaction becomes prominant (shown in figure 5.7). At 800 μs after the pulse, the absorbance begins to reach a plateau, which indicates that the polymeric materials formed by the electron pulse have been formed and the reaction has been completed.

An absorption spectrum for transient species produced in neat 2-EHA based on the absorption 800 μs after the pulse is shown in figure 5.10. It was determined from decay curves measured at a series of wavelengths, and each value shown in this spectrum is based on three measurements which were averaged. The largest absorption maximum in the system remains in the 310 - 330 nm wavelength region (corresponding to the initiating acrylate monomer radicals). Notice that the absorbance within this wavelength region is lower at 800 μs after the pulse ($A_{800\mu s}^{320nm} = 0.004 \pm 0.001$) than it is at 2 μs after the pulse ($A_{2\mu s}^{320nm} = 0.017 \pm 0.003$); this result is expected since the concentration of monomer radicals decreases significantly with time. A new absorbance also appears to be emerging in the 360 - 370 nm region. This new absorbance is believed to represent the formation of oligomers, and its position closer to the visible region of the spectrum is consistent with other studies of acrylate polymerizations which studied the changes in the shape of the transient spectrum as a function of time after the pulse [47]. It also fits what would be expected based on the structures of the species that are anticipated to be generated at different times after the pulse. The conjugation present in acrylate monomers is expected to absorb closer to the UV region, while nonconjugated oligomers

are expected to absorb closer to the visible region of the spectrum. This oligomer absorbance is also broader than that corresponding to the monomer, probably due to the fact that it is being generated from species which have a distribution of molecular weights (dimers, trimers, etc....).

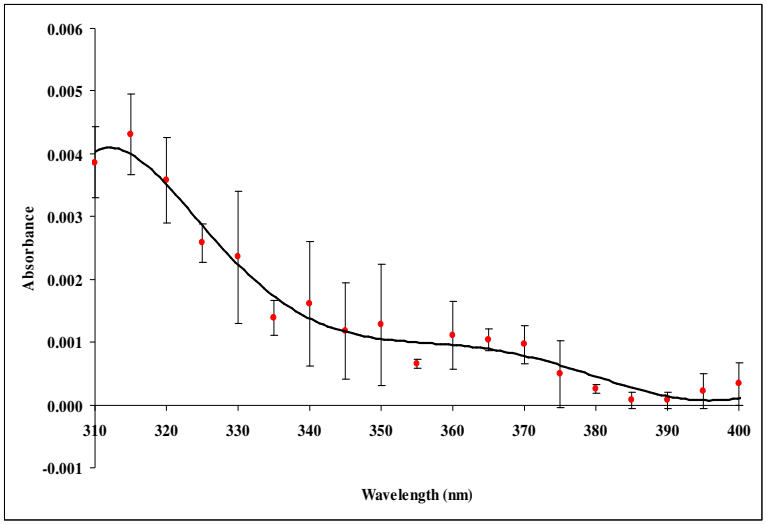

Figure 5.10. Absorption spectrum for transient species produced in neat 2-ethylhexyl acrylate based on the absorption 800 μs after a 3 μs pulse and a dose of 80 Gy/pulse ([2-EHA] = 4.80 mol dm^{-3}, argon saturated).

Notice that although the 360 – 370 nm absorption appears to become more prominent with time when compared to the absorption within the 310 – 330 nm region, it is still decreasing with time. I.e., the 360 – 370 nm absorption increases with time when compared to that of the 310 – 330 nm absorption, but it decreases with time when compared to itself.

5.2 2-Ethylhexyl Acrylate in Methanol

As was described in the introductory section of this chapter, most of the pulse radiolysis studies of the polymerization of 2-EHA have been performed in dilute cyclohexane solutions. Methanol is another solvent which is compatible with 2-EHA, and a pulse radiolysis investigation of 2-EHA in methanol is reported in this section. Figure 5.11 shows the reactions that typically take place during the radiolysis of methanol in the neat [55]. One of the major transient species that is produced is the hydroxymethyl radical ($^{\bullet}CH_2OH$), and radicals of this type tend to undergo termination either through recombination with one another to form ethylene glycol ($(CH_2OH)_2$) or through disproportionation to yield formaldehyde (CH_2O) and methanol (CH_3OH) [56].

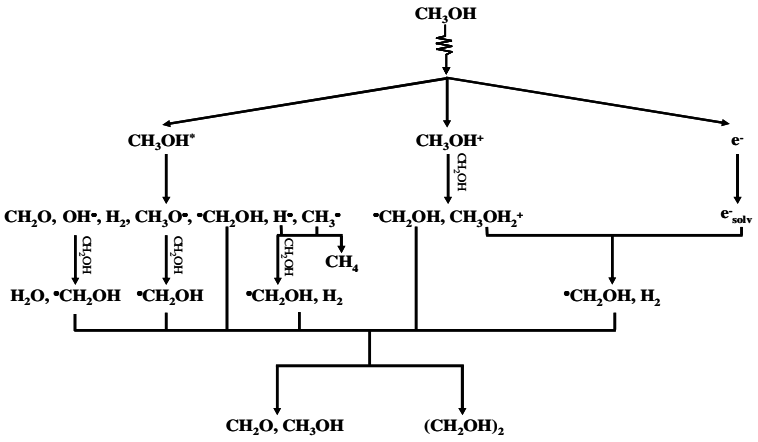

Figure 5.11. Radiolysis of neat methanol [56].

The transient absorption spectrum of neat methanol is shown in figure 5.12, and was measured in order to clearly distinguish the 2-EHA transients generated during the polymerization reaction from those which arise from the solvent. It was determined from build-up curves measured at a series of wavelengths, and each value shown in this

spectrum is based on the average of three repeat measurements. The absorption maximum was observed to be located in the 280 – 300 nm wavelength range, and is assigned to the hydroxylmethyl radical. The absorption maximum for radiolytic species produced from methanol is outside of the range of interest for 2-EHA radicals, which may thus be easily seen during measurements of 2-EHA/MeOH solutions.

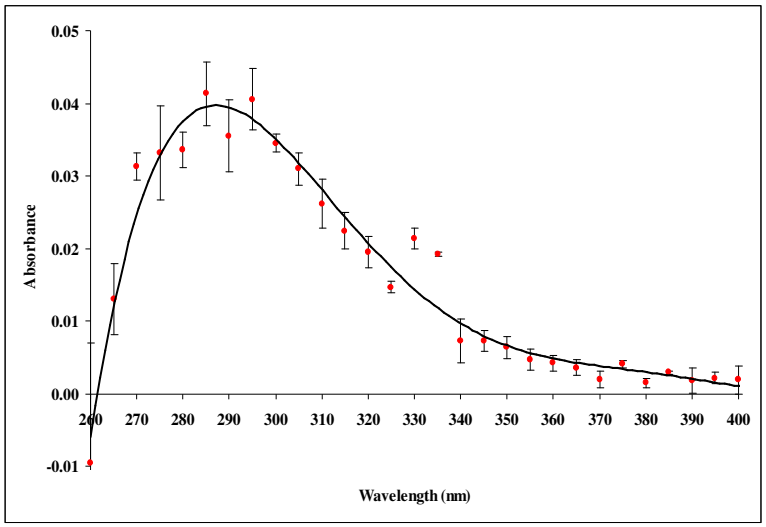

Figure 5.12. Transient absorption spectrum of neat methanol based on the absorption 2 μs after a 3 μs pulse and a dose of 100 Gy/pulse ([MeOH] = 24.7 mol dm^{-3}, argon saturated).

Since methanol was the predominant constituent of the 2-EHA/MeOH solutions investigated in this study, most of the energy deposited by the electron beam irradiation will generate radiolytic species of this solvent, particularly hydroxymethyl radicals. These species may then react with the acrylate to form species which are capable of initiating the polymerization reaction. The transient absorption spectrum for a 32.7 mol% 2-EHA / 67.3 mol% MeOH solution before and after subtraction of the neat methanol transient spectrum is shown in figure 5.13. After subtraction, the overall shape of the 2-EHA/MeOH spectrum remains the same, but the absorption maximum region is located in a slightly longer wavelength region. This phenomenon is what would be expected

based on observation of the shape of the neat MeOH transient spectrum, which suggests that methanol makes an increasing contribution to the absorbance observed in 2-EHA/MeOH solutions as the wavelength becomes shorter.

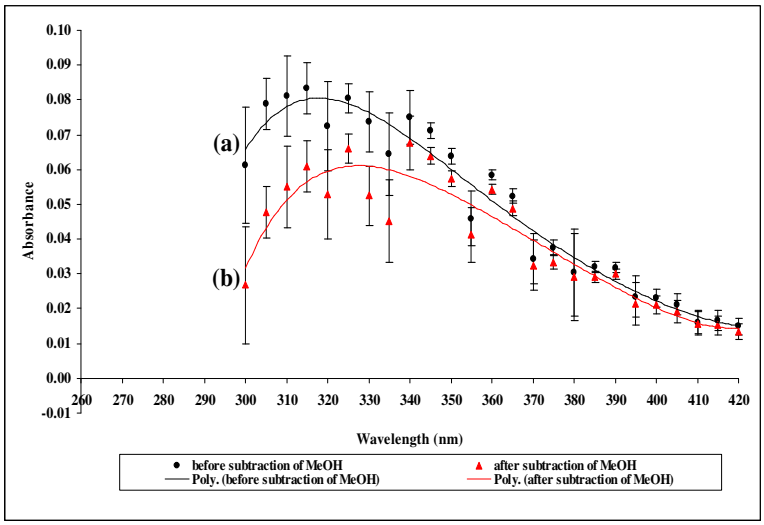

Figure 5.13. Transient absorption spectrum of a 2-EHA/MeOH solution based on the absorption 2 μs after a 3 μs pulse and a dose of 100 Gy/pulse ([2-EHA] = 3.36 mol dm^{-3} (32.7 mol%), [MeOH] = 6.92 mol dm^{-3} (67.3 mol%), argon saturated) (a) before subtraction of the MeOH spectrum and (b) after subtraction of the MeOH spectrum.

The homopolymerization of 2-EHA in methanol is expected to take place in the manner shown in figure 5.14. Hydroxymethyl radicals are the first generation of transient which can be observed using the experimental setup employed in this work (3 μs pulse width, ≤ 100 Gy/pulse, [2-EHA] = 3.36 mol dm^{-3} (32.7 mol%), [MeOH] = 6.92 mol dm^{-3} (67.3 mol%)). A 2-EHA monomer molecule can add to this hydroxymethyl radical to form a solvent-monomer radical adduct, which can then undergo the propagation and termination steps of the reaction. We propose that the transients observed in the 320 – 330 nm absorption maximum range of the subtracted 2-EHA/MeOH spectrum shown in figure 5.13 are a mixture of MeOH/2-EHA radical adducts 2-EHA monomer radicals. Notice that the value of the absorbance in the 2-

EHA/MeOH solution in this range even after subtraction of methanol ($A_{2\mu s}^{320nm}$ = 0.035 ± 0.004) is approximately twice that obtained at the absorption maximum for transients in neat 2-EHA ($A_{2\mu s}^{320nm}$ = 0.017 ± 0.003). This may be due to an enhancement in the rate of production of the 2-EHA radical in the presence of methanol.

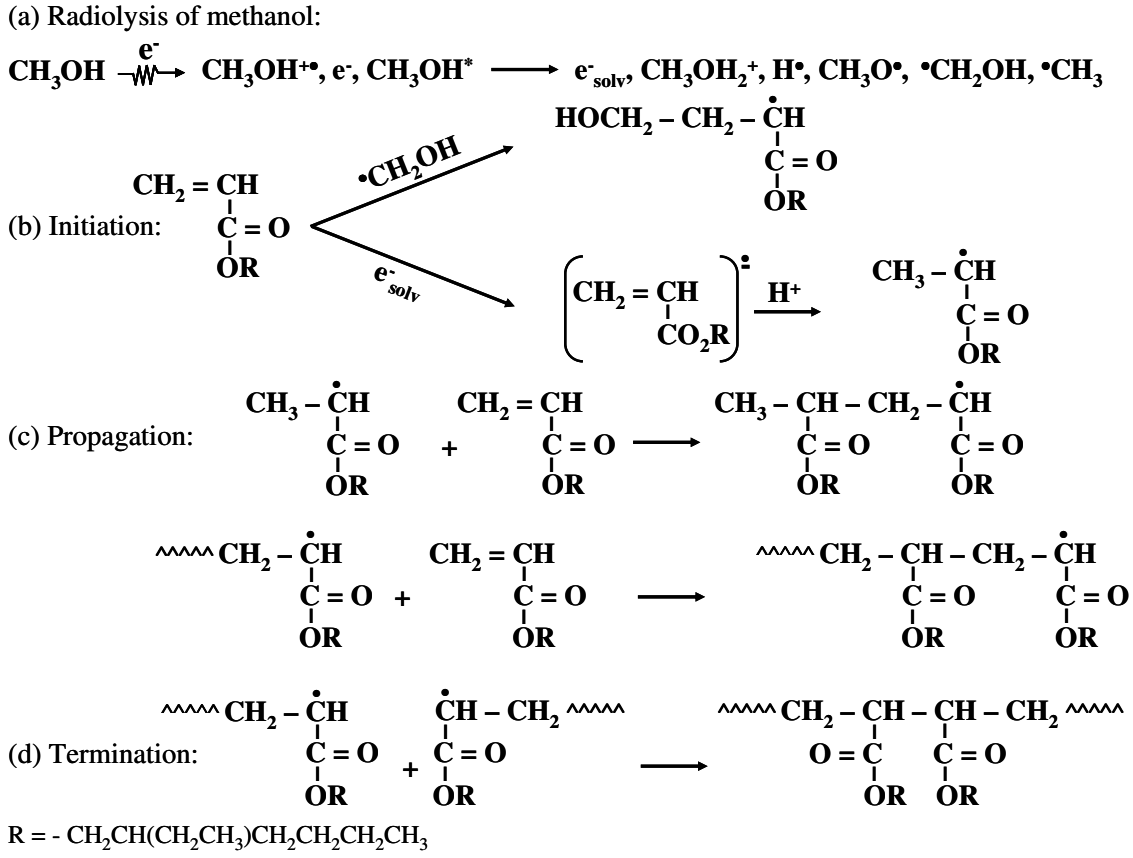

Figure 5.14. Homopolymerization of 2-EHA in MeOH (a) radiolysis of MeOH, (b) initiation, (c) propagation, (d) termination.

According to the reaction mechanism shown in figure 5.14, the major transient species expected to be produced during radiolysis of 2-EHA/MeOH solutions are similar to those produced in neat 2-EHA (radical anions, neutral free radicals, propagating radicals, etc....), except that there will also be a substantial number of hydroxymethyl

radicals produced in addition. Methanol is anticipated to affect mostly the mechanism and rate of the initiation step of the reaction. Measurement of the pH of the 2-EHA/MeOH solutions studied in this work indicated greater acidity ($[H^+] = 1 \times 10^{-5}$ mol dm^{-3}) compared to neat 2-EHA ($[H^+] = 1 \times 10^{-6}$ mol dm^{-3}). A higher concentration of H^+ in this system compared to that in the neat is expected to lead to faster rates of build-up of the 2-EHA radicals.

5.2.1 Build-up

A typical absorbance build-up curve for the formation of transient species in the 2-EHA/MeOH solutions studied is shown in figure 5.15. The build-up in absorbance that this curve represents should correspond to the production of the solvent-monomer MeOH/2-EHA radical adducts formed in the early stages of the polymerization reaction:

$$A = \log\left(\frac{V_0}{V}\right) = \varepsilon_{MeOH-EHA^\bullet}.[MeOH - EHA^\bullet]l \qquad (66)$$

where $\varepsilon_{MeOH-EHA^\bullet}$ and [MeOH-EHA$^\bullet$] are the molar absorptivity and concentration of the solvent-monomer radical adduct.

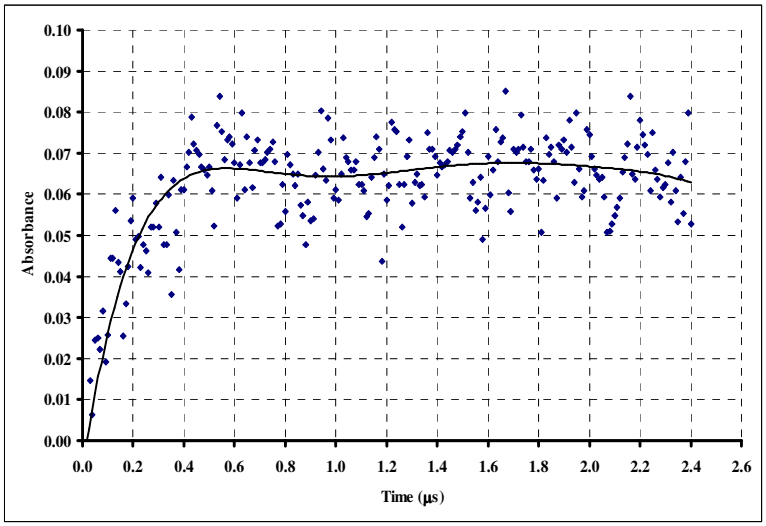

Figure 5.15. Build-up of transients in 2-EHA/MeOH solution ([2-EHA] = 3.36 mol dm^{-3} (32.7 mol%), [MeOH] = 6.92 mol dm^{-3} (67.3 mol%), argon saturated, 330 nm, 100 Gy/pulse, 3 μs pulse width).

We propose that the build-up observed at 330 nm in a 32.7 mol% 2-EHA / 67.3 mol% MeOH solution corresponds to the addition of a 2-EHA monomer molecule to the hydroxymethyl radical to form a solvent-monomer radical adduct. The concentration of the two species participating in this reaction are expected to be comparable enough that this reaction should follow a second order rate law. The rate coefficient for the build-up of transients in 2-EHA/MeOH solution was calculated according to the following equation for a second order rate law:

$$\frac{1}{(A_\infty - A_t)} = \frac{2kt}{\varepsilon_{MeOH-EHA}.l} \qquad (67)$$

where A_∞ is the absorbance 2 μs after the pulse. Figure 5.16 shows a plot of $1/(A_\infty - A_t)$ vs. t which was used to calculate this rate coefficient within the first μs after the pulse.

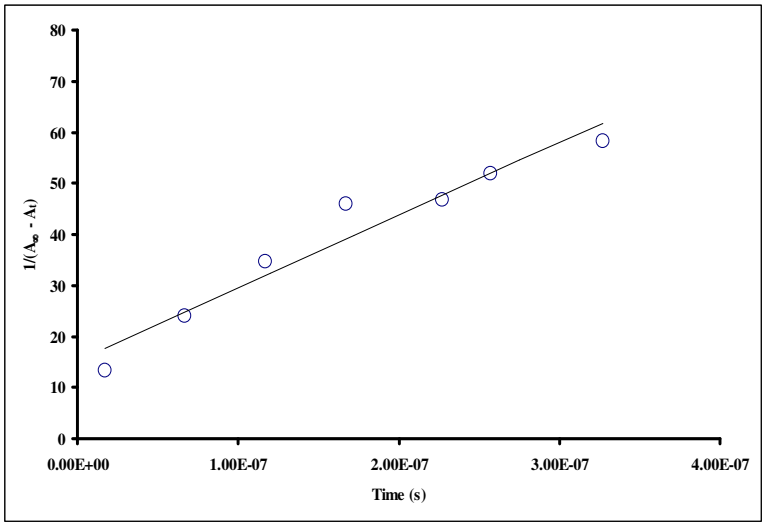

Figure 5.16. Straight line fitted to data for the build-up of transient species in 2-EHA/MeOH solution to a second order rate law ([2-EHA] = 3.36 mol dm^{-3} (32.7 mol%), [MeOH] = 6.92 mol dm^{-3} (67.3 mol%), argon saturated, 330 nm, 100 Gy/pulse, 3 μs pulse width).

The slope of the trend line from this plot is proportional to the rate constant associated with this build-up (slope = $2k / \varepsilon_{MeOH-EHA\bullet} . l$). Table 5.3 shows the results of three repeat calculations of the rate coefficient for build-up in 2-EHA/MeOH solution.

Table 5.3. Rate coefficients for the build-up of transients in 2-EHA/MeOH solution.

[2-EHA] (mol dm^{-3})	[MeOH] (mol dm^{-3})	Dose/ pulse (Gy)	Wavelength (nm)	Path length (cm)	$2k / \varepsilon_{MeOH-EHA\bullet} . l$ (s^{-1})	$k_{obs}\varepsilon_{MeOH\text{-}EHA\bullet}$
3.36	6.92	100	330	3	1.62×10^8	1.08×10^8
3.36	6.92	100	330	3	8.46×10^8	5.64×10^8
3.36	6.92	100	330	3	1.42×10^8	0.947×10^8

After removal of the 5.64×10^8 result as an outlier, an average of the other two results gave an observed rate coefficient for build-up of transients in 2-EHA/MeOH solution as $k_{obs} = ((1 \pm 0.07) \times 10^8)\varepsilon_{MeOH\text{-}EHA\bullet}$. This rate coefficient is reported in terms of the molar absorptivity of the MeOH-EHA radical adduct since the value for this property could not be found in any published reports on the chemistry of these compounds. The rate build-

up of transients in 2-EHA/MeOH solution is smaller but is the same order of magnitude as in neat 2-EHA. A slightly slower build-up of 2-EHA radicals in solution is expected since these radicals are formed in a less direct manner than they are in the neat.

5.2.2 Decay

Figure 5.17 shows a typical decay curve for transients produced after a single pulse of electron irradiation in 32.7 mol% 2-EHA / 67.3 mol% MeOH solution. This absorption decay should correspond to the consumption of 2-EHA chain radicals, and may be described by equation (62). It represents the propagation step of the reaction and is expected to follow pseudo-first order kinetics since the unreacted 2-EHA monomer concentration during this time range should remain so large compared to the concentration or 2-EHA radical produced ($[EHA]_0 >> [EHA^{\bullet}]$) that it may be considered to remain 'constant'.

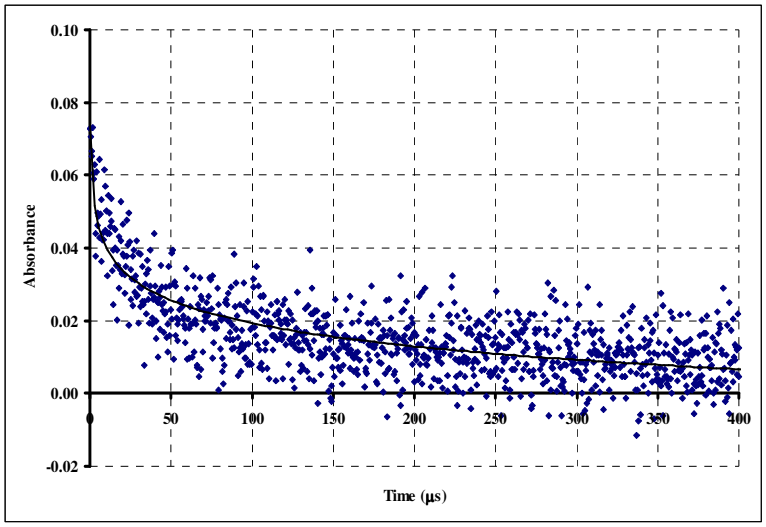

Figure 5.17. Decay of transients in 2-EHA/MeOH solution ([2-EHA] = 3.36 mol dm^{-3} (32.7 mol%), [MeOH] = 6.92 mol dm^{-3} (67.3 mol%), argon saturated, 330 nm, 100 Gy/pulse, 3 µs pulse width).

A pseudo-first order rate law (described by equation (64)) was fitted to the decay shown in figure 5.17. A plot of ln (A_t) vs. t was then used to determine the rate coefficient associated with this decay, and is shown in figure 5.18.

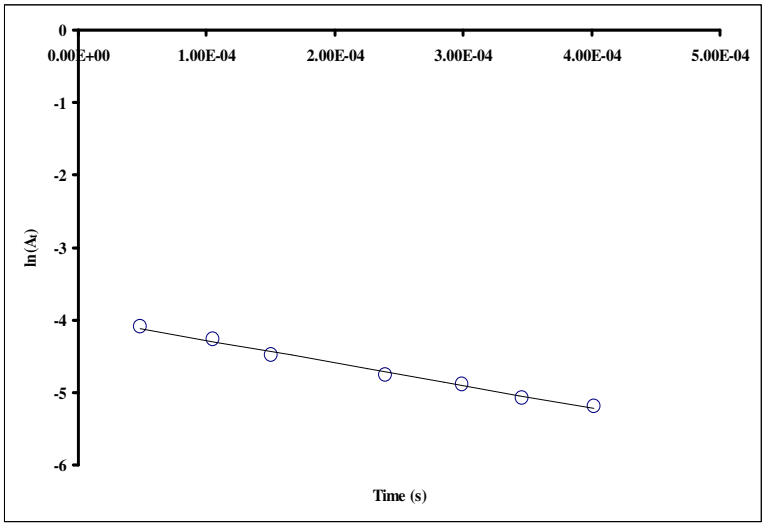

Figure 5.18. Straight line fitted to data for the decay of transient species in 2-EHA/MeOH solution to a pseudo-first order rate law within the first 400 μs after the pulse ([2-EHA] = 3.36 mol dm^{-3} (32.7 mol%), [MeOH] = 6.92 mol dm^{-3} (67.3 mol%), argon saturated, 330 nm, 100 Gy/pulse, 3 μs pulse width).

The slope of the trend line from this plot is proportional to the rate coefficient associated with the decay (slope = $-k_p[EHA]_0$). This slope is then divided by the initial concentration of 2-EHA monomer to calculate the rate coefficient of propagation as follows:

$$k_p = \frac{2.78\times10^4}{[EHA]_0} = \frac{2.78\times10^4}{3.36} = 8.27\times10^3\, mol^{-1} dm^3 s^{-1} \qquad (68)$$

where $[EHA]_0$ = 3.36 mol dm^{-3} is the initial concentration of 2-EHA monomer in the solution. Table 5.4 shows the results of three repeat calculations of this type for the rate coefficient associated with the decay within the first 400 μs after the pulse.

Table 5.4. Rate coefficients for the decay of transients in 2-EHA/MeOH solutions.

[2-EHA] (mol dm^{-3})	[MeOH] (mol dm^{-3})	Dose/ pulse (Gy)	Wavelength (nm)	Path length (cm)	$k_p[EHA]_0$ (s^{-1})	k_p (mol^{-1} dm^3 s^{-1})
3.36	6.92	100	330	3	2.78×10^4	8.27×10^3
3.36	6.92	100	330	3	3.72×10^4	10.1×10^3
3.36	6.92	100	330	3	2.57×10^4	7.65×10^3

An average of the three results gave an average rate coefficient for the decay of transients in 2-EHA/MeOH solution as $k_p = (9 \pm 1) \times 10^3$ mol^{-1} dm^3 s^{-1}. This value is an order of magnitude greater than that obtained from our measurements of this rate coefficient for 2-EHA in the neat ($k_p = ((5 \pm 1) \times 10^2$ mol^{-1} dm^3 s^{-1}). The faster decay observed for 2-EHA propagating radicals in solution may be due to contributions from chain transfer reactions with the MeOH solvent which competes with the addition of 2-EHA monomers to the growing chain.

5.3 Mixtures of 2-Ethylhexyl Acrylate and Acrylic Acid

Most of the pulse radiolysis investigations involving acrylic acid have been in dilute aqueous solutions of this compound in its polymeric form [57, 58]. These studies usually focus on the reaction of radiolytic species generated from water with poly(acrylic acid) to induce a crosslinking reaction [59]. Kinetic studies of acrylic acid in the neat have been reported under air-saturated conditions, since this compound in its deaerated form tends to polymerize very quickly and become cloudy upon irradiation. A study by

Pankasem *et al.* reported free radicals as the dominant radiolytic species produced in neat aerated acrylic acid, due to the enormous sensitivity of the polymerization reaction to oxygen [60].

The synthesis of a 2-EHA/AA copolymer is expected to proceed in the manner shown in figure 5.19. Upon irradiation of a mixture of the acrylate and acrylic acid monomers, initiation will take place primarily through the generation of carbon-centered 2-EHA free radicals, since this is the constituent of highest concentration in the system. The propagation reaction will then proceed by head-to-tail addition of acrylic acid and acrylate monomers. The propagating species will possess the radical centered on the more highly substituted carbon of the vinyl group of the monomer that has added to the growing chain. Termination of the polymerization reaction takes place primarily through a bimolecular combination mechanism [5, 11, 17, 18].

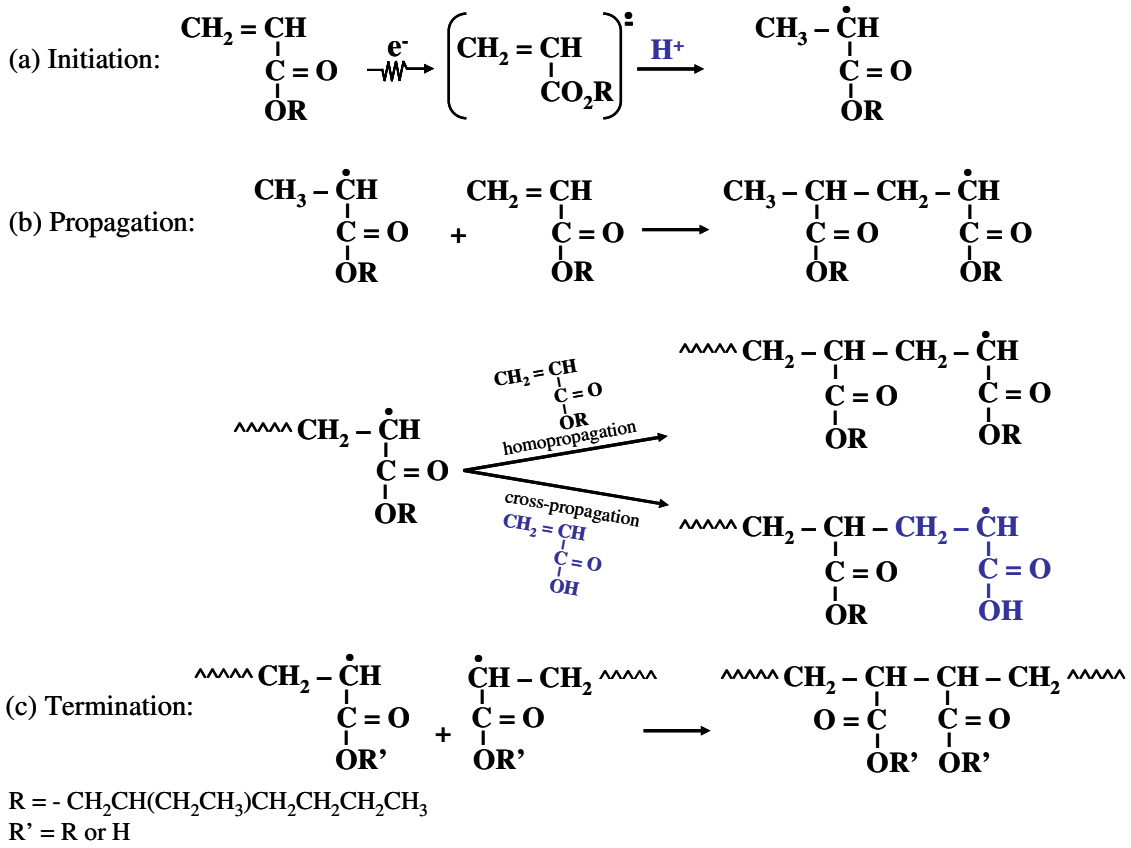

Figure 5.19. Copolymerization of 2-ethylhexyl acrylate and acrylic acid (a) initiation, (b) propagation, and (c) termination.

5.3.1 Build-up

A typical absorbance build-up curve for the formation of transient species in the 2-EHA/AA mixtures studied in this work is shown in figure 5.20. The build-up in absorbance that this curve represents should correspond to the production of neutral 2-EHA monomer radicals. The absorbance is assigned to this species because the initial concentration of 2-EHA monomer is greater than that of the AA monomer. We thus propose that the absorbance measured during this build-up can be described by equation (60). However, the neutralization step of the reaction is influenced by the presence of acrylic acid, which may generate a higher concentration of H^+ ions. Measurement of the

pH of the 4.7 mol% 2-EHA / 25.3 mol% AA mixtures studied in this work indicated proton concentrations of $[H^+] = 1 \times 10^{-4}$ mol dm^{-3}. This is anticipated to cause the rate of build-up in the neutral 2-EHA radical to be faster in the presence of AA than it is in the neat.

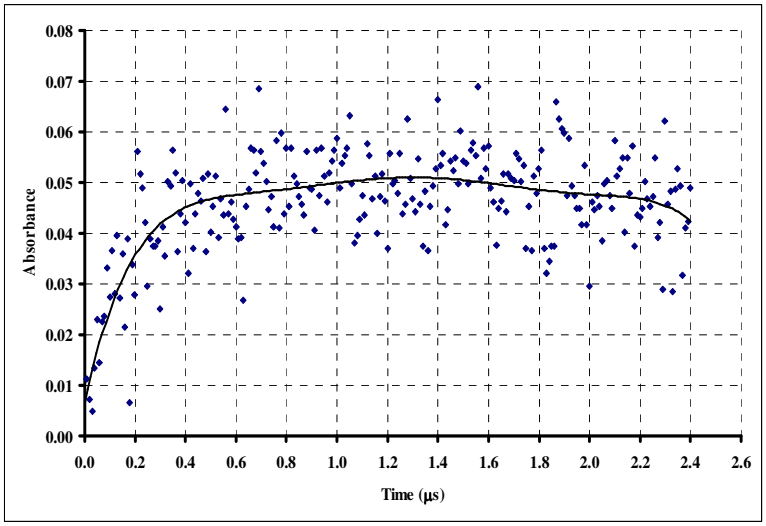

Figure 5.20. Build-up of transients in a 2-EHA/AA mixture ([2-EHA] = 4.32 mol dm^{-3} (74.7 mol%), [AA] = 1.46 mol dm^{-3} (25.3 mol%), argon saturated, 330 nm, 80 Gy/pulse, 3 μs pulse width).

The concentration of H^+ ions during the time period that the build-up curve shown in figure 5.20 was measured is assumed to be so large compared to the concentration of 2-EHA monomer radicals produced ($[H^+]_0 >> [EHA^\bullet]$) that it may be considered to remain 'constant'. The build-up of transients in 4.7 mol% 2-EHA / 25.3 mol% AA mixtures is therefore expected to follow a pseudo-first order rate law, which is described by the following equation:

$$\ln(A_t) - \ln(A_0) = k[H^+]_0 t \qquad (69)$$

where $[H^+]_0 = 1 \times 10^{-4}$ mol dm^{-3} is the initial concentration of H^+ ions in a 74.7 mol% 2-EHA / 25.3 mol% AA mixture. The presence of acrylic acid is thus expected to transform the rate of 2-EHA monomer radical build-up from second order (in the neat) to pseudo-first order.

The rate coefficient associated with the build-up of transients in a 74.7 mol% 2-EHA / 25.3 mol% AA mixture may be determined from a plot of ln (A_t) vs. t. Figure 5.21 shows a plot of a straight line fitted to the data.

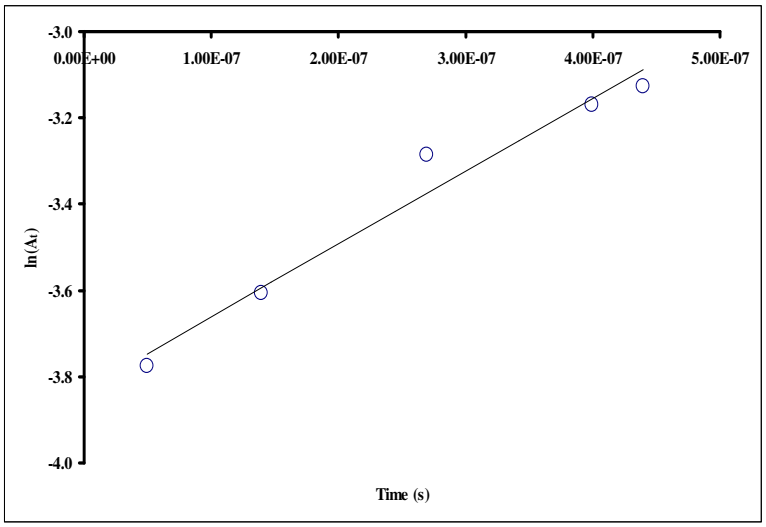

Figure 5.21. Straight line fitted to data for the build-up of transient species in a 2-EHA/AA mixture to a pseudo-first order rate law within the first μs after the pulse ([2-EHA] = 4.32 mol dm^{-3} (74.7 mol%), [AA] = 1.46 mol dm^{-3} (25.3 mol%), argon saturated, 330 nm, 80 Gy/pulse, 3 μs pulse width).

The slope of the line from this plot is proportional to the rate coefficient which corresponds to the build-up (slope = $k[H^+]_0$). Thus since the concentration of H^+ ions is assumed to remain 'constant' throughout this time period, the experimentally determined slope must be divided by this concentration in order to obtain the actual rate coefficient

associated with this build-up. The slope of the line shown in figure 5.21 may be used to calculate this rate coefficient as follows:

$$k = \frac{1.69 \times 10^6}{[H^+]_0} = \frac{1.69 \times 10^6}{1 \times 10^{-4}} = 1.69 \times 10^{10}\, mol^{-1} dm^3 s^{-1} \qquad (70)$$

k is an empirical rate coefficient characterizing the build-up of radicals in the mixed 2-EHA/AA system. Table 5.5 shows the results of five repeat calculations of this type for the rate coefficient associated with the build-up in a 74.7 mol% 2-EHA / 25.3 mol% AA mixture within the first μs after the pulse.

Table 5.5. Rate coefficients for the build-up of transients in 2-EHA/AA mixtures.

[2-EHA] (mol dm^{-3})	[AA] (mol dm^{-3})	Dose/ pulse (Gy)	Wavelength (nm)	Path length (cm)	$k[H^+]_0$ (s^{-1})	k (mol^{-1} dm^3 s^{-1})
4.32	1.46	80	330	3	1.26×10^6	1.26×10^{10}
4.32	1.46	80	330	3	1.69×10^6	1.69×10^{10}
4.32	1.46	80	330	3	1.89×10^6	1.89×10^{10}
4.32	1.46	80	330	3	1.63×10^6	1.63×10^{10}
4.32	1.46	80	330	3	1.18×10^6	1.18×10^{10}

An average rate coefficient for the build-up of transients in a 74.7 mol% 2-EHA / 25.3 mol% AA mixture was found to be $k = (1.5 \pm 0.3) \times 10^{10}$ mol^{-1} dm^3 s^{-1}.

5.4 Mixtures of 2-Ethylhexyl Acrylate and Acrylic Acid in Methanol

Methanol is the predominant constituent of the 2-EHA/AA/MeOH solutions studied in this work, thus most of the electron beam energy will be deposited on this solvent to generate hydroxymethyl radicals. These solvent radicals will then react with 2-

EHA to produce acrylate monomer radicals, which then undergo propagation and termination. Acrylic acid is expected to participate in the neutralization step of any acrylate monomer radical anions that are produced, and to also undergo copolymerization with 2-EHA.

The transient absorption spectrum for a 33.4 mol% 2-EHA / 10.1 mol% AA / 56.5 mol% MeOH solution is shown in figure 5.22. Although it contains regions of enhanced absorption in the 300 - 310 and 350 - 370 nm wavelength ranges, it does not appear to possess a clearly defined absorption maximum.

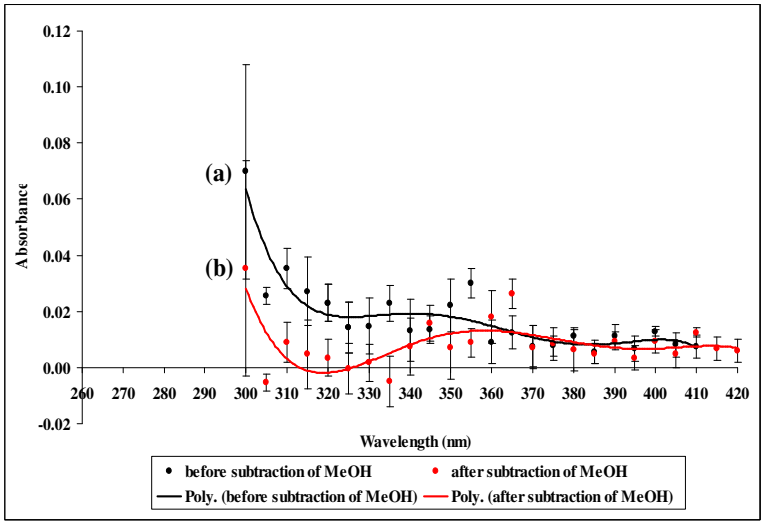

Figure 5.22. Transient absorption spectrum of a 2-EHA/AA/MeOH solution based on the absorption 2 μs after a 3 μs pulse and a dose of 80 Gy/pulse ([2-EHA] = 3.36 mol dm^{-3} (33.4 mol%), [AA] = 1.02 mol dm^{-3} (10.1 mol%), [MeOH] = 5.68 mol dm^{-3} (56.5 mol%), argon saturated) (a) before subtraction of the MeOH spectrum and (b) after subtraction of the MeOH spectrum.

5.4.1 Build-up

A typical absorbance build-up curve for the formation of transient species in the 2-EHA/AA/MeOH solutions is shown in figure 5.23. The build-up in absorbance that this curve represents should correspond to the production of the solvent-monomer

MeOH/2-EHA radical adducts that are expected to form during the early stages of the polymerization reaction, as described by equation (66). However, the rate of this build-up is also expected to be influenced by the presence of acrylic acid, which will change the H^+ ion concentration in the system and affect the rate of neutralization of any 2-EHA radical anions which may be present in the system.

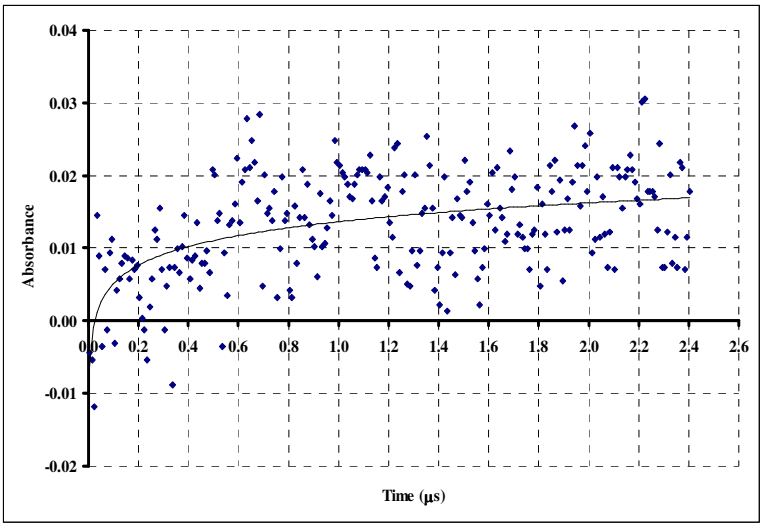

Figure 5.23. Build-up of transients in a 2-EHA/AA/MeOH solution (argon saturated, [2-EHA] = 3.36 mol dm^{-3} (33.4 mol%), [AA] = 1.02 mol dm^{-3} (10.1 mol%), [MeOH] = 5.68 mol dm^{-3} (56.5 mol%), 330 nm, 43 Gy/pulse, 3 μs pulse width).

The presence of both AA and MeOH in the system (which leads to $[H^+]_0 >> [EHA^\bullet]$) is expected to cause this build-up in 2-EHA monomer radicals to follow pseudo-first order kinetics, as is described by equation (68). In the case of a 33.4 mol% 2-EHA / 10.1 mol% AA / 56.5 mol% MeOH solution, the initial concentration of protons is $[H^+]_0 = 1 \times 10^{-3}$ mol dm^{-3}. The rate coefficient of this build-up can be determined from a plot of ln (A_t) vs. t, which is shown in figure 5.24.

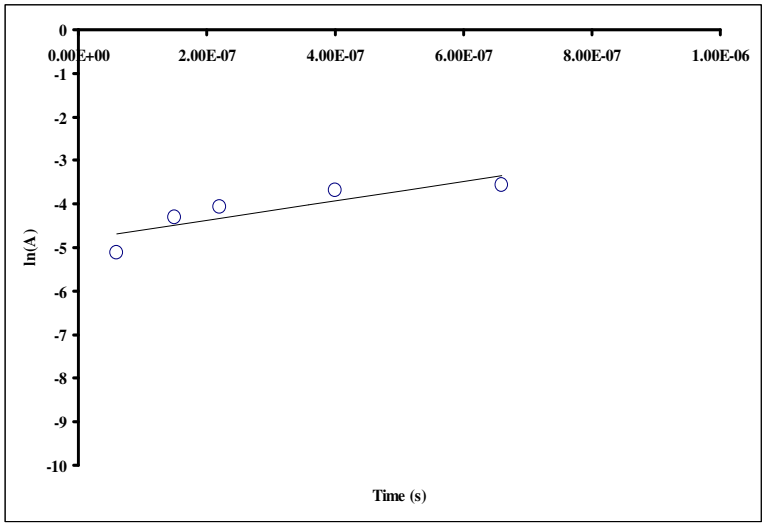

Figure 5.24. Straight line fitted to data for the build-up of transient species in a 2-EHA/AA/MeOH solution to a pseudo-first order rate law within the first μs after the pulse ([2-EHA] = 3.36 mol dm^{-3} (33.4 mol%), [AA] = 1.02 mol dm^{-3} (10.1 mol%), [MeOH] = 5.68 mol dm^{-3} (56.5 mol%), argon saturated, 330 nm, 43 Gy/pulse, 3 μs pulse width).

The slope of the line from this plot should be proportional to the rate coefficient associated with this build-up (slope = $k[H^+]_0$). The rate coefficient is calculated by dividing the observed slope by the initial concentration of H^+ ions. Table 5.6 shows the results of six repeat calculations of this type for the rate coefficient of the build-up in a 33.4 mol% 2-EHA / 10.1 mol% AA / 56.5 mol% MeOH solution within the first μs after the pulse.

Table 5.6. Rate coefficients for the build-up of transients in 2-EHA/AA/MeOH solutions.

[2-EHA] (mol dm^{-3})	[AA] (mol dm^{-3})	[MeOH] (mol dm^{-3})	$k[H^+]_0$ (s^{-1})	k (mol^{-1} dm^3 s^{-1})
3.36	1.02	5.68	1.31×10^6	1.31×10^9
3.36	1.02	5.68	3.39×10^6	3.39×10^9
3.36	1.02	5.68	2.25×10^6	2.25×10^9
3.36	1.02	5.68	3.81×10^6	3.81×10^9
3.36	1.02	5.68	3.02×10^6	3.02×10^9
3.36	1.02	5.68	1.13×10^6	1.13×10^9

An average rate coefficient for the build-up of transients in a 33.4 mol% 2-EHA / 10.1 mol% AA / 56.5 mol% MeOH solution was found to be $k = (2.5 \pm 1) \times 10^9$ mol^{-1} dm^3 s^{-1}.

5.4.2 Decay

Figure 5.25 shows a typical decay curve for transients produced after a single pulse of electron irradiation in a 3.4 mol% 2-EHA / 10.1 mol% AA / 56.5 mol% MeOH solution. This decay in the absorption should correspond to the consumption of 2-EHA monomeric radicals as they undergo the propagation step of the reaction.

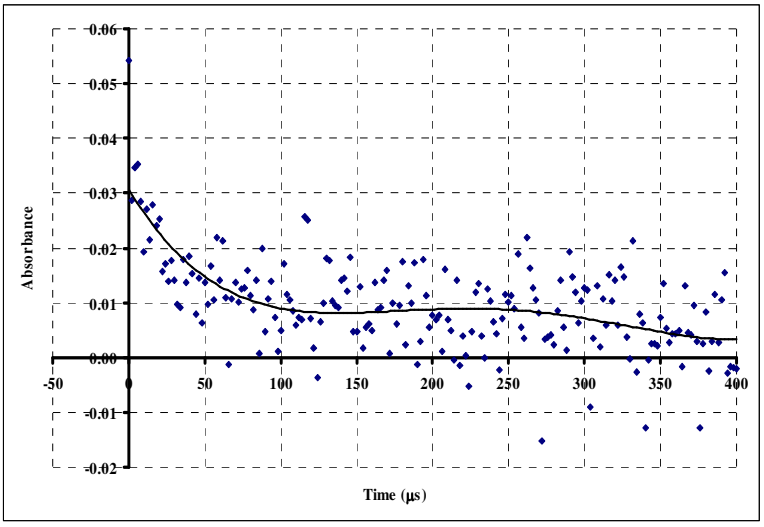

Figure 5.25. Decay of transients in 2-EHA/AA/MeOH solution ([2-EHA] = 3.36 mol dm^{-3} (33.4 mol%), [AA] = 1.02 mol dm^{-3} (10.1 mol%), [MeOH] = 5.68 mol dm^{-3} (56.5 mol%), argon saturated, 330 nm, 51 Gy/pulse, 3 μs pulse width).

This decay may be fitted by a pseudo-first order rate law. A plot of ln (A_t) vs. t can then be used to determine the rate coefficient associated with this decay, and is shown in figure 5.26.

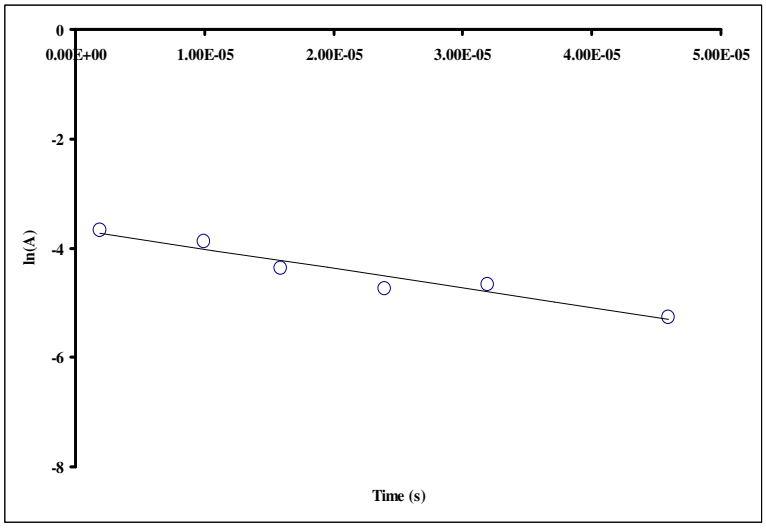

Figure 5.26. Straight line fitted to data for the decay of transient species in 2-EHA/AA/MeOH solution to a pseudo-first order rate law ([2-EHA] = 3.36 mol dm^{-3} (33.4 mol%), [AA] = 1.02 mol dm^{-3} (10.1 mol%), [MeOH] = 5.68 mol dm^{-3} (56.5 mol%), argon saturated, 330 nm, 51 Gy/pulse, 3 μs pulse width).

The slope of the line from this plot is proportional to the rate coefficient which corresponds to the decay (slope = $-k_p[EHA]_0$), and it is divided by the initial concentration of 2-EHA monomer to determine the rate coefficient of propagation. Table 5.7 shows the results of three repeat calculations of this type for the rate coefficient associated with the decay within the first 50 μs after the pulse.

Table 5.7. Rate coefficients for the decay of transients in 2-EHA/AA/MeOH solutions.

[2-EHA] (mol dm^{-3})	[AA] (mol dm^{-3})	[MeOH] (mol dm^{-3})	$k_p[EHA]_0$ (s^{-1})	k_p (mol^{-1} dm^3 s^{-1})
3.36	1.02	5.68	3.47×10^4	1.03×10^4
3.36	1.02	5.68	4.57×10^4	1.36×10^4
3.36	1.02	5.68	3.59×10^4	1.07×10^4

An average rate coefficient of $k_p = (1 \pm 0.1) \times 10^4$ mol^{-1} dm^3 s^{-1} was obtained for the decay of transients in a 3.4 mol% 2-EHA / 10.1 mol% AA / 56.5 mol% MeOH solution. This value is of the same order of magnitude as that obtained in the 2-EHA/MeOH

solutions investigated, which makes sense since the initial concentration of 2-EHA monomer in both of these solutions is the same. It also supports our proposition that acrylic acid is more influential in the rate of the initiating steps of the reaction (although it is undergoing copolymerization with the 2-EHA), whereas the rate of the propagation step of the reaction is not as affected by the presence of AA.

5.5 Summary of Results and Conclusions

Table 5.8. Summary of pulse radiolysis results.

	Composition (mol dm^{-3})	Build-up	Decay
Neat 2-EHA	[2-EHA] = 4.80	A_{max}: 310-330 nm 2nd order **$k = ((7 \pm 3) \times 10^8)\varepsilon_{EHA\bullet}$**	A_{max}: 310–330 nm 360 – 370 nm 2nd order **$k_p = (5 \pm 1) \times 10^2$ mol^{-1} dm^3 s^{-1}**
2-EHA/MeOH	[2-EHA] = 3.36 [MeOH] = 6.92	A_{max}: (i) 280-290 nm (ii) 310-330 nm 2nd order **$k = ((1 \pm 0.1) \times 10^8)\varepsilon_{EHA\bullet}$**	2nd order **$k_p = (9 \pm 1) \times 10^3$ mol^{-1} dm^3 s^{-1}**
2-EHA/AA	[2-EHA] = 4.32 [AA] = 1.46	2nd order **$k = (1.5 \pm 0.3) \times 10^{10}$ mol^{-1} dm^3 s^{-1}**	N/A
2-EHA/AA/MeOH	[2-EHA] = 3.36 [AA] = 1.02 [MeOH] = 5.68	2nd order **$k = (2.5 \pm 1) \times 10^9$ mol^{-1} dm^3 s^{-1}**	2nd order **$k_p = (1 \pm 0.1) \times 10^4$ mol^{-1} dm^3 s^{-1}**

Pulse radiolysis investigations have demonstrated the presence of initiating 2-EHA monomer radicals in the 310 - 330 nm wavelength range, and oligomeric radicals in the 360 - 370 nm wavelength range. The build-up in absorbance of these free radicals is very fast, and the rate of the build-up is enhanced in the presence of acrylic acid.

The propagation rate coefficient determined from decay curves of the 2-EHA radical measured at 330 nm was observed to be on the same order of magnitude as that

reported by Feng *et al.* (k_p = 280 mol^{-1} dm^3 s^{-1}, measured by PR-KSD), but two orders of magnitude lower than that reported by Beuermann *et al.* (k_p = 12 243 - 18 096 mol^{-1} dm^3 s^{-1}, measured by PLP-MWD). This large difference in propagation rate coefficient may indicate a limitation of the PR-KSD technique used in this work. Propagation rate coefficients of acrylates determined by PLP-MWD have been demonstrated to be significantly reduced when performed at temperatures above 30 °C, due to the predominance of chain transfer to polymer within this temperature range.

6. Poly(2-ethylhexyl acrylate-co-acrylic acid) Ionomer Formation

The most extensively studied type of polymeric matrix for nanocomposite materials is that made of block copolymers. The morphologies of these types of polymers have been heavily investigated and demonstrated to provide a great deal of control over the distribution of inorganic clusters. The main drawback of block copolymers lies in the fact that the synthesis process required is relatively complex, which often limits the types of polymers which may be used for nanocomposites.

One of the most frequently cited investigations of the production of iron oxide nanoparticles in a polymeric matrix was reported by Ziolo *et al* [61]. This study involved the production of γ-Fe_2O_3 in an ion-exchange resin known as Dowex® (manufactured by Dow Chemical Company). The matrix employed in this work was composed of a sulfonated styrene-divinylbenzene copolymer, into which iron was incorporated through mixture with $FeCl_2$ or $FeCl_3$. Sodium hydroxide was used to ion-exchange with the iron to form an iron hydroxide, which was then transformed into oxide nanoclusters through the application of heat and hydrogen peroxide. The sizes of the particles produced were 50 – 100 nm in diameter, and were found not to possess any coercivity or retentivity at room temperature, which is characteristic behavior of superparamagnetic particles.

Although 2-EHA/AA copolymers are widely employed for radiation-cured adhesive applications, there have been no studies demonstrating the use of these materials as matrices for nanocomposites. This chapter includes studies on the synthesis and characterization of 2-EHA/AA ionomeric materials which may serves as precursors to magnetic nanocomposites.

6.1 Ionomer Synthesis

Figure 6.1 shows a schematic drawing of the samples at various stages in the experiment, including the 2-EHA/AA copolymer (a), the copolymer/metal salt mixture (b), and the ionomer (c). Acrylic acid has a tendency to hydrogen bond to itself, and the copolymer structure shown in figure 6.1(a) shows these linkages between the acrylic acid segments. In nonpolar solvents, acrylic acid tends to form hydrogen-bonded cyclic dimers. The formation of this dimer structure is driven by the enhancement of its compatibility with nonpolar environments, since its polarity is reduced by the formation of these hydrogen-bonded bridges [62]. (Its polarity is reduced by the formation of these hydrogen-bonded bridges, thereby enhancing its miscibility with nonpolar environments.)

If the more polar acrylic acid segments of the copolymer microphase separate and form ionic multiplets, these regions may serve to confine inorganic components as they are incorporated into the material. By changing the amount of acrylic acid in the copolymer, the morphology and the sizes of these multiplets can potentially be modified to limit the size of and spacing between the magnetic particles which form.

In addition to serving as a comonomer, acrylic acid functions as a means of incorporation of metal salts into the polymer. When the 2-EHA/AA copolymer is mixed with ferric chloride, and a reaction is expected to take place in which the ferric cations displace the protons of the carboxylic acid groups. Figure 6.1 shows a schematic of the hydrogen-bonded structure of the copolymer (a), and the mixture of this copolymer with ferric chloride (b). The hydrogen bonding between carboxylic acid groups may be intermolecular, intramolecular, or a combination of both types. Although two and three

acid groups are expected to associate with each ferrous and ferric cation, respectively, these structures have not yet been confirmed by experiment. Iron may also exist in a number of hydroxide forms (e.g., $FeOH^{+}$, $FeOH^{2+}$, $Fe(OH)_2^{+}$), depending on the pH of the system. An ionomer is formed after the removal of the unassociated hydrogen and acetate or chloride ions through dialysis, and FTIR spectroscopy provides a means of identifying the formation of the ionomer. This ionomer may then serve as a precursor to a nanocomposite material.

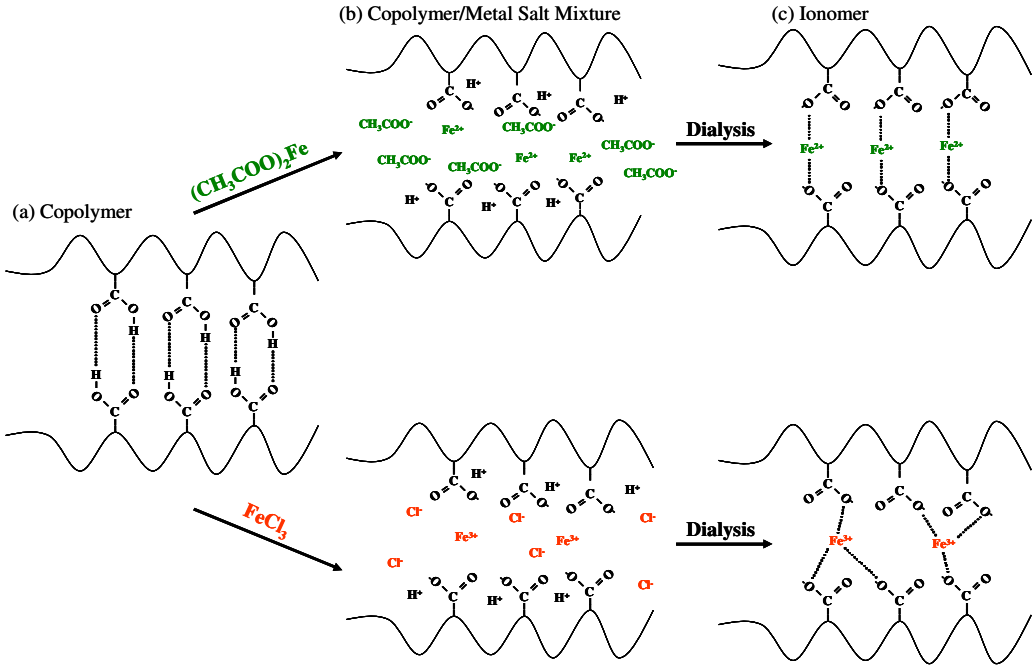

Figure 6.1. Schematic drawing of (a) copolymer, (b) copolymer/metal salt mixture, (c) ionomer.

6.2 Ionomer Characterization

6.2.1 FTIR Spectroscopy

Figure 6.2 shows the FTIR-ATR spectrum of 2-ethylhexyl acrylate monomer. The spectral assignments for each band displayed in this spectrum are shown in table 6.1.

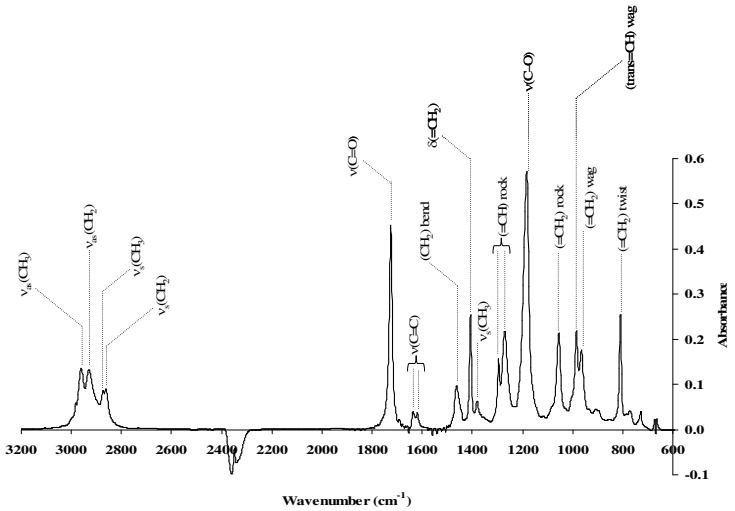

Figure 6.2. FTIR-ATR spectrum of 2-ethylhexyl acrylate monomer.

Table 6.1. FTIR-ATR spectral assignments for 2-ethylhexyl acrylate monomer.

Wavenumber (cm^{-1})	Assignment
2960	$\nu_{as}(CH_3)$ asymmetric stretch
2930	$\nu_{as}(CH_2)$ asymmetric stretch
2877	$\nu_s(CH_3)$ symmetric stretch
2875	$\nu_s(CH_2)$ symmetric stretch
1730	$\nu_s(C=O)$ symmetric stretch
1640	ν(C=C) stretch
1620	ν(C=C) stretch
1470	$\delta(CH_2)$ bend
1410	$\delta(=CH_2)$ bend
1380	$\delta(CH_3)$ bend
1300, 1270	(=CH) rock
1185	ν(C-O) stretch
1060	$(=CH_2)$ rock
990	(trans-CH) wag
960	$(=CH_2)$ wag
810	$(=CH_2)$ twist

Figure 6.3 shows the FTIR-ATR spectrum of acrylic acid monomer. The spectral assignments for each band displayed in this spectrum are shown in table 6.2.

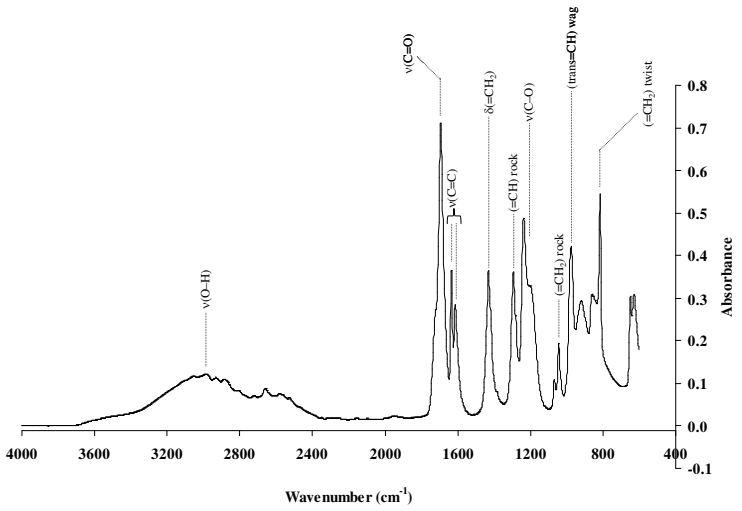

Figure 6.3. FTIR-ATR spectrum of acrylic acid monomer.

Table 6.2. FTIR-ATR spectral assignments for acrylic acid monomer.

Wavenumber (cm^{-1})	Assignment
3000	ν(O-H) stretch
1695	ν_s(C=O) symmetric stretch
1635	ν(C=C) stretch
1630	ν(C=C) stretch
1430	δ(CH_2) bend
1295	(=CH) rock
1240	ν(C-O) stretch
1045	(=CH_2) rock
975	(trans-CH) wag
815	(=CH_2) twist

Figure 6.4 shows an overlay of the FTIR spectra of 2-EHA and AA monomers and suggested peak assignments. Notice that there is overlap of almost every band in the 1100 – 1800 cm^{-1} region of these two compounds. A distinction between these two monomers is thus not made in the spectra of the copolymer and ionomer. A comparison of the individual monomer spectra is important for interpretation of additional FTIR

spectra measured at later stages in the modification of this system, the major steps of which include polymerization and metal incorporation.

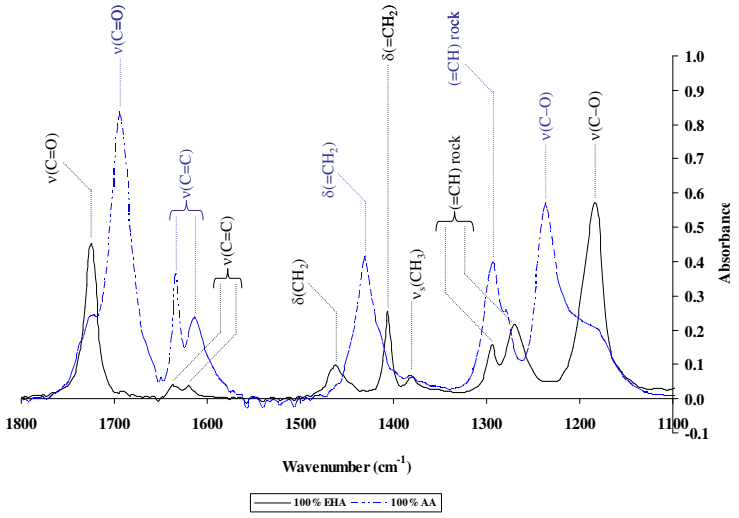

Figure 6.4. Overlay of FTIR-ATR spectra of 2-ethylhexyl acrylate monomer and acrylic acid monomer.

During the copolymerization of 2-EHA and AA, the addition of each new repeat unit to the growing chain involves the breakage of an alkene bond which is transformed into a methylene bond. The total number of alkene bonds in the system should therefore decrease with increased radiation dose and conversion into polymer, and this process may be studied by FTIR spectroscopy [63, 64].

Figure 6.5 shows the overlay of a 2-EHA/AA mixture before and after exposure to γ-irradiation. There are four characteristic alkene absorbances shown in this spectrum: two stretching bands (1637, 1622 cm^{-1}), an olefinic in-plane bending absorbance (1407 cm^{-1}), and an olefinic twisting absorbance (810 cm^{-1}) [65]. These bands may be used to monitor the extent of the polymerization reaction since their relative intensities diminish as the amount of monomer converted into polymer increases.

However, a quantitative analysis of this type was not performed on the copolymers synthesized in this work since there is a great deal of overlap between the 2-EHA and AA bands and it is difficult to distinguish each type of monomer.

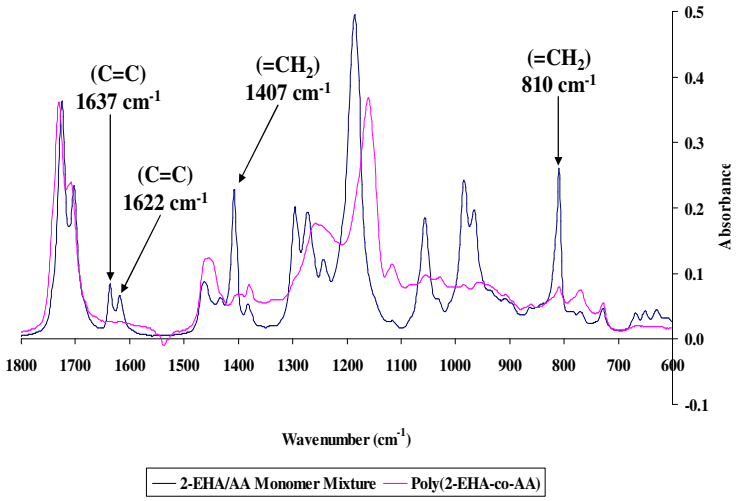

Figure 6.5. FTIR spectrum of a mixture of 2-EHA and AA before and after irradiation (starting monomer composition: [2-EHA] = 4.32 mol dm^{-3} (74.7 mol%), [AA] = 1.46 mol dm^{-3} (25.3 mol%), 100 Gy dose of γ-irradiation, 0.83 Gy s^{-1} dose rate).

The FTIR spectrum of the ionomer formed from ferrous acetate ($Fe(CO_2CH_3)_2$) is shown in figure 6.6 with two different formulated compositions, one of which involves mixture of the copolymer with a 1:2 mole ratio of Fe^{2+} to AA (blue), and the other of which involves mixture with a 2:1 mole ratio of Fe^{2+} to AA (pink). An overlay of the FTIR spectrum of the copolymer (dotted line) shows that after dialysis a new absorbance appears close to 1600 cm^{-1}. This absorbance is associated with an asymmetric stretching vibration of the carboxylic acid salt, and indicates the formation of an ionomer. Aside from the amount of ferrous acetate added to the system to form these ionomers, they were prepared in the same manner. The first step of this involved dissolving the copolymer into THF, followed by addition of the metal salt to the solution. This mixture was then

transferred into a dialysis bag which was then placed into a solvent mixture of chloroform and methanol (1:1 volume ratio of $CHCl_3$ to MeOH; $[CHCl_3]$ = 6.25 mol dm^{-3}, [MeOH] = 12.3 mol dm^{-3}). The FTIR measurements shown in this figure were performed after nine days of dialysis. A more intense absorbance band was observed in the sample to which a greater concentration of the metal salt was added.

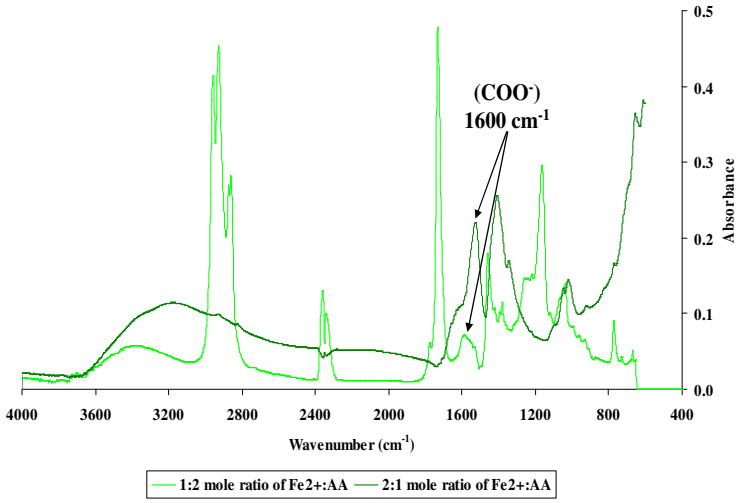

Figure 6.6. FTIR spectra of poly(2-EHA-co-AA)/Fe^{2+} ionomer formed from sample formulated compositions based on 1:2 (blue) and 2:1 (pink) mole ratio of Fe^{2+} to AA (starting monomer composition: [2-EHA] = 4.32 mol dm^{-3} (74.7 mol%), [AA] = 1.46 mol dm^{-3} (25.3 mol%), 100 Gy dose of γ-irradiation, 0.83 Gy s^{-1} dose rate).

The FTIR spectrum of the ionomer formed from ferric chloride ($FeCl_3$) is shown in figure 6.7 with two different formulated compositions, one of which involves mixture of the copolymer with a 1:3 mole ratio of Fe^{3+} to AA (blue), and the other of which involves mixture with a 3:1 mole ratio of Fe^{3+} to AA (pink). An overlay of the FTIR spectrum of the copolymer (dotted line) shows the appearance of the carboxylic acid salt stretch near 1600 cm^{-1}, with the intensity of this band increasing as the concentration of $FeCl_3$. This absorbance is associated with an asymmetric stretching vibration of the

carboxylic acid salt, and indicates the formation of an ionomer. These spectra also show the appearance of a more intense absorbance band in the sample to which a greater concentration of the metal salt was added.

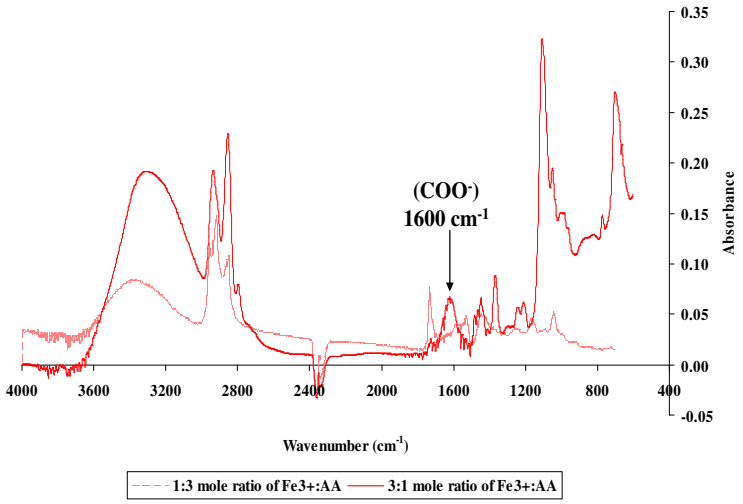

Figure 6.7. FTIR spectra of poly(2-EHA-co-AA)/Fe^{3+} ionomer formed from sample formulated compositions based on 1:3 (blue) and 3:1 (pink) mole ratio of Fe^{3+} to AA (starting monomer composition: [2-EHA] = 4.32 mol dm^{-3} (74.7 mol%), [AA] = 1.46 mol dm^{-3} (25.3 mol%), 100 Gy dose of γ-irradiation, 0.83 Gy s^{-1} dose rate).

The effect of the choice of metal salt used in the formation of the ionomer was investigated through comparison of results obtained from ferrous acetate ($(CH_3COO)_2Fe$) and ferric chloride ($FeCl_3$). The FTIR spectra of ionomers synthesized from a 2-EHA/AA copolymer and each of these metal salts are shown in figure 6.8.

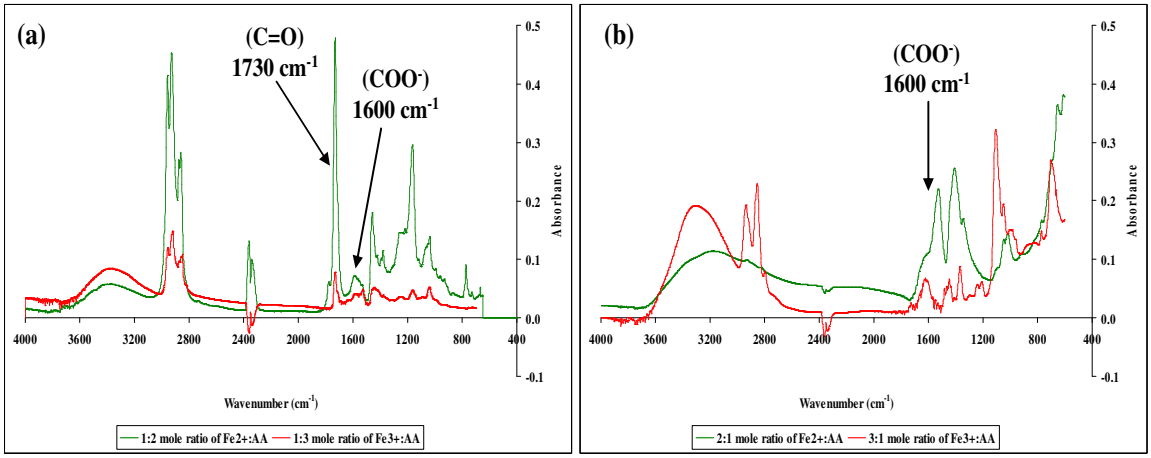

Figure 6.8. FTIR spectra of poly(2-EHA-co-AA)/Fe^{2+} ionomer and poly(2-EHA-co-AA)/Fe^{3+} ionomer made from formulated compositions based on (a) 1:2 and 1:3 mole ratios of Fe^{2+} and Fe^{3+} to AA and (b) 2:1 and 3:1 mole ratios of Fe^{2+} and Fe^{3+} to AA.

At both of the metal salt concentrations investigated, the ionomer containing Fe^{2+} displayed a stronger absorbance at 1600 cm^{-1}. This indicates a greater relative ease of reaction of iron with the copolymer when ferrous acetate is employed.

A study by Clay *et al.* on the effect of the metal salt employed for incorporation of metal into block copolymers reported a similar phenomenon [66]. This investigation included a comparison of the uptake of iron cations from ferrous acetate and ferric chloride into a norbonene block copolymer functionalized with carboxylic acid groups. A greater amount of metal ion uptake was observed when the acetate salt was used, and the explanation for this was given by comparison of the stability constants of the various species which form during the reaction, which may be described as follows:

$$ML_{n-1} + L = ML_n \qquad (71)$$

where *M* is the metal cation, and *L* is the acetate anion (CH_3COO^-). The stability constant for this reaction is given by:

$$K_n = \frac{[ML_n]}{[ML_{n-1}][L]} \tag{72}$$

When metal chloride is used, the reaction leads to the formation of hydrochloric acid (HCl). The stability constant for HCl is zero, so the free H^+ ions in solution inhibit the binding of the metal to the polymer. When metal acetate is used, the reaction leads to the formation of acetic acid (CH_3COOH). The stability constant for acetic acid is relatively high (10^5 (mol dm^{-3})$^{-1}$), thus the ease with which H^+ ions bind to acetate anions facilitates the binding of the metal to the carboxylate anion group of the copolymer. We propose that the stronger 1600 cm^{-1} absorbance band observed from the poly(2-EHA-co-AA) ionomers formed from ferrous acetate is due to the stronger binding of H^+ ions to acetate ions rather than chloride ions. Another contribution to the greater absorbance observed in the spectra of poly(2-EHA-co-AA)/Fe^{2+} ionomers may be due to the fact that ferrous acetate is more miscible with the acrylate copolymer than ferric chloride.

The peak in the FTIR spectra shown in figure 6.8(a) located near 1730 cm^{-1} corresponds to carbonyl group (C=O) stretching, including those associated with both the 2-EHA and AA repeat units. Notice that the FTIR spectra shown in figure 6.8(b) of the ionomers formed from higher concentrations of ferrous acetate and ferric chloride did not show this carbonyl absorbance. The disappearance of this band upon this type of reaction was also reported in the study performed by Clay *et al* [66]. It verifies that metal ions have successfully been incorporated into the copolymer.

6.2.2 X-ray Photoelectron Spectroscopy

Analysis of samples before and after iron incorporation using XPS may be used to study changes in bonding which take place during each step of the modification process, since the binding energy positions and intensities are sensitive to changes in the chemical environment [67]. This technique may be used as an additional means of studying the interactions that take place between the copolymer and the ferric cations, and may provide information that confirms the formation of the ionomer.

Figure 6.10 shows the oxygen 1s XPS spectra of the copolymer before (a) and after mixture with $FeCl_3$ (b). If the reaction leading to the formation of the ionomer takes place, then this region of the spectrum is expected to exhibit some of the most dramatic changes which may be used to verify the success of this process. The spectrum of the copolymer contains two peaks which correspond to the two types of oxygen in the copolymer: oxygen single-bonded to carbon and oxygen double-bonded to carbon, which are positioned at 533.1 and 531.7 eV, respectively. The spectrum of the copolymer/$FeCl_3$ mixture also contains peaks for oxygen single-bonded to carbon and double-bonded to carbon at 533.6 and 532.1 eV, respectively. An additional peak at 530.6 eV appears in the spectrum after mixture of $FeCl_3$ with the copolymer. This peak may correspond to the formation of a linkage between the ferric cations and the oxygens of the acrylic acid segments of the copolymer, but the exact origin of this peak requires further study to determine if this peak serves as evidence of formation of the ionomer.

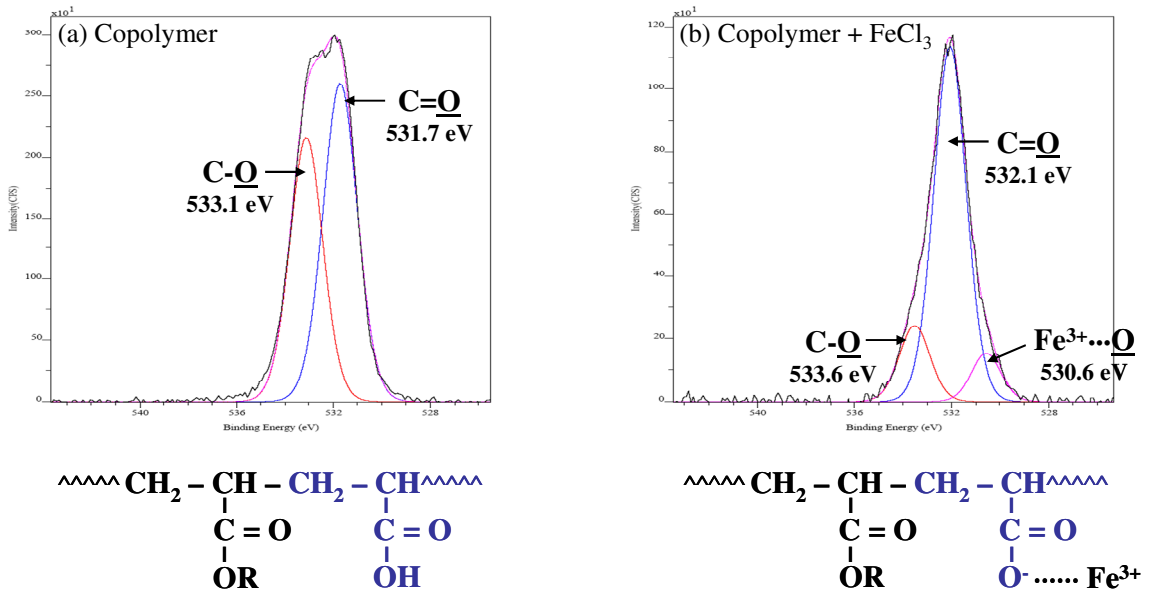

Figure 6.9. O 1s XPS of (a) copolymer (starting monomer composition: [2-EHA] = 4.32 mol dm^{-3} (74.7 mol%), [AA] = 1.46 mol dm^{-3} (25.3 mol%), 100 Gy dose of γ-irradiation, 0.83 Gy s^{-1} dose rate) and (b) copolymer/$FeCl_3$ mixture (formulated composition based on 1:3 mole ratio of $FeCl_3$ to AA).

6.2.3 Energy Dispersive X-ray Spectroscopy

Additional analysis of the elemental composition of the ionomeric materials formed was performed by EDS. Figure 6.11 show the EDS spectra of the ionomers synthesized from ferrous acetate (1:2 mole ratio of Fe^{2+}:AA) and ferric chloride (1:3 mole ratio of Fe^{3+}:AA). The spectra of both of these ionomers show the presence of iron within the sample indicated by K_α and K_β peaks near 6.5 and 7 keV, respectively. A K_α peak for carbon appears near 0.25 keV as one of the elements exhibiting the greatest signal. Copper lines from the grid on which the sample is placed during TEM/EDS analysis shows strong signals near 0.9 and 8 keV. Contamination from chromium appears near 5.4 and 5.9 keV, which possibly originates from the tweezers used to handle the sample grids.

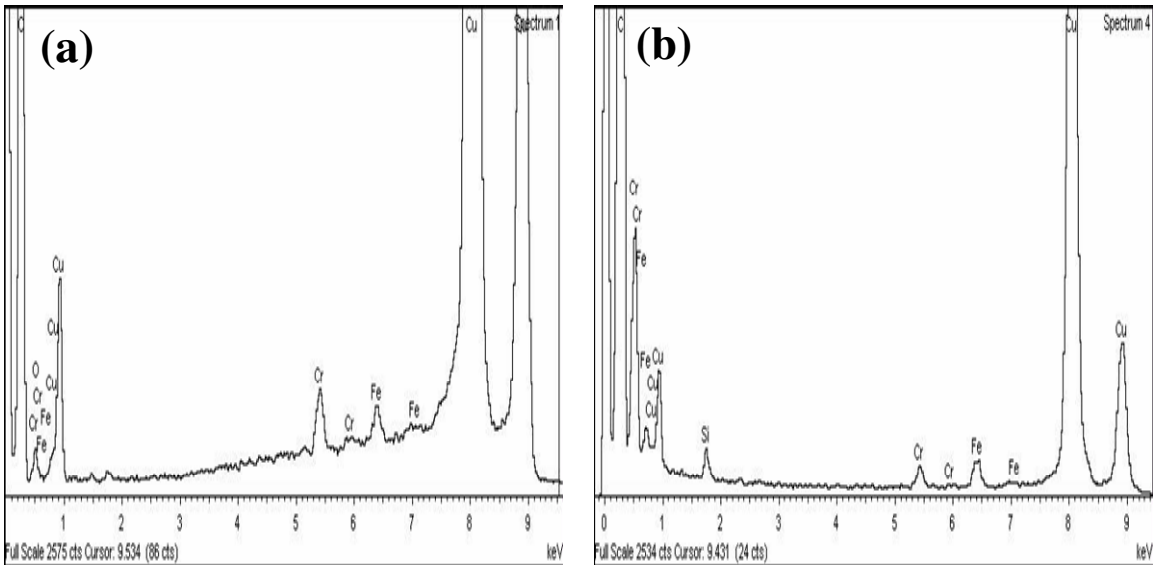

Figure 6.10. EDS spectra of (a) poly(2-EHA-co-AA)/Fe^{2+} ionomer (from formulated compositions based on 1:2 mole ratio of Fe^{2+} to AA) and (b) poly(2-EHA-co-AA)/Fe^{3+} ionomer (from formulated compositions based on 1:3 mole ratio of Fe^{3+} to AA).

Figure 6.12 shows the EDS of ionomers synthesized at higher concentrations of ferrous acetate and ferric chloride. Quantitative analysis of selected regions of these samples indicated that the ionomers formed from ferrous acetate contained iron concentrations in the 2 – 12 at% range, and carbon concentrations in the 88 – 97 at% range. Ionomers formed from ferric chloride contained iron concentrations of 12 – 16 at%, chlorine concentrations of 4 – 15 at%, and carbon concentrations of 70 – 84 at%. The fact that such a large concentration of chloride was detected in this sample even after nine days of dialysis, indicates that there is a significant amount of residual $FeCl_3$ salt remaining in the sample. Therefore, a more exhaustive removal of the salt which is not bound to the copolymer must be performed in order to obtain quantitative measurements which more accurately reflect the extent of iron cation uptake by the polymer.

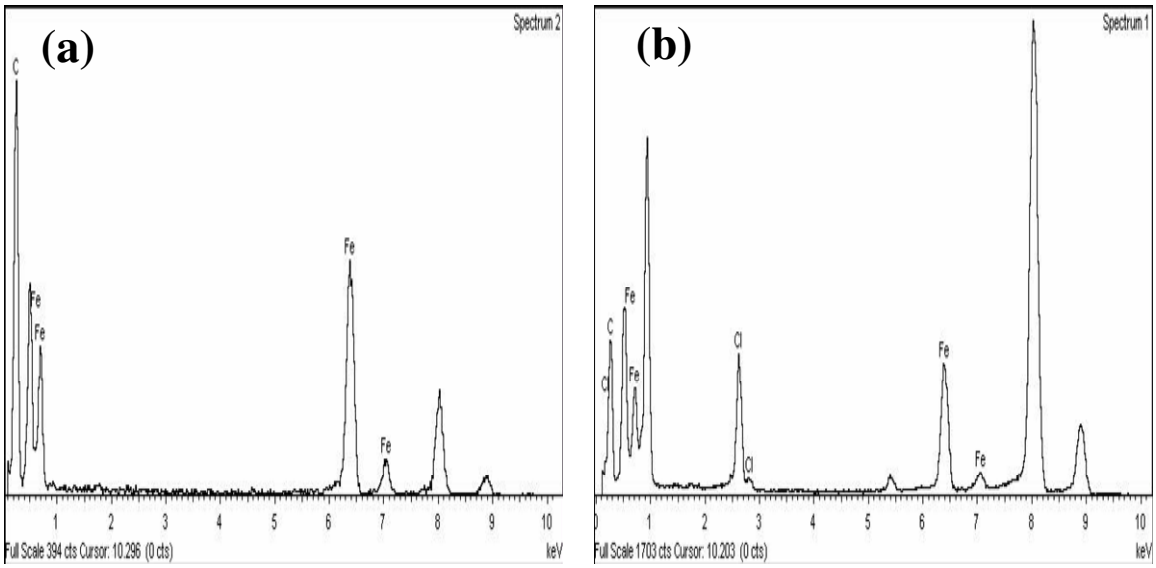

Figure 6.11. EDS spectra of (a) poly(2-EHA-co-AA)/Fe^{2+} ionomer (from formulated compositions based on 2:1 mole ratio of Fe^{2+} to AA) and (b) poly(2-EHA-co-AA)/Fe^{3+} ionomer (from formulated compositions based on 3:1 mole ratio of Fe^{3+} to AA).

A greater iron content (compared to carbon content) is observed in the spectra of the ionomers synthesized from higher concentrations of the metal salts. However, this type of analysis does not make as clear a distinction between the various states that the iron cation may be in with regards to its interactions with the polymer as is made by FTIR spectroscopy. It is not as easy to tell which metal ions are bound to the copolymer and those which may be associated with residual salt that was not completely removed from the sample during dialysis. For example, if the sample contains residual acetate that has not been removed during dialysis, the contribution that it makes to the atomic percent of carbon measured in the sample is more difficult to evaluate by EDS than in would be by FTIR measurement. This is due to the fact that the FTIR spectra of these materials show a clear distinction among the various functional groups to which carbon may belong.

6.2.4 Transmission Electron Microscopy

Figure 6.13 shows the TEM images of the ionomers made from ferrous acetate (1:2 mole ratio of Fe^{2+}:AA) and ferric chloride (1:3 mole ratio of Fe^{3+}:AA). Both types of ionomers show dark regions of less than 1 nm which may correspond to clusters of iron cations.

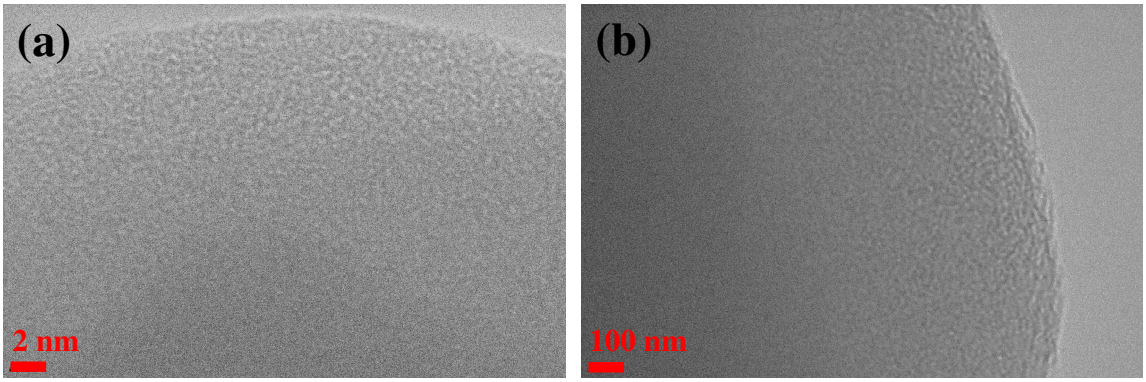

Figure 6.12. TEM images of (a) poly(2-EHA-co-AA)Fe^{2+} ionomer (from formulated compositions based on 1:2 mole ratio of Fe^{2+} to AA) and (b) poly(2-EHA-co-AA)/Fe^{3+} ionomer (from formulated compositions based on 1:3 mole ratio of Fe^{3+} to AA).

Figure 6.14 shows the TEM images of the ionomers made from higher concentrations of ferrous acetate (2:1 mole ratio of Fe^{2+}:AA) and ferric chloride (3:1 mole ratio of Fe^{3+}:AA). These samples contain dark regions of roughly 100 nm in diameter, which may correspond to iron clusters of up to approximately 350 iron cations (based on an atomic radius of 0.14 nm).

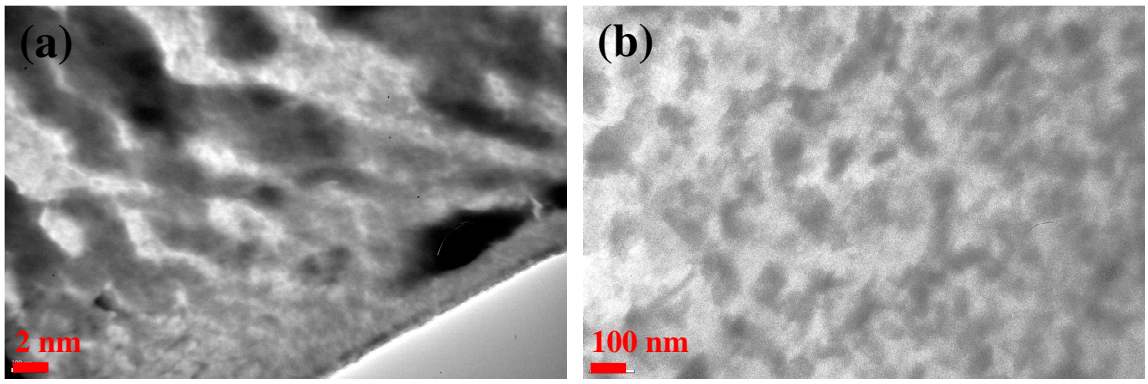

Figure 6.13. TEM images of (a) poly(2-EHA-co-AA)Fe^{2+} ionomer (from formulated compositions based on 2:1 mole ratio of Fe^{2+} to AA) and (b) poly(2-EHA-co-AA)/Fe^{3+} ionomer (from formulated compositions based on 3:1 mole ratio of Fe^{3+} to AA).

6.3 Summary of Results and Conclusions

(1) FTIR measurement clearly showed changes in the 2-EHA/AA samples in the steps leading up to the formation of the ionomer. This included the reduction in the size of the alkene bands at 1637, 1622, 1407, and 810 cm^{-1} after irradiation to form the copolymer, and the emergence of an asymmetric carboxylate stretching band at 1600 cm^{-1} upon formation of the ionomer.

(2) Comparison of ionomers made at 1:2 and 2:1 mole ratio of $FeAc_2$ to AA and 1:3 and 3:1 mole ratio of $FeCl_3$ to AA indicated a greater uptake of the iron in samples which were mixed with higher concentrations of the metal salt, indicated by a greater magnitude of the COO^- stretch at 1600 cm^{-1}. The FTIR spectra of the samples formed at higher concentrations did not display a symmetric carbonyl stretching band at 1700 cm^{-1}, which further confirmed successful formation of the ionomer.

(3) Comparison of the FTIR spectra of ionomers formed from $FeAc_2$ and $FeCl_3$ indicated that a greater uptake of the iron took place when $FeAc_2$ was used. This phenomenon was attributed to the greater stability constant of acetic acid compared with that for hydrochloric acid, which drives the incorporation of the iron cations into the copolymer.

(4) XPS analysis of the 2-EHA/AA copolymer before and after mixture with $FeCl_3$ showed the emergence of a new peak near 530 eV. This peak may correspond to an interaction between the oxygen in the copolymer and the ferric cations. However, more experimental work is required to conclusively determine the origin of this peak, since it did not appear consistently within all of the samples measured by XPS.

(5) EDS measurements of the ionomers formed from ferrous acetate and ferric chloride indicated a relatively greater atomic percent of iron in samples formed from 2:1 and 3:1 mole ratios of ferrous acetate and ferric chloride to AA, respectively. However, elemental analysis demonstrated a significant amount of chlorine remained in the poly(2-EHA-co-AA)/Fe^{3+} samples, which indicated the presence of residual $FeCl_3$ salt. These measurements therefore indicate that the dialysis procedure employed in this work did not completely remove the ions in the material which were not bound to the copolymer.

(6) TEM images of ionomers formed from ferrous acetate (2:1 mole ratio of Fe^{2+}:AA) and ferric chloride (3:1 mole ratio of Fe^{3+}:AA) contained dark regions of at least 100 nm in diameter which may represent clusters of approximately 350 iron cations.

7. Recommendations for Future Work

7.1 Radiation-Induced Copolymerization of 2-Ethylhexyl Acrylate and Acrylic Acid

(1) ^{13}C NMR measurements would provide significant pieces of information related to the structure of the polymer synthesized in this work. For example, they could be used to determine the crosslink density of the material.

(2) Gel Permeation Chromatography (GPC) measurements would provide additional useful information about the polymer composition. Although ^{1}H NMR could be used to determine the total amount of monomer of each type which had been incorporated into the polymer as a function of dose, it did not indicate the distribution of molecular masses of the polymers produced. However, there are several challenges to the measurement of molecular weight distributions of 2-EHA/AA copolymers which would require some time to resolve. One is the appropriate mobile phase which is compatible with both the 2-EHA and AA comonomers, despite the large differences in their polarities, which would also be compatible with the packing material in the GPC column. An attempt was made to perform GPC analysis on copolymer samples which were formed from a starting monomer mixture composition containing 4.32 mol dm^{-3} 2-EHA monomer and 0.253 mol dm^{-3} AA monomer, but difficulties arose with the transport of the sample through the column (mobile phase: THF). This particular monomer mixture composition contained the highest concentration of AA used in this work, and the high polarity of AA may have led to an undesired reaction with the packing material. Therefore a solvent mixture of

THF with a solvent of higher polarity (such as methanol) could be tried to compatibilize the sample with the particular column that was used.

(3) An investigation of the effect of pulse frequency on the extent of conversion of the materials produced would be useful in developing more sophisticated methods of synthesis of 2-EHA/AA copolymers using pulsed electron beam irradiation. Our group has previously studied this parameter for the homopolymerization of neat 2-EHA. It would be useful to repeat this investigation in the presence of acrylic acid, particularly since the ^{1}H NMR analysis method employed in this would enable the individual conversion profiles of each comonomer to be monitored.

7.2 Pulse Radiolysis

(1) A shorter (ns) electron pulse width would enable us to see the ionic precursors to the neutral carbon-centered free radical of 2-EHA. The radical anion which is expected to form upon irradiation of 2-EHA does not have a long enough lifetime to be observed using the experimental measurement parameters employed in this work. Rather, it is expected to form and decay during the 3 μs electron pulse which was applied to the samples studied in the work presented in this dissertation. It is thus difficult to obtain information regarding the mechanism of radical formation when a pulse of this length is employed. A shorter pulse would also diminish the overlap of Čerenkov radiation with build-up of 2-EHA neutral free radicals, thereby enhancing the certainty in the absorbance region used for fitting to data for the build-up.

(2) EPR measurements of neat 2-EHA would be very useful in elucidating the structure of the radicals generated by electron irradiation. This would also be helpful in acquiring information regarding the mechanism of the polymerization reaction.

(3) Pulse radiolysis measurements across a range of doses per pulse would enable a clearer distinction between the values of the propagation and termination rate coefficients. The propagation step of the reaction would predominate at lower dose rates, while the termination step would predominate at higher dose rates.

(4) Pulse radiolyis studies with additional variations in the concentrations of 2-EHA, AA, and MeOH would help to clarify the role that each species plays in the radiation-induced reactions that are taking place.

7.3 Poly(2-ethylhexyl acrylate-co-acrylic acid) Ionomer Formation

(1) Mössbauer spectroscopy, micro-x-ray fluorescence could be very informative with regards to the speciation of the iron (i.e., the local environment of the iron, including such characteristics as the number of carboxylic acid groups bound to the cation).

(2) The ionomer formed in this work may be employed as a precursor material to a magnetic composite. Metal nanoparticle-organic polymer composites have become a fascinating area of interdisciplinary research with a broad range of applications over the past few decades. This interest extends from the difference in properties between particles and their corresponding bulk material forms. Currently there is tremendous

interest in magnetic nanoparticles in many areas of technological application, including magnetic data storage, medical diagnostic imaging, and drug delivery [61, 68, 69]. This can be attributed to the potential of creating substances with properties which are not available in coarser-grained materials.

Most of the challenges to the development of nanoparticles concern the handling of nanoscale powders [70]. One of the greatest obstacles to the technological structural application of nanoobjects is in the prevention of the agglomeration phenomena which take place due to the instability of the surfaces of the particles as their size diminishes [71]. An understanding of the nature of the agglomeration process and its mechanism is essential for the resolution of the stability issues associated with these nanoparticle interactions [69].

There are a broad variety of techniques currently under investigation for the preparation of stable metal or metal oxide nanoparticles. One of the most popular approaches involves their formation within 'nanoreactor' environments, which are usually based on micelle self-assembly with the use of surfactants and/or polymers. In particular, polymer systems with regular architecture such as block copolymers, dendrimers, star, and brush polymers, or a combination of these are widely used for the preparation of inorganic nanoparticles. The polymers used for such functions as prevention of agglomeration of nanoparticles are often composed of two immiscible components (amphiphilic) covalently bound so that the system cannot undergo macrophase separation. The system instead undergoes what is known as microphase separation, in which the hydrophilic and hydrophobic portions segregate into well-

defined regions [72, 73]. This process may generate very distinct regions of hydrophilic nature into which an inorganic component may be incorporated.

Diblock copolymers constitute a relatively simple system that is widely used to design templates for inorganic particle synthesis. They exhibit a range of morphologies which may be manipulated through modification of the block length, some of which the most common include lamellar, cylindrical, and spherical phases [74]. The size and shape of the particles formed within these domains may thus be controlled by the resultant polymer morphology.

Although block copolymers are the most extensively studied microphase-separating polymeric systems, there exist a number of other systems which have been reported to undergo this process, including interpenetrating polymer networks, polyelectrolytes (under conditions of weak charge in poor solvents), random copolymers, and ionomers. The microdomain structure and morphology of ionomers have been heavily investigated over the years [75].

Ionomers are random copolymers containing a small fraction (usually less than 15 mol%) of segments containing ionic salts. Although such polar repeat units are attracted to each other, their covalent attachment to the polymer chain prevents them from separating out, and they instead form ionic aggregates known as multiplets [76, 77]. It has been demonstrated that the multiplet structures displayed by ionomers are analogous to the microdomain structures of block copolymers, and microphase separation theory can be applied and extended to ionomeric materials [73].

Ionomers can therefore be used as matrices for nanocomposites. An example of such a system has been reported by J.Y. Kim *et al.* in which a urethane-acrylate

copolymer was used as the matrix for an iron salt which was converted to a magnetic composite containing γ-Fe_2O_3 (maghemite) and Fe_3O_4 nanoparticles (magnetite) [78]. In this study it was demonstrated that methods which produced greater microphase separation displayed higher saturation magnetization, since they contain enhanced levels of interactions between the polymer and the metal salt precursor.

The most common type of ionomer is based on an ethylene nonionic backbone copolymerized with acrylic acid or methacrylic acid. An example of such a material is Surlyn® (manufactured by DuPont), and is based on poly(ethylene-co-methacrylic acid), in which the acidic groups are neutralized with sodium or zinc cations [79]. Although relatively small concentrations of acidic groups are incorporated into the polymer, they generate significant changes in the morphology and properties of the material, including a reduction in long-chain branching, lower melting point, and enhanced clarity and toughness. The combination of lower crystallinity (enhanced clarity) due to the incorporation of methacrylic acid units, along with the ease of processing and useful mechanical properties of polyethylene, make this ionomeric material useful for packaging applications.

When the concentration of acidic units in the ionomer is relatively low, the ion pairs will be isolated from one another. When their concentration is raised above a particular level, they will group together to form ionic regions known as multiplets [80]. In the dry state, this aggregation behavior is governed primarily by dipole-dipole interactions, whereas in the hydrated state it is governed by the phase separation into hydrophilic and hydrophobic regions. This aggregation phenomenon is thermally reversible, since it is based on physical bonding. Above a critical temperature, the

clusters become destabilized. This cluster order-disorder transition takes place at a temperature above the matrix glass transition.

Appendix: Kinetics Calculations for Pulse Radiolysis [5]

Case I: First Order, Reactant Absorbs

(a) $A \rightarrow M$

(b) $A + B \rightarrow N$ (where $[B]_0 >> [A]_0$)

(c) Reactions of type (a) and/or (b)

If only A absorbs: $$\frac{-d[A]}{dt} = k_1[A]$$

where in case: (i) $k_1 = k$

(ii) $k_1 = k[B]_0$

(iii) $k_1 = k_1 + k_2 + ... + k_m[B]_0 + k_m + [B]_0 + ...$

$$\int_{[A]_0}^{[A]} d\ln[A] = -\int_0^t k_1 dt$$

$$\ln[A]_t - \ln[A]_0 = -k_1 t$$

Assume Beer's law: $$D = optical\ density = \log_{10}\left(\frac{I_0}{I_{tr}}\right) = \varepsilon^{\lambda} cl$$

where ε^{λ} is the decadic molar extinction coefficient.

$$\ln D_t = -k_1 t + \ln D_0$$

$$2.303 \log_{10} D_t = -k_1 t + 2.303 \log_{10} D_0$$

A plot of $log_{10}D_t$ vs. t gives a straight line with:

$$slope = \frac{-k_1}{2.303}$$

At time τ when $D_t = 1/2D_0$:

$$\ln\left(\frac{1}{2}\right) = -k_1 \tau$$

$$\tau = \frac{0.693}{k_1} \quad and \quad k_1 = \frac{0.693}{\tau}$$

Case II: First Order, Product Absorbs

(a) $A \rightarrow M$

(b) $A + B \rightarrow M$ (where $[B]_0 >> [A]_0$)

If only M absorbs: $\frac{d[M]}{dt} = k_1[A]$

where in case: (i) $k_1 = k$

(ii) $k_1 = k[B]_0$

Let: $x = [M]$ and by stoichiometry $[A]_0 - x = [A]$:

$$\int_0^{[M]_t} \frac{dx}{([A]_0 - x)} = \int_0^t k_1 dt$$

$$-\ln([A]_0 - [M]_t) + \ln([A]_0) = k^1 t$$

If the reaction goes essentially to completion, we will have:

$$[A]_0 \cong [M]_\infty$$

$$\ln([M]_\infty - [M]_t) - \ln([M]_\infty) = -k^1 t$$

Assume Beer's law: $\ln(D_\infty - D_t) = -k^1 t + \ln(D_\infty)$

A plot of $ln(D_\infty - D_t)$ vs. t gives a straight line with: slope = $-k^1$

where k^1 is defined above.

Case III: Second Order, Reactant Absorbs

(a) $A + A \rightarrow M$

(b) $A + B \rightarrow N$ where $[A]_0 = [B]_0$

If only A absorbs: $$\frac{-d[A]}{dt} = k^1[A]^2$$

where in case: (i) $k^1 = 2k$

(ii) $k^1 = k$

$$-\int_{[A]_0}^{[A]_t} \frac{d[A]}{[A]^2} = \int_0^t k^1 dt$$

$$\frac{1}{[A]_t} - \frac{1}{[A]_0} = k^1 t$$

Assume Beer's law: $$\frac{1}{D_t} = \frac{k^1 t}{\varepsilon^\lambda l} + \frac{1}{D_0}$$

A plot of $1/D_t$ vs. t gives a straight line with: slope = $\frac{k^1}{\varepsilon^\lambda l}$

where k_1 is defined above.

Case IV: Second Order, Product Absorbs

(a) $A + A \rightarrow M$

(b) $A + B \rightarrow M$ where $[A]_0 = [B]_0$

If only M absorbs: $$\frac{d[M]}{dt} = k[A]^2$$

Case (i): Let x = [M] and by stoichiometry $[A] = [A]_0 - 2x$

$$\int_0^{[M]_t} \frac{dx}{([A]_0 - 2x)^2} = \int_0^t k dt$$

$$\frac{1}{2([A]_0 - 2[M]_t)} - \frac{1}{2[A]_0} = kt$$

If the reaction goes to completion, we will have: $[A]_0 \cong 2[M]_\infty$

$$\frac{1}{4([M]_\infty - [M]_t)} - \frac{1}{4[M]_\infty} = kt$$

Assume Beer's law: $\frac{1}{D_\infty - D_t} = \frac{4kt}{\varepsilon^\lambda l} + \frac{1}{D_\infty}$

A plot of $[D_\infty - D_t]^{-1}$ vs. t gives a straight line with: slope = $\frac{4k}{\varepsilon^\lambda l}$

Case (ii): Let x = [M] and by stoichiometry $[A] = [A]_0 - 2x$

$$\int_0^{[M]_t} \frac{dx}{([A]_0 - x)^2} = \int_0^t kdt$$

By similar arguments to those above:

$$\frac{1}{D_\infty - D_t} = \frac{kt}{\varepsilon^\lambda l} + \frac{1}{D_\infty}$$

A plot of $[D_\infty - D_t]^{-1}$ vs. t gives a straight line with: slope = $\frac{k}{\varepsilon^\lambda l}$

Case V: Second Order, Two Reactants

$A + B \rightarrow M$ where $[A]_0 \neq [B]_0$

If only A absorbs:

Let x = [M] and by stoichiometry $[A] = [A]_0 - x$ and $[B] = [B]_0 - x$

$$\frac{dx}{dt} = k([A]_0 - x)([B]_0 - x)$$

$$\int_0^x \frac{dx}{([A]_0 - x)([B]_0 - x)} = \int_0^t kdt$$

$$\ln\left(\frac{[B]_0 - x}{[A]_0 - x}\right) - \ln\left(\frac{[B]_0}{[A]_0}\right) = ([B]_0 - [A]_0)kt$$

$$\ln\left(\frac{[B]_t}{[A]_t}\right) = [A]_0\left(\frac{[B]_0}{[A]_0} - 1\right)kt + \ln\left(\frac{[B]_0}{[A]_0}\right)$$

By stoichiometry: d[A] = d[B]

Integrating: $[A]_t - [A]_0 = [B]_t - [B]_0$

$$[B]_t = [A]_t + [B]_0 - [A]_0 = [A]_t$$

$$\left\{1 + \frac{[A]_0}{[A]_t}\left(\frac{[B]_0}{[A]_0} - 1\right)\right\}$$

Let: $$\alpha = \left(\frac{[B]_0}{[A]_0} - 1\right)$$

Then by substitution: $$\ln\left(1 + \alpha\frac{[A]_0}{[A]_t}\right) = \alpha[A]_0 kt + \ln(\alpha + 1)$$

Assume Beer's law: $$\ln\left\{1 + \alpha\frac{D_0}{D_t}\right\} = \frac{\alpha D_0 k}{\varepsilon^{\lambda} l}t + \ln(\alpha + 1)$$

$$\ln\left(\frac{D_t + \beta}{D_t}\right) = \frac{\beta k}{\varepsilon^{\lambda} l}t + \ln\left(\frac{\beta}{D_0} + 1\right) \qquad \text{where } \beta = \alpha D_0$$

Plot $\ln\left(\frac{D_t + \beta}{D_t}\right)$ vs. t, choosing the value of β by trial and error so that a straight line is obtained.

Then S = Slope = $\frac{\beta k}{\varepsilon^{\lambda} l}$ or $k = \frac{\varepsilon^{\lambda} l s}{\beta}$

Case VI: Mixed First and Second Order, Method I

If A disappears by both a first and a second order process, and if only A absorbs:

$$\frac{-d[A]}{dt} = k_1[A] + 2k_2[A]^2$$

where k_1 may be a pseudo-first order rate constant

$$\int_{[A]_t}^{[A]_{t^1}} \frac{d[A]}{[A](2k_2[A] + k_1)} = -\int_{t}^{t^1} dt$$

Let $[A]_t = x$ and $[A]_{t1} = y$

$$\ln\left(\frac{2k_2x + k_1}{x}\right) - \ln\left(\frac{2k_2y + k_1}{y}\right) = -k_1\left(t^1 - t\right) = k_1\theta$$

$$\ln\left(\frac{2k_2 + k_1/x}{2k_2 + k_1/y}\right) = k_1\theta$$

$$2k_2 + \frac{k_1}{x} = \left[2k_2 + \frac{k_1}{y}\right]e^{k_1\theta}$$

$$\frac{1}{x} = \frac{e^{k_1\theta}}{y} + \frac{2k_2}{k_1}\left[e^{k_1\theta} - 1\right]$$

Assume Beer's law: $\frac{1}{D_t} = \frac{e^{k_1\theta}}{D_{t^1}} + \frac{2k_2}{\varepsilon^{\lambda} l k_1}\left[e^{k_1\theta} - 1\right]$

Choose some fixed time interval θ. Read D_{t1} at any arbitrary time t^1 and then read D^t at time t which is θ later than t^1.

A plot of $1/D_t$ vs. $1/D_{t1}$ is a straight line with

S = Slope = $e^{k_1\theta}$

and I = Intercept = $\frac{2k_2}{\varepsilon^{\lambda} l k_1}\left[e^{k_1\theta} - 1\right]$

Thus $k_1 = \frac{\ln(S)}{\theta}$ and $2k_2 = \frac{\varepsilon^{\lambda} lI \ln(S)}{\theta(S-1)}$

Case VII: Mixed First and Second Order, Method II

If A disappears by both a first and a second order process, and if only A absorbs:

$$\frac{-d[A]}{dt} = k_1[A] + 2k_2[A]^2$$

where k_1 may be a pseudo-first order rate constant

$$\int_{[A]_0}^{[A]_t} \frac{d[A]}{[A](2k_2[A] + k_1)} = \int_0^t dt$$

$$\ln\left(\frac{2k_2[A]_t + k_1}{[A]_t}\right) = k_1 t + \ln\left(\frac{2k_2[A]_0 + k_1}{[A]_0}\right)$$

Assume Beer's law: $\ln\left(\frac{D_t + \alpha}{D_t}\right) = k_1 t + \ln\left(\frac{D_0 + \alpha}{D_0}\right)$

where $\alpha = \frac{k_1 \varepsilon^{\lambda} l}{2k_2}$

Plot $\ln\left(\frac{D_t + \alpha}{D_t}\right)$ vs. t, choosing the value of α by trial and error so that a straight line is obtained. Then S = Slope = k_1 and I = Intercept = $\ln\left(\frac{D_0 + \alpha}{D_0}\right)$ Thus k_1 = S and $2k_2$ = $\frac{S\varepsilon^{\lambda} l}{\alpha}$

REFERENCES

1. Tsoulfanidis, N., *Measurement and Detection of Radiation*. 2nd ed. 1995, Washington, DC: Taylor & Francis.

2. Pierpoint, S.B., *Radiation-Induced Changes Affecting Polyester Based Polyurethane Binder, Ph.D. thesis*. 2002, University of Maryland: College Park.

3. Woods, R.J. and A.K. Pikaev, *Applied Radiation Chemistry: Radiation Processing*. 1994, New York: John Wiley & Sons, Inc.

4. Al-Sheikhly, M., et al., *Radiation-Induced Polymerization of Acrylated Systems*, in *10th "Tihany" Symposium on Radiation Chemistry*. 2002: Sopron, Hungary.

5. Tang, F.W., *The Effects of Small Amounts of Methanol on the Ionizing Radiation Induced Polymerization and Photopolymerization of Styrene, Ph.D. thesis*. 1990, University of Maryland: College Park.

6. Jones, C.G., *Radiation-Induced Remediation of Polychlornated Biphenyls Contained in Industrial Transformer Oil from Electrical Generating Stations, Ph.D. thesis*. 2001, University of Maryland: College Park.

7. Werst, D.W. and A.D. Trifunac, *Early Events Following Radiolytic and Photogeneration of Radical Cations in Hydrocarbons.* Radiation Physics and Chemistry, 1993. **41**(1-2): p. 127-133.

8. Tabata, Y., ed. *Pulse Radiolysis*. 1991, CRC Press: Boca Raton, FL.

9. Painter, P.C. and M.M. Coleman, *Fundamentals of Polymer Science: An Introductory Text*. 2nd Ed. ed. 1997, Boca Raton, FL: CRC Press LLC.

10. Rodriguez, F., et al., *Principles of Polymer Systems*. 5th Ed. ed. 2003, New York: Taylor & Francis.

11. *Polymer Handbook*. 4th Ed. ed, ed. J. Brandrup. 1999, New York: John Wiley & Sons, Inc.

12. Odian, G., *Principles of Polymerization*. 3rd Ed. ed. 1991, New York: John Wiley & Sons, Inc.

13. Ham, G.E., *Kinetics and Mechanisms of Polymerization, Volume 1: Vinyl Polymerization*. 1967, New York: Marcel Dekker, Inc.

14. Plessis, C., et al., *Intramolecular chain transfer to polymer in the emulsion polymerization of 2-ethylhexyl acrylate.* Macromolecules, 2001. **34**(17): p. 6138-6143.

15. Heatley, F., P.A. Lovell, and T. Yamashita, *Chain transfer to polymer in free-radical solution polymerization of 2-ethylhexyl acrylate studied by NMR spectroscopy.* Macromolecules, 2001. **34**(22): p. 7636-7641.

16. Allen, P.E.M. and C.R. Patrick, *Kinetics and Mechanisms of Polymerization Reactions: Applications of Physico-chemical Principles*. 1974, New York: John Wiley & Sons, Inc.

17. Buback, M., et al., *Consistent Values of Rate Parameters in Free-Radical Polymerization Systems .2. Outstanding Dilemmas and Recommendations.* Journal of Polymer Science Part a-Polymer Chemistry, 1992. **30**(5): p. 851-863.

18. *The Effect Polymerization Inhibitors Have on Acrylate Monomers and Formulations*. 2005 [cited; Available from: www.sartomer.com/TechLit/5040.pdf

19. Eisenberg, A. and J.S. Kim, *Introduction to Ionomers*. 4th Ed. ed. 1998, New York: John Wiley & Sons, Inc.

20. *Encyclopedia of Chemical Technology*, R.E. Kirk, Editor. 1991, John Wiley & Sons, Inc.: New York.

21. Koleske, J.V., *Radiation Curing of Coatings*. 2002, West Conshohocken, PA: ASTM International.

22. Clough, R.L., *High-energy radiation and polymers: A review of commercial processes and emerging applications.* Nuclear Instruments & Methods in Physics Research Section B-Beam Interactions with Materials and Atoms, 2001. **185**: p. 8-33.

23. Takacs, E., K. Dajka, and L. Wojnarovits, *Study of high-energy radiation initiated polymerization of butyl acrylate.* Radiation Physics and Chemistry, 2002. **63**(1): p. 41-44.

24. Defoort, B., D. Defoort, and X. Coqueret, *Electron-beam initiated polymerization of acrylate compositions, 2 - Simulation of thermal effects in thin films.* Macromolecular Theory and Simulations, 2000. **9**(9): p. 725-734.

25. Clegg, D.W. and A.A. Collyer, *Irradiation Effects on Polymers*. 1991, New York: Elsevier Applied Science.

26. Feng, H., *The Radiation-Induced Bulk Polymerization of 2-Ethylhexyl Acrylate*. 2002, University of Maryland: College Park.

27. Asahara, J., et al., *Crosslinked acrylic pressure-sensitive adhesives. I. Effect of the crosslinking reaction on the peel strength.* Journal of Applied Polymer Science, 2003. **87**(9): p. 1493-1499.

28. Aymonier, A., et al., *Design of pressure-sensitive adhesives by free-radical emulsion copolymerization of methyl methacrylate and 2-ethylhexyl acrylate. 1. Kinetic study and tack properties.* Chemistry of Materials, 2001. **13**(8): p. 2562-2566.

29. Weiss, D.E. and D.S. Dunn, *Pulsed polymerization of acrylate monomers using electron beam. Conditions for achieving single-phase heterogeneous polymerization.* Radiation Physics and Chemistry, 2002. **65**(3): p. 281-288.

30. Vazquez, B., et al., *Polymeric hydrophilic hydrogels with flexible hydrophobic chains. Control of the hydration and interactions with water molecules.* Macromolecules, 1997. **30**(26): p. 8440-8446.

31. *Sigma-Aldrich Catalog and Handbook*. 2007 [cited; Available from: www.sigmaaldrich.com.

32. *Airgas Catalog*. 2007 [cited; Available from: www.airgas.com.

33. *Wheaton Science Products Catalog*. 2007 [cited; Available from: www.wheatonsci.com.

34. *Alfa Aesar Chemicals, Metals, and Materials Catalog*. 2006 - 2007 [cited; Available from: www.alfa.com.

35. *Fisher Scientific Catalog*. 2007 [cited; Available from: www.fishersci.com.

36. Ebert, M., et al., *Pulse Radiolysis*. 1965, New York: Academic Press, Inc.

37. *Bruker Catalog*. 2007 [cited; Available from: www.bruker.com.

38. *Cambridge Isotope Laboratories Catalog*. 2007 [cited; Available from: www.isotope.com.

39. *Thermo Scientific Catalog*. 2007 [cited; Available from: www.thermo.com.

40. *Kratos Analytical Catalog*. 2007 [cited; Available from: www.kratos.com.

41. *JEOL Catalog*. 2007 [cited; Available from: www.jeol.com.

42. *Electron Microscopy Sciences Catalog*. 2007 [cited; Available from: www.emsdiasum.com.

43. *The Aldrich Library of NMR Spectra*. 2nd Ed. ed, ed. C.J. Pouchert. 1983, Milwaukee, WI: Aldrich Chemical Company Library.

44. Lambert, J.B., et al., *Organic Structural Spectroscopy*. 2nd Ed. ed. 1998, Upper Saddle River, NJ: Prentice-Hall, Inc.

45. Beuermann, S., et al., *Determination of free-radical propagation rate coefficients of butyl, 2-ethylhexyl, and dodecyl acrylates by pulsed-laser polymerization.* Macromolecules, 1996. **29**(12): p. 4206-4215.

46. Takacs, E., S.S. Emmi, and L. Wojnarovits, *Pulse radiolysis study on polymerization kinetics in organic solvent: 2-ethylhexyl acrylate.* Nuclear Instruments & Methods in Physics Research Section B-Beam Interactions with Materials and Atoms, 1999. **151**(1-4): p. 346-349.

47. Takacs, E., L. Wojnarovits, and K. Dajka, *Kinetics of the early stages of high-energy radiation initiated polymerization.* Macromolecular Chemistry and Physics, 2000. **201**(16): p. 2170-2175.

48. Davis, T.P., et al., *Copolymerization Propagation Kinetics of Styrene with Alkyl Acrylates.* Polymer International, 1991. **24**(2): p. 65-70.

49. Lyons, R.A., et al., *Pulsed-laser polymerization measurements of the propagation rate coefficient for butyl acrylate.* Macromolecules, 1996. **29**(6): p. 1918-1927.

50. Takacs, E., S.S. Emmi, and L. Wojnarovits, *Study of polymerization kinetics of acrylic and methacrylic acid esters at low conversions.* Radiation Physics and Chemistry, 1999. **55**(5-6): p. 621-624.

51. Feng, H.X., et al., *Polymerization of neat 2-ethylhexyl acrylate induced by a pulsed electron beam.* Journal of Polymer Science Part a-Polymer Chemistry, 2003. **41**(1): p. 196-203.

52. Feng, H.X., et al., *The role of pulse frequency and acrylic acid in the radiation-induced bulk polymerization of 2-ethylhexyl acrylate.* Radiation Physics and Chemistry, 2003. **67**(3-4): p. 347-352.

53. Knolle, W. and R. Mehnert, *Primary reactions in the electron-induced polymerization of acrylates.* Nuclear Instruments & Methods in Physics Research Section B-Beam Interactions with Materials and Atoms, 1995. **105**(1-4): p. 154-158.

54. Houston, P.L., *Chemical Kinetics and Reaction Dynamics*. 2001, New York: McGraw-Hill.

55. Mostafavi, M., et al., *Transient and stable silver clusters induced by radiolysis in methanol.* Journal of Physical Chemistry A, 2002. **106**(43): p. 10184-10194.

56. Wang, W.F., et al., *Termination of (CH2OH)-C-center dot/CH2O center dot-radicals in aqueous solution.* Journal of Physical Chemistry, 1996. **100**(39): p. 15843-15847.

57. Rosiak, J.M. and P. Ulanski, *Synthesis of hydrogels by irradiation of polymers in aqueous solution.* Radiation Physics and Chemistry, 1999. **55**(2): p. 139-151.

58. Ulanski, P. and J.M. Rosiak, *Pulse-Radiolysis of Poly(Acrylic Acid) in Deoxygenated Aqueous-Solution.* Journal of Radioanalytical and Nuclear Chemistry-Letters, 1994. **186**(4): p. 315-324.

59. Ulanski, P., et al., *Radiolysis of Poly(Acrylic Acid) in Aqueous-Solution.* Radiation Physics and Chemistry, 1995. **46**(4-6): p. 909-912.

60. Pankasem, S., et al., *Pulse radiolysis of vinyl monomers, in the pure state and with added pyrene.* Radiation Physics and Chemistry, 1996. **47**(6): p. 827-833.

61. Ziolo, R.F., et al., *Matrix-Mediated Synthesis of Nanocrystalline Gamma-Fe2o3 - a New Optically Transparent Magnetic Material.* Science, 1992. **257**(5067): p. 219-223.

62. Joshi, M.S., K. Singer, and J. Silverman, *Radiation-Induced Crosslinking of Polyethylene in Presence of Bifunctional Vinyl Monomers.* Radiation Physics and Chemistry, 1977. **9**(4-6): p. 475-488.

63. Patacz, C., B. Defoort, and X. Coqueret, *Electron-beam initiated polymerization of acrylate compositions 1: FTIR monitoring of incremental irradiation.* Radiation Physics and Chemistry, 2000. **59**(3): p. 329-337.

64. Buback, M., et al., *Quantitative IR spectroscopic analysis of ethylene-acrylate copolymers.* European Polymer Journal, 1997. **33**(3): p. 375-379.

65. Gunzler, H. and H.U. Gramlich, *IR Spectroscopy*. 2002, Federal Republic of Germany: Wiley-VCH.

66. Clay, R.T. and R.E. Cohen, *Synthesis of metal nanoclusters within microphase-separated diblock copolymers: sodium carboxylate vs carboxylic acid functionalization.* Supramolecular Science, 1998. **5**(1-2): p. 41-48.

67. Ghosh, P.K., *Introduction to Photoelectron Spectroscopy*. 1983, New York: John Wiley & Sons, Inc.

68. LesliePelecky, D.L. and R.D. Rieke, *Magnetic properties of nanostructured materials.* Chemistry of Materials, 1996. **8**(8): p. 1770-1783.

69. Leslie-Pelecky, D.L. and R.D. Rieke, *Magnetic properties of nanostructured materials.* Chemistry of Materials, 1996. **8**(8): p. 1770-1783.

70. Willard, M.A., et al., *Chemically prepared magnetic nanoparticles.* International Materials Reviews, 2004. **49**(3-4): p. 125-170.

71. Chien, C.L., *Granular Magnetic Solids.* Journal of Applied Physics, 1991. **69**.

72. Wilson, J.L., et al., *Synthesis and magnetic properties of polymer nanocomposites with embedded iron nanoparticles.* Journal of Applied Physics, 2004. **95**(3): p. 1439-1443.

73. Nyrkova, I.A., A.R. Khokhlov, and M. Doi, *Microdomains in Block-Copolymers and Multiplets in Ionomers - Parallels in Behavior.* Macromolecules, 1993. **26**(14): p. 3601-3610.

74. Jones, R.A., *Soft Condensed Matter*. 2002, New York: Oxford University Press, Inc.

75. Schlick, S., *Ionomers: characterization, theory, and applications*. 1996, New York: CRC Press, Inc.

76. Tant, M.R., K.A. Mauritz, and G.L. Wilkes, *Ionomers: synthesis, structure, properties, and applications*. 1997, New York: Van Nostrand Reinhold Company, Inc.

77. Eisenberg, A., *Clustering of ions in organic polymers: a theoretical approach.* Macromolecules, 1970. **3**.

78. Kim, J.Y., J.W. Lee, and K.D. Suh, *Synthesis of magnetic nanocomposites using amphiphilic polyurethane networks.* Macromolecular Rapid Communications, 2001. **22**(17): p. 1432-1437.

79. Siuzdak, D.A., P.R. Start, and K.A. Mauritz, *Surlyn (R)/silicate hybrid materials. I. Polymer in situ sol-gel process and structure characterization.* Journal of Applied Polymer Science, 2000. **77**(13): p. 2832-2844.

80. Eisenberg, A., B. Hird, and R.B. Moore, *A New Multiplet-Cluster Model for the Morphology of Random Ionomers.* Macromolecules, 1990. **23**(18): p. 4098-4107.